Skeletal muscle plasticity:
The LIM domain protein nTRIP6 in muscle regeneration, nuclear function of the mTORC1 activator RHEB in muscle growth

Zur Erlangung des akademischen Grades einer

DOKTORIN DER NATURWISSENSCHAFTEN

(Dr. rer. nat.)

von der KIT-Fakultät für Chemie und Biowissenschaften

des Karlsruher Instituts für Technologie (KIT)

genehmigte

DISSERTATION

von

Tannaz Norizadeh Abbariki

1. Referent: Apl. Prof. Dr. Andrew Cato

2. Referent: Prof. Dr. Martin Bastmeyer

Tag der mündlichen Prüfung: 08.12.2020

Erklärung zur Urheberschaft

Hiermit erkläre ich, diese Dissertation selbstständig verfasst und keine anderen als die angegebenen Hilfsmittel verwendet zu haben. Wörtliches oder indirekt übernommenes Gedankengut ist nach bestem Wissen als solches gekennzeichnet worden. Dies ist mein erster Dissertationsversuch, ich habe keine erfolglosen Dissertationsversuche unternommen. Die Dissertation wurde bisher zu keinem Zeitpunkt als Prüfarbeit verwendet oder als Dissertation bei einer anderen Fakultät vorgelegt.

_____

Tannaz Norizadeh Abbariki

I Zusammenfassung

Skelettmuskelregenerierung und Muskelwachstum sind zwei essentielle Aspekte der Muskelplastizität. Die Muskelregenerierung basiert auf dem komplexen und hoch konzertierten Prozess der Myogenese, der die Aktivierung der Muskelstammzellen, sogenannter Satellitenzellen, beinhaltet. Diese rufen proliferierende Vorläuferzellen hervor, die Myoblasten. Die Myoblasten verlassen den Zellzyklus und differenzieren zu gewidmeten Präkursoren, den Myozyten. Am Ende führt die Verschmelzung von mehreren Myozyten zur Bildung von Myofasern.

Im ersten Teil meiner Doktorarbeit habe ich die Rolle des transkriptionellen Co-regulators nTRIP6 bei der Regulierung der Myogenese untersucht. Frühere *in vitro* Arbeiten legen nahe, dass nTRIP6 eine Rolle bei der Myogenese, genauer am Übergang zwischen Proliferation und Differenzierung, spielen könnte. In einem *in vitro* Model der Myogenese mit der C2C12-Maus-Myoblasten-Zelllinie konnte ich zeigen, dass selektives Blockieren der nTRIP6-Funktion eine beschleunigte Expression der frühen Differenzierungsmarker hervorrief, ohne dabei die Dynamik der Zellzyklus-Terminierung zu verändern. Diese vorzeitige frühe Differenzierung führte zu einer Verzögerung der Expression von späten Differenzierungsmarkern und der Verschmelzung der Myozyten. Somit verhindert nTRIP6 die vorzeitige Differenzierung der Myoblasten und ermöglicht in den späteren Stadien die korrekte Differenzierung und Verschmelzung der Myozyten. Dementsprechend führt ein Gen-Knockout des TRIP6-Gens in den Satellitenzellen von Mäusen zu deregulierten Skelettmuskelregenerationsdynamiken. Als Indikator für die Verschmelzung wurde eine erhöhte Anzahl an Myozyten sowie eine Verzögerung bei der Erhöhung des Myofaser-Durchmessers verwendet. Folglich trägt nTRIP6 Expression zur zeitlichen Kontrolle der Myogenese und der Skelettmuskelregeneration bei.

Im zweiten Teil dieser Arbeit habe ich die Regulierung der Myofaser-Größe untersucht. Der Hauptinduktor der Muskelhypertrophie, die hauptsächlich auf der Vergrößerung der Myofaser basiert, ist der mTORC1-(mechanistic target of rapamycin complex 1) Signalweg. Der Upstream-Aktivator von mTORC1 ist das kleine G-Protein RHEB, das der Lysosomen-Membran zugeordnet und dabei farnesylierungsabhängig ist. RHEB wurde bereits im Zellkern gefunden, jedoch ist die nukleare Funktion von

RHEB, insbesondere im Zusammenhang mit dem Muskelwachstum, noch nicht erforscht. Mit Zebrafischen als *in vivo* Model konnte ich zeigen, dass RHEB in Myofasern adulter Fische vor allem zytosolisch ist. Im Gegensatz dazu befindet sich RHEB in Myofasern von Embryos ausschließlich im Nukleus. Nukleares RHEB könnte somit eine Besonderheit von schnell wachsenden Muskeln sein. Des Weiteren konnte *in vitro* gezeigt werden, dass in Zellen, in denen RHEB sowohl zytosolisch als auch nuklear vorkommt, die Verwendung eines Farnesylierungstransferase-Inhibitors die nukleare Lokalisation von RHEB erhöht. Dies deutet darauf hin, dass ein wesentlicher Faktor der nuklearen Anreicherung von RHEB ein Mangel an Farnesylierung ist. Darüber hinaus förderte eine konstitutive aktive Mutante von RHEB, welche nur im Zellkern vorhanden war, eine Vergrößerung der Myofaser in Zebrafisch-Embryonen, während eine dominant negative Mutante Atrophie verursachte. Erstaunlicherweise hemmte weder die Verwendung einer RHEB-Mutante mit reduzierter mTORC1-Interaktion, noch die Verwendung eines mTORC1-Inhibitors, die Fähigkeit der konstitutiven aktiven RHEB Mutante, zur Vergrößerung der Myofaser. Somit fördert nukleares RHEB das Myofaser-Wachstum mTORC1-unabhängig. Schließlich konnte ich durch *in vitro* Experimenten zeigen, dass nukleares RHEB die Transkription von ribosomaler RNA - einer essenziellen Voraussetzung des Myofaser Wachstums - bei Zebrafischen fördert. Dieser Teil meiner Arbeit identifizierte eine nukleare Funktion von RHEB bei der Kontrolle des Muskelwachstums über einen mTORC1-unabhängigen Mechanismus. Zusammengenommen zeigen die Ergebnisse dieser Arbeit die Vielfalt und Komplexität der Mechanismen, die an der Regulierung der Skelettmuskelplastizität beteiligt sind.

II Abstract

Skeletal muscle regeneration and muscle growth are two essential aspects of skeletal muscle plasticity. Muscle regeneration relies on the highly orchestrated process of myogenesis, which involves the activation of muscle stem cells, the so-called satellite cells. These cells then give rise to proliferating progenitors, the myoblasts, which subsequently exit the cell cycle and differentiate into committed precursors, the myocytes. Ultimately, the fusion of myocytes leads to myofibre formation. In the first part of my thesis, I investigated the role of the transcriptional co-regulator nTRIP6, the nuclear isoform of the LIM-domain protein TRIP6, in the regulation of myogenesis. Previous work *in vitro* suggested that nTRIP6 may play a role in myogenesis at the transition between proliferation and differentiation. In an *in vitro* model of myogenesis using the C2C12 mouse myoblast cell line, I showed that selectively blocking nTRIP6 function results in accelerated expression of early differentiation marker genes without modifying the dynamics of cell cycle exit. This premature early differentiation was associated with delays in the expression of late differentiation marker genes and in myocyte fusion. Thus, nTRIP6 prevents premature myoblast differentiation, allowing proper myocyte differentiation and fusion at later stages. Accordingly, knocking out the *Trip6* gene in satellite cells in the mouse leads to deregulated skeletal muscle regeneration dynamics, with increased numbers of myocytes and a delay in the increase in myofibre diameter, used as an index of fusion. Thus, nTRIP6 expression contributes to the temporal control of myogenesis and of skeletal muscle regeneration.

In the second part of this work, I investigated the regulation of myofibre size. The main inducer of muscle hypertrophy, which primarily relies on increases in myofibre size, is the mTORC1 (mechanistic target of rapamycin complex 1) pathway. The immediate upstream activator of mTORC1 is the small G-protein RHEB, which is associated to lysosomal membranes in a farnesylation-dependent manner. RHEB has also been found in the nucleus, however its nuclear functions have not been investigated, in particular in the context of muscle growth. Using the zebrafish as an *in vivo* model, I showed that RHEB is mostly cytosolic in myofibres from adult fish. In contrast, RHEB was nearly exclusively nuclear in myofibres from embryos. Thus, nuclear RHEB might be a feature of fast-growing muscles. Furthermore, *in vitro* in cells where RHEB is both cytosolic and nuclear, a farnesyl transferase inhibitor increased the nuclear

localisation of RHEB, suggesting that the lack of farnesylation is a major determinant of RHEB nuclear accumulation. In addition, a nuclear-targeted, constitutively active mutant of RHEB promoted an increase in myofibre size in zebrafish embryo, while a nuclear-targeted dominant negative mutant induced atrophy. Surprisingly, a mutation that reduces RHEB interaction with mTORC1, as well as treatment with an mTORC1 inhibitor did not hamper the ability of the constitutive active RHEB mutant to increase myofibre size. Thus, nuclear RHEB promotes myofibre growth in an mTORC1-independent manner. Finally, *in vitro* experiments showed that nuclear RHEB stimulated zebrafish ribosomal RNA transcription, which is an essential requirement for myofibre growth. Thus, this part of my work uncovered a nuclear function for RHEB in the control of muscle growth via an mTORC1-independent mechanism. Together, the data presented in this thesis illustrate the diversity and complexity of the molecular mechanisms involved in the regulation of skeletal muscle plasticity.

III Index

I Zusammenfassung 4

II Abstract 6

III Index 8

IV Figure Index 9

V Abbreviations 10

1. Introduction 11

1.1 Skeletal muscle plasticity 11

1.2 Skeletal muscle regeneration 12

1.3 Control of muscle size 18

1.4 Hypotheses and aims 29

2. Materials and methods 31

2.1 Materials 31

2.2 Methods 43

3. Results 60

3.1 Function of nTRIP6 in myogenesis and skeletal muscle regeneration 60

3.2 Nuclear function of RHEB in muscle growth in the zebrafish embryo 69

4. Discussion 82

4.1 Skeletal muscle regeneration 82

4.2 Muscle growth 84

4.3 Conclusion 88

5. References 89

6.Acknowledgments 107

IV Figure Index

Figure 1 Transcription factors involved in the control of adult myogenesis 13
Figure 2 Schematic representation of the LIM domain protein TRIP6 17
Figure 3 Schematic representation of the alternative translation of *Trip6* mRNA 18
Figure 4 Schematic representation of mTOR Complexes 1 (mTORC1) and mTORC2 20
Figure 5 Schematic representation of mTORC1 activation 23
Figure 6 Effects of mTORC1 on ribosome biogenesis 24
Figure 7 Schematic representation of RHEB structure 26
Figure 8 Schematic representation of RHEB mutants 27
Figure 9 The blocking peptide does not interfere with the cytosolic functions of TRIP6 61
Figure 10 Blocking nTRIP6 function accelerates early differentiation and delays late differentiation 62
Figure 11 Blocking nTRIP6 function does not affect myoblast proliferation and cell cycle exit 63
Figure 12 Blocking nTRIP6 function delays late differentiation 64
Figure 13 Blocking nTRIP6 function leads to impaired myocyte fusion 65
Figure 14 Skeletal muscle regeneration in *Trip6* knockout mice 67
Figure 15 Subcellular localisation of mTOR and RHEB in C2C12 myoblasts 69
Figure 16 Nonfarnesylated RHEB accumulates in the nuclei of C2C12 myoblast cells 70
Figure 17 Localisation of mTOR and RHEB in Zebrafish myofibres 71
Figure 18 Effect of RHEB mutants on myofibre size 72
Figure 19 Effect of cytosolic RHEB mutants on myofibre size 73
Figure 20 Effect of nuclear RHEB mutants on myofibre size 74
Figure 21 Effect of nuclear RHEB on myocyte fusion 76
Figure 22 Effect of cytosolic constitutive active RHEB-I39K mutant on myofibre size 77
Figure 23 Effect of nuclear constitutive active RHEB-I39K mutant on myofibre size 78
Figure 24 Effect of Rapamycin on RHEB-mediated increase in myofibre size 79
Figure 25 RHEB is not localised in the nucleolus 80
Figure 26 Effect of RHEB on rRNA transcription 81

V Abbreviations

BP	Blocking peptide
cBPP	Control blocking peptide
dpf	Days post fertilization
dpi	Days post injury
Edu	5-Ethynyl-2´-deoxyuridine
FTI	Farnesyl transferase inhibitor
hpf	Hours post fertilization
IRES	Internal ribosome entry site
LSM	Laser scanning confocal microspoe
M-MLV RT	Moloney murine leukemia virus reverse transcriptase
MRF	Myogenic regulatory factor
mTOR	Mechanistic target of rapamycin
NES	Nuclear export signal
NLS	Nuclear localization sequence
NLuc	NanoLuc luciferase
PBS -/-	Phosphate buffered saline without calcium and magnesium
PHIC	Phosphatase inhibitor cocktail
PIC	Protease inhibitor cocktail
PMSF	Phenylmethylsulfonyl fluoride
Pol	Polymerase
PTU	Phenylthiourea
rDNA	Ribosomal DNA
RIPA	Radioimmunoprecipitation assay
rRNA	Ribosomal RNA
rSAP	Recombinant shrimp alkaline phosphatase
S.D.	Standard deviation
siRNA	Small interfering RNA
TRIS	Tris(hydroxymethyl)-aminomethane
WT	Wild type
ZF	Zebrafish

1. Introduction

1.1 Skeletal muscle plasticity

Skeletal muscle is a plastic and dynamic tissue which plays essential roles in the body including movement, generating force and power, control of breathing and metabolism. Skeletal muscle represents a different proportion of total body mass in different classes of vertebrates. In humans, for example, skeletal muscle represents approximately 40% of total body mass (Karagounis and Hawley, 2010), while in the zebrafish, the muscle mass is never fixed and increase continuously throughout life until reaching up to more than half of the body mass (Mommsen, 2001).

The long syncytial muscle cells, the so-called myofibres, are arranged in bundles and surrounded by a layer of connective tissue. Each single myofibre is made of thousands of myofibrils which are assembled together in a very orderly pattern and form a repeated contractile unit, the sarcomere. Each sarcomere is composed of two main contractile proteins, myosin and actin, and regulatory proteins such as the calcium-dependent troponin complex, tropomyosin and actinin, and other associated protein like titin and nebulin, which contribute to the mechanical and physiological properties of muscle (Frontera and Ochala, 2015).

On the basis of these plastic cells, skeletal muscle has the great capability to change its structure and function in response to different stimuli such as the availability of nutrients and growth factors, mechanical overload (physical activity) and pathophysiological conditions (Chromiak and Antonio, 2008). Due to this plasticity, skeletal muscle is able to maintain its mass, repair and regenerate itself, for example after injury or prolonged periods of immobilization and lack of nutrition. During aging and in certain pathological situations, the regeneration capacity of muscle declines (Carosio et al., 2011), muscle mass is lost, and these strongly affect the whole-body function, and consequently the quality of life. Hence, the homeostatic maintenance of muscle mass is crucial for human health (Wolfe, 2006).

In this work, I have investigated two aspects of skeletal muscle plasticity, muscle regeneration and the control of muscle size.

1.2 Skeletal muscle regeneration

Skeletal muscle regeneration is a highly orchestrated process which relies on the process of adult myogenesis and is based on resident muscle stem cells, the so-called satellite cells. These cells are normally in a quiescent state and located between the sarcolemma and the basal lamina of muscle fibres (Yin et al., 2013). The muscle repair process after an injury involves two major phases: degeneration and regeneration. During the degeneration phase, inflammatory cells, initially neutrophils then macrophages, infiltrate the injured muscle through blood vessels and remove the necrotic tissue and disrupted myofibrils (Ciciliot and Schiaffino, 2010; Karalaki et al., 2009). The other important role of macrophages is the activation of satellite cells to promote the regeneration phase (Tidball and Wehling-Henricks, 2007). In the regeneration phase, satellite cells are activated, enter the cell cycle and proliferate to give rise to a population of proliferating progenitor cells, the myoblasts, which then differentiate into myocytes after exiting from the cell cycle. Myocytes then finally undergo terminal differentiation. At the first step of terminal differentiation, myocytes fuse to already existing myofibres or together to form new multinucleated immature muscle fibres, called myotubes (Chal and Pourquié, 2017) characterised by presence of centrally located nuclei (Ciciliot and Schiaffino, 2010). The newly formed myotubes then finally mature into functional contractile myofibres with nuclei positioned at their periphery (Cadot et al., 2015).

1.2.1 Transcriptional control of adult myogenesis

Myogenesis as a multistep process is tightly regulated by a network of transcription factors. The target genes of these transcription factors must be expressed only at the certain time point during the myogenesis process. Therefore, the expression of each transcription factor is highly temporally controlled. The paired domain transcription factor PAX7, basic helix-loop-helix myogenic regulatory transcription factors (MRFs) and members of the MADS-box transcription factor family, in particular the myocyte

enhancer factor-2 (MEF2) contribute to the activation of satellite cells, proliferation and differentiation during adult myogenesis (Karalaki et al., 2009) (Fig. 1).

PAX7 is expressed in all quiescent satellite cells and is required for their postanal maintenance. PAX7 is also essential for satellite cells function to promote proliferation and inhibit differentiation during muscle regeneration. It has been reported that mouse lacking PAX7 showed a sever reduction in satellite cells pool and a limited muscle regeneration due to premature differentiation into committed myocytes without their normal proliferation (von Maltzahn et al., 2013). PAX7 acts upstream of myogenic regulatory factors which comprised of Myf5, MyoD, Myf4 (Myogenin), and MRF4, which promote the progression between the different stages of adult myogenesis (Karalaki et al., 2009).

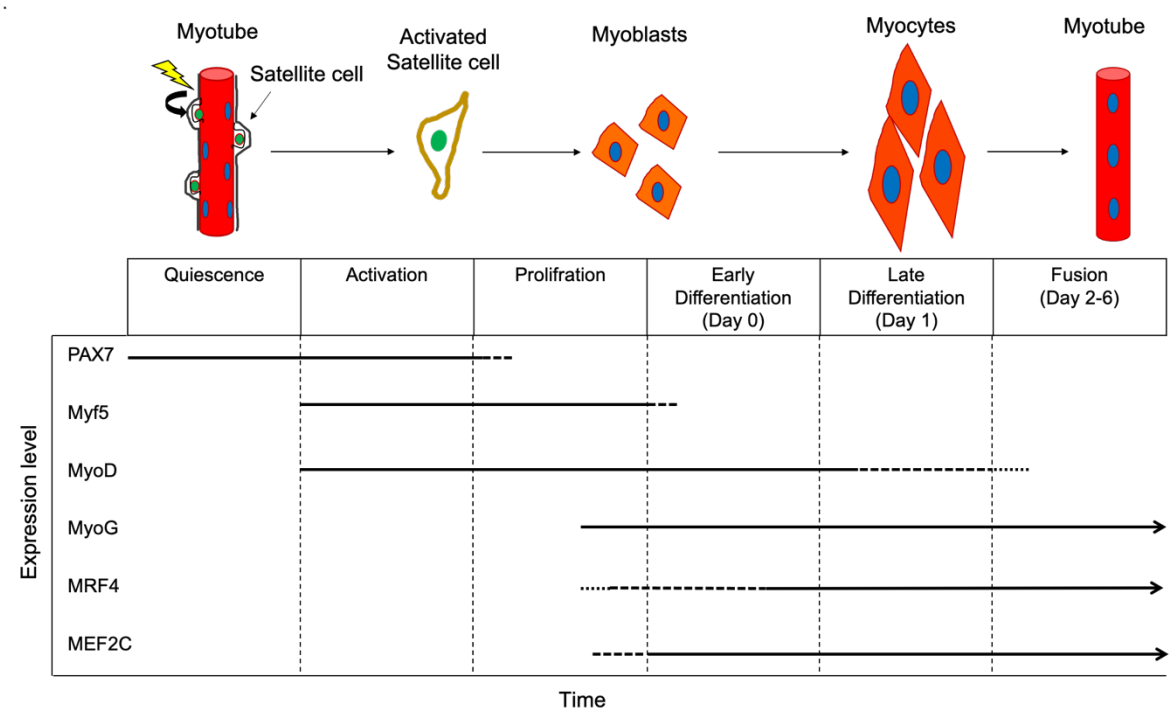

Figure1- Transcription factors involved in the control of adult myogenesis. Upon injury, quiescent satellite cells are activated and proliferate to give rise to a population of proliferating progenitor cells, the myoblasts. After a certain number of cell cycle, myoblasts stop proliferating and differentiate into committed myocytes which then fuse with each other to form new multinucleated myotubes. Each stage of this process is regulated by a network of myogenic transcription factors. The expression of these transcription factors is restricted to certain stages of myogenesis. Modified from Bentzinger et al., (2012).

Upon muscle damage, PAX7 positive quiescent satellite cells enter the cell cycle and begin to express Myf5 and MyoD at the same time. Therefore, myoblasts are characterized by high expression of Myf5 and MyoD. However, they play distinct roles during myogenesis. Myf5 is expressed during the proliferation phase but is unable to initiate myogenic differentiation. The loss of Myf5 results in a slow muscle regeneration with more mononucleated cells and also high levels of degenerated fibres, since the formation of new myofibres is impaired (Yamamoto et al., 2018).

MyoD plays a key role in the regulation of adult myogenesis. Activated satellite cells follow one of two fates depending of MyoD activity: the myoblasts which downregulate PAX7 but keep MyoD expression commit to differentiate into myocyte. The ones which maintain PAX7 expression but lose MyoD expression, proliferate slowly, return to quiescent and repopulate the satellite cells pool (Karalaki et al., 2009; Shi and Garry, 2006).

Proliferation and differentiation are coregulated in an opposite manner in such a way that proliferating myoblasts do not differentiate, and that differentiating cells have stopped proliferating. MyoD plays crucial role in this dual regulation. Thereby, in proliferating myoblasts, MyoD induces the expression of Id3 and NP1 which inhibits the function of pre-differentiation regulatory factors, to prevent untimely differentiation (Wyzykowski et al., 2002). Then, at the proper time point MyoD activates the expression of differentiation promoting transcription factors such as Myf4 (Myogenin) and MRF4 to activate differentiation (Ishibashi et al., 2005). Therefore, the loss of MyoD leads to a high increase in the satellite cells pool, a cell proliferation defect and a delay in terminal differentiation (Yamamoto et al., 2018).

Myogenin is essential for initiating terminal differentiation. When MyoD directs the expression of Myogenin, myoblasts exit the cell cycle and differentiate into myocytes (Zammit, 2017). Myogenin is also expressed in myotubes and *in vivo* targeted mutation in this gene causes an extreme reduction in myotube fusion, subsequently severe skeletal muscle deficiency (Karalaki et al., 2009; Musarò, 2014). Furthermore, Myogenin promotes the expression of important genes which are associated with late differentiation and skeletal muscle maturation such as myosin heavy chains (MHC) (Sartore et al., 1982) and troponin 1 type 2 (Tnni2) (Yoshimoto et al., 2020). Moreover,

Myogenin is required for MRF4 expression, the last member of the MRF family (Musarò, 2014; Zhou and Bornemann, 2001).

MRF4 is expressed in the late stage of terminal differentiation, when myotubes are fused and undergo maturation. Less is known about the function of MRF4 during muscle differentiation. However, it has been reported that MRF4 over-expression promotes early differentiation and myotube formation (Cornelison and Wold, 1997; Pavlath et al., 2003), while MRF4 knockdown in adult skeletal muscle leads to remarkable increase in muscle fibre size (Hernández-Hernández et al., 2017).

The MEF2 family belongs to MADS domain (MCM1, Agamous, Deficiens and SRF) transcription factors and includes four members, MEF2A, B, C and D. MEF2 factors alone are unable to activate satellite cells or to promote myogenesis, but they cooperate with other members of myogenic transcription factors such as MyoD to regulate muscle regeneration at late stages (Liu et al., 2014; Taylor and Hughes, 2017). Among MEF2 proteins, MEF2C plays an essential role during terminal differentiation and myotube maturation. MEF2C regulates the expression of late differentiation factors such as MRF4 to promote terminal differentiation and fusion (Moretti et al., 2016). MEF2C also promotes the expression of sarcomeric proteins, including the M-line-specific proteins Myomesin and M protein (Hinits and Hughes, 2007). Although involved in late differentiation, fusion and myotube maturation, MEF2C starts to be expressed in proliferating myoblasts (Liu et al., 2014; Mokalled et al., 2012). Therefore, a tight temporal control of MEF2C is necessary to suppress its transcriptional activity in proliferating myoblasts and to induce it differentiating cells.

Several mechanisms, involving transcriptional co-repressors and co-activators contribute to keep MEF2C inactive during proliferation and active in the differentiation phase. For example, GRIP-1 and CARM1 (coactivator-associated arginine methyltransferase-1) directly interact with MEF2C during the differentiation phase and cooperatively activate MEF2C activity (Chen et al., 2002). In parallel, Class IIa histone deacetylases (HDACs) such as HDAC4 and HDAC5 are examples of transcriptional co-repressors which bind MEF2C during the proliferation phase to suppress untimely differentiation during myogenesis (Thébault et al., 2001). However, these mechanisms seem not to be sufficient to timely control the activity of MEF2C during adult myogenesis, in particular at the transition between myoblast proliferation and

differentiation. Interestingly, our group has reported that nTRIP6, the nuclear isoform of the LIM domain protein TRIP6, acts as a co-repressor for MEF2C in the nucleus of myoblasts (Kemler et al., 2016).

1.2.2 The LIM domain-containing protein TRIP6 and its nuclear isoform nTRIP6

The LIM domain, first identified in the Lin-11, Isl-1 and Mec-3 homeodomain transcription factors, is 50-60 amino acids in size with highly conserved cysteine-rich structures consisting of a double zinc finger motif which are linked with two amino acids (Karlsson et al., 1990). The structures containing zinc fingers are typically organized to bind DNA but LIM domain mediate protein-protein interactions. LIM domain proteins usually harbour several LIM domains and act as adaptor molecule which recruit and interact with various proteins to regulate several fundamental cellular processes (Aoyagi and Archer, 2008; Dawid et al., 1998; Karlsson et al., 1990).

LIM domain proteins are classified based on the arrangement and position of LIM domains (Zheng and Zhao, 2007). One particularly interesting class of LIM domain proteins belong to the ZYXIN and PAXILLIN families. These proteins are enriched in the cytosol at focal adhesion (FA) plaques and cell-cell contacts, where they regulate cytoskeletal dynamics, signal transduction, cell adhesion and migration (Smith et al., 2014). However, most of these so-called focal adhesion LIM domain proteins have been shown to also regulate transcription in the nucleus, by shuttling between the cytoplasmic and nuclear compartments (Hervy et al., 2006; Wang and Gilmore, 2003).

TRIP6 (thyroid hormone receptor interacting protein 6) is a member of the ZYXIN family which harbours three LIM domains in its C-terminal region. It is located in the cytoplasm because of a functional proline-rich nuclear export signal (NES) within the N-terminal pre-LIM region (Fig. 2). Like the other Zyxin family members, TRIP6 is detected mostly at focal adhesion plaques and cell-cell contacts, where it acts as an adaptor protein for a broad range of proteins involved in cell adhesion, migration and actin cytoskeletal rearrangement (Lin and Lin, 2011; Wang et al., 1999). It also regulates transcription in the nucleus. Thus, like the other members of the ZYXIN family, TRIP6 has been hypothesized to shuttle between the cytoplasm and the nucleus (Hervy et al., 2006; Wang and Gilmore, 2003). However, our group has

demonstrated that TRIP6 is not shuttling, but that its transcriptional regulatory functions are mediated by a shorter isoform which is exclusively expressed in nucleus; therefore, our group named this nuclear isoform nTRIP6 (Kassel et al., 2004).

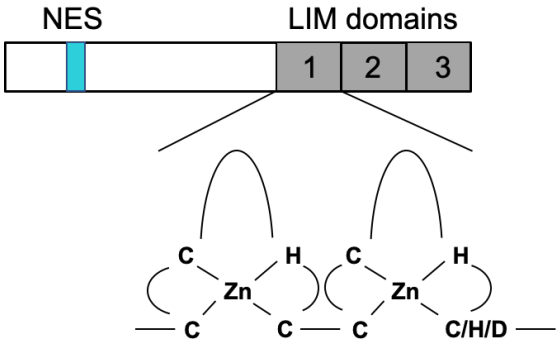

Figure 2- Schematic representation of the LIM domain protein TRIP6. TRIP6 contains three C-terminal LIM domains, each consisting of two zinc-fingers. A nuclear export signal (NES) is located within the N-terminal half.

Unpublished results of the group have shown that TRIP6 and nTRIP6 are generated from the same mRNA by an alternative translation mechanism. The mRNA contains two in frame AUG initiation codons. The first AUG codon is responsible to initiate the translation of TRIP6. However, AUG1 is not in a perfect Kozak sequence which leads to leaky ribosomal scanning. Thereby, during the scanning phase of translation initiation, some small ribosomal subunits skip this AUG and continue to scan until they reach the second AUG (AUG2) in an appropriate Kozak context to start translation. AUG (AUG2) is located in the middle of the NES encoding sequence. Therefore, initiation at this AUG leads to the translation of a shorter protein with a truncated, non-functional NES, which is therefore localised in the nucleus (Fig. 3).

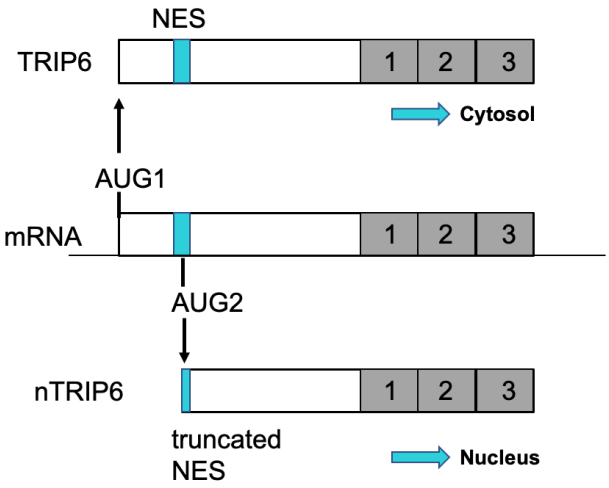

Figure 3- Schematic representation of the alternative translation of *Trip6* mRNA. Translation initiation at the first AUG produces the TRIP6 protein, which harbours a nuclear export signal (NES) and is therefore expressed in the cytosol. Translation initiation at the second AUG located within the NES-encoding sequence, produces nTRIP6, which is shorter in size and harbours a truncated, non-functional NES and is therefore in the nucleus.

nTRIP6 still harbours the three C- terminal LIM domains as well as two protein-protein interaction motifs in its N-terminal pre-LIM region (Kassel et al., 2004). A short peptide has been developed that blocks the interaction of other proteins with these domains (Diefenbacher et al., 2008, 2010; Kassel et al., 2004). In the nucleus, nTRIP6 interacts with various transcription factors such as AP-1, NF-κB and the glucocorticoid receptor (GR) and increases their transcriptional activity via the recruitment of other transcriptional co-activators such as THRAP3 to the transcription factor-bound promoters of target genes (Diefenbacher et al., 2014). Surprisingly, our group has recently reported that nTRIP6 acts as a co-repressor for MEF2C in myoblasts. nTRIP6 exerts this co-repressor function by interacting with MEF2C via its N-terminal pre-LIM region. At the MEF2C-bound regulatory region of target genes, nTRIP6 mediates the recruitment of HDAC5 to repress transcription (Kemler et al., 2016). This co-repressor function for MEF2C raises the hypothesis of a role for nTRIP6 in the regulation of myogenesis.

1.3 Control of muscle size

Skeletal muscle mass is determined mostly by the size of myofibres (Rennie et al., 2004). Thus, alteration in muscle size occurs largely from the growth or shrinkage of

pre-existing myofibres rather than an increase or decrease in cell number, hyperplasia or hypoplasia respectively (Goodman et al., 2011). Single myofibres consist of approximately 80% of structural and functional proteins. The loss or dysfunction of one of these proteins results in the reduction in myofibre size and muscle atrophy (Bonaldo and Sandri, 2013), while the increase in protein synthesis leads to muscle hypertrophy (Marcotte et al., 2015). Hence myofibre size depends on the balance between the rates of protein synthesis and degradation (Goldberg, 1969; Rennie et al., 2004). More specifically, myofibre size in both muscle hypertrophy and atrophy is controlled by several factors and signalling pathways that regulate gene expression on the transcriptional and translational level or interfere with protein degradation and autophagy (Sandri, 2008).

The main signaling pathway which acts as a positive regulator of muscle growth is the insulin-like growth factor 1 (IGF1)/phosphoinositide-3-kinase (PI3K)/Akt-protein kinase B (PKB)/mechanistic target of rapamycin (mTOR) pathway (Schiaffino and Mammucari, 2011). The mTOR pathway is central to the regulation of muscle size, as most of the atrophy-inducing signals also converge to suppress mTOR activity (Lee, 2004; Sandri, 2008; Schiaffino et al., 2013). Therefore, muscle mass is ultimately regulated by the activity of mTOR signalling, a key modulator of protein synthesis (You et al., 2015).

1.3.1 The mechanistic target of rapamycin (mTOR)

The mechanistic (originally mammalian) target of rapamycin (mTOR) is a Serine/Threonine kinase which is conserved throughout evolution. The mTOR pathway regulates a broad range of cellular processes including cell metabolism, growth, differentiation, migration and development in response to intra- and extracellular signals such as the availability of nutrients, growth factors, hormones, oxygen and mechanical loading (physical activity) (Liu and Sabatini, 2020). Dysregulation of mTOR, in response to stress, nutritional modification or hypoxia (Hoppeler et al., 2008), disturbs cellular homeostasis and leads to many diseases such as cancers, metabolic, autoimmune and age-related diseases (Kou et al., 2019; Perl, 2015).

mTOR is the catalytic subunit of two structurally and functionally distinct complexes known as mTOR complex 1 (mTORC1) and mTORC2. These complexes are identified by their protein composition, their distinctive substrates and signalling roles in the cell, as well as different sensitivity to the chemical inhibitor rapamycin (Jhanwar-Uniyal et al., 2019).

mTORC1 (Fig. 4A) is composed of mTOR and two other core components, mammalian lethal with Sec13 protein 8 (mLST8, also known as GβL) and the scaffold regulatory associated protein of mTOR (RAPTOR). mLST8 acts as a stabilizer of the kinase activation loop, although mice lacking mLST8 do not show effects on mTORC1 kinase activity. RAPTOR acts as a bridge between mTORC1 and its substrates (Kim et al., 2002, 2003). It has been reported that ablation of RAPTOR leads to an early lethality during mice embryo development (Guertin et al., 2006). In general, RAPTOR is essential for regulating mTORC1 activity and its proper subcellular localisation (Sancak et al., 2008). In addition to the core components mTORC1 comprises also two inhibitory components, proline rich AKT substrate 40 kDa (PRAS40) and DEP domain containing mTOR interacting protein (DEPTOR) which interacts with RAPTOR (Wang et al., 2007). Rapamycin, which gave its name to mTOR, is a chemical inhibitor, that inhibits mTORC1 activity through binding to the small cytosolic FK506-binding protein of 12 kDa (FKBP12) and interacts with the binding domain (FRB) of mTOR (Yin Zheng, 2018). mTORC1 is responsible for the regulation of cell growth and metabolism by promoting various processes such as biosynthesis of proteins (Hara et al., 1998), lipids (Peterson et al., 2011), nucleotides (Robitaille et al., 2013) and ATP (Thoreen et al., 2009), while preventing autophagic breakdown of cellular components (Chen et al., 2012).

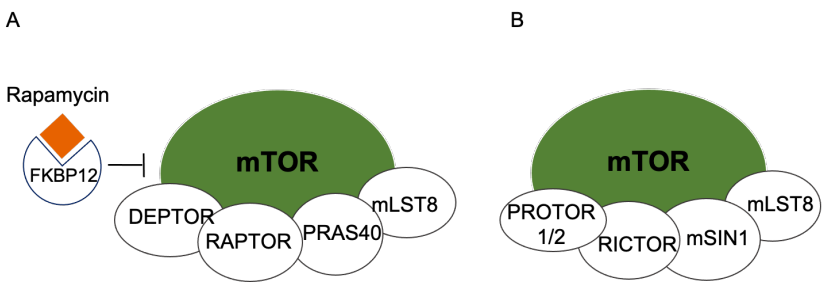

Figure 4- Schematic representation of mTOR Complexes 1 (mTORC1) and mTORC2. A) mTORC1 comprises mTOR, DEPTOR, RAPTOR, PRAS40 and mLST8 and is sensitive to rapamycin, while mTORC2 **(B)** comprises mTOR, DEPTOR, PROTOR1/2, RICTOR, mSin1 and mLST8 and is insensitive to rapamycin.

mTORC2 consists also of mTOR, mLST8 and DEPTOR (Fig. 4B). But instead of RAPTOR, mTORC2 is characterized by rapamycin insensitive companion of mTOR (RICTOR). RICTOR binds MAPK interacting protein 1 (mSIN1) and protein associated with RICTOR 1 or 2 (PROTOR 1/2) to assemble mTORC2 (Frias et al., 2006). Mice embryos lacking mLST8 and RICTOR show the same phenotype and die at the early stages of development, due to the essential role of mLST8 in interaction between RICTOR and mTOR. Thus, mLST8 and RICTOR are both required for mTORC2 signalling activity (Guertin et al., 2006). RICTOR blocks the FKBP12–rapamycin complex binding site on mTOR, thereby mTORC2 is not sensitive to acute rapamycin treatment. However, rapamycin can inhibit mTORC2 after prolonged treatment in some cell types by preventing mTOR component to nucleate new mTORC2 (Yin Zheng, 2018). Less is known about the function of mTORC2, however it has been shown that mTORC2 plays a key role in cell survival via phosphorylation and activation of several members of the AGC family of protein kinases, such as Akt, a key effector of PI3K signalling to promote metabolism and to suppress apoptosis (Sarbassov et al., 2005). mTORC2 also activates protein kinase C (PKC), a regulator of cytoskeleton remodelling and cell migration (Jacinto et al., 2004), and serum- and glucocorticoid-induced protein kinase (SGK1) a regulator of ion transport (García-Martínez and Alessi, 2008).

There is some evidence that mTORC1 and mTORC2 components such as mTOR, mLST8, RAPTOR, RICTOR and mSIN1 can be detected in both the cytoplasm and the nucleus but at significantly higher levels in the cytoplasm (Rosner and Hengstschläger, 2008). However, the function of these components in the nucleus is not clear.

1.3.2 mTORC1 activation

Numerous studies have focused more specifically on mTORC1 because of its critical role in regulating protein biosynthesis as the most resource-intensive process in growing cells and in promoting, for example, skeletal muscle hypertrophy (Marcotte et al., 2015). In order to regulate the function of mTORC1 in the regulation of muscle growth, both activation and inhibition of several signalling cascades are required

(Kobayashi et al., 2019). The Insulin like growth factor I (IGF-I)/Akt/mTORC1 pathway is thought to be one of the important regulatory mechanism (Glass, 2003). This pathway is mainly influenced by physical activity, nutrition, and various diseased conditions (Rommel et al., 2001). This signalling pathway indirectly activate mTORC1 via an upstream small G protein, RHEB (Ras homolog enriched in brain). The activation of mTORC1 by RHEB is illustrated in Fig. 5. RHEB is a member of the RAS super family of GTPase which predominantly localises at the surface of lysosomes (Parmar and Tamanoi, 2010; Sanders et al., 2019). The GDP-bound form of RHEB is inactive, RHEB is active in GTP-bound form. The active RHEB interacts with mTORC1 through its switch I/II region, relieves an inhibitory interaction between mTOR and a binding protein (FKBP38), consequently activating mTORC1 (Long et al., 2005). This process is further regulated by an upstream GTPase-activating protein (GAP), called tuberous sclerosis complex (TSC1/TSC2 heterodimer). TSC2 maintain RHEB in the GDP bound state, therefore prevents its ability to activate mTORC1 (Inoki, 2003). Upon stimulation, the TSC complex dissociates from RHEB through Akt-dependent phosphorylation, resulting in the accumulation of GTP-bound RHEB, which recruits mTORC1 to the surface of lysosomes. This recruitment induces the activation of mTORC1 via conformational changes which lead to the activation of the mTOR kinase domain (Blaauw et al., 2017; Li et al., 2004) (Fig. 5). Upon activation, mTORC1 directly phosphorylates PRAS40 and DEPTOR, which releases their inhibitory interaction with mTORC1 (Peterson et al., 2009). Several canonical downstream targets of mTORC1 contain a specific TOR signalling motif (TOS). RAPTOR may recognize TOS motif of mTORC1 substrates, interact with them and facilitate their phosphorylation (Nojima et al., 2003).

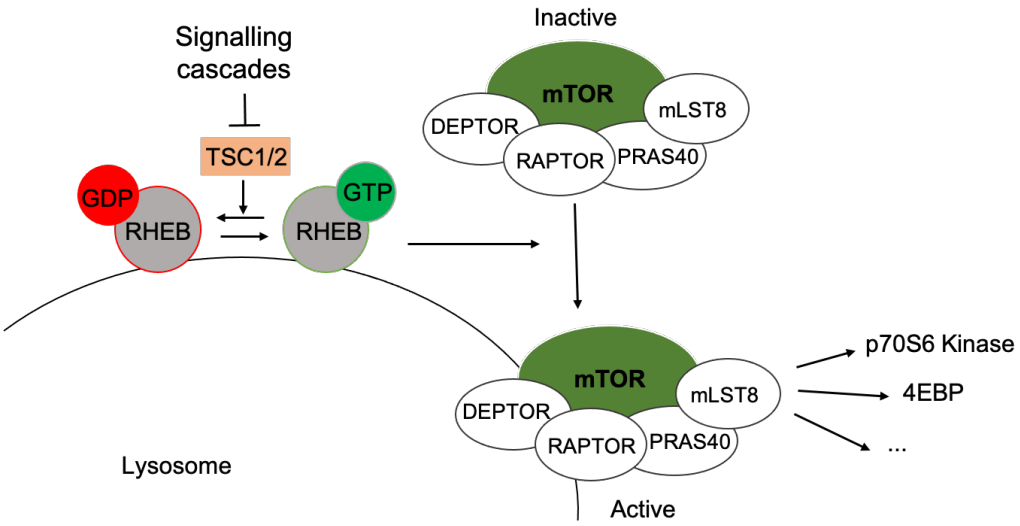

Figure 5- Schematic representation of mTORC1 activation. Upstream signals activate mTORC1 through signaling cascades which converge to inhibit the TSC1/2 complex, the inactive GDP-bound RHEB switch to the active form (GTP-bound), recruits mTORC1 on the surface of the lysosome, leading to its activation. Activated mTORC1 phosphorylates various downstream targets.

1.3.3 Molecular functions of mTORC1

To regulate the biosynthesis of proteins, which is highly required for the muscle fibre growth, mTORC1 phosphorylates the eukaryotic initiation factor 4E (eIF4E)- binding protein 1 (4E- BP1) and the p70 ribosomal S6 kinase 1 (S6K1). Phosphorylation of 4EBP promotes cap dependent translation through releasing its inhibitory interaction with eukaryote initiation factor E (eIF4E), which activates an essential eukaryote initiation factor complex (eIF4F). EIF4F complex is important to recruit small ribosomal subunit (40S) to promote cap-dependent translation initiation (Gingras et al., 1999). Activated mTORC1 also phosphorylates S6K1 which results in the degradation of translational machinery associated components including programmed cell death protein 4 (Pdcd4). Upon Pdcd4 degradation several substrates linked to translation initiation, such as eukaryote initiation factor 3 (eIF3) complex are released. EIF3 complex serves as a scaffold for mTOR and S6K1 and also interacts with eukaryote initiation factor 4B (eIF4B), a positive regulator of eIF4F complex to facilitate cap-dependent translation initiation (Dorrello et al., 2006; Harris et al., 2006). Phosphorylation of S6K1 is also proposed to activate the translation of a specific

subset of mRNAs. These mRNAs bear terminal oligopyrimidine (TOP) tracts at their 5' end encoding ribosomal components and translation elongation factors. However, the mechanism is still unclear (Pende et al., 2004).

Furthermore, it has been recently shown that mTORC1 contributes to the regulation of several steps of ribosome biogenesis. Beside stimulating the translation of ribosomal proteins and other proteins required for ribosome assembly, mTORC1 also stimulates the transcription of ribosomal RNAs (Fig. 6).

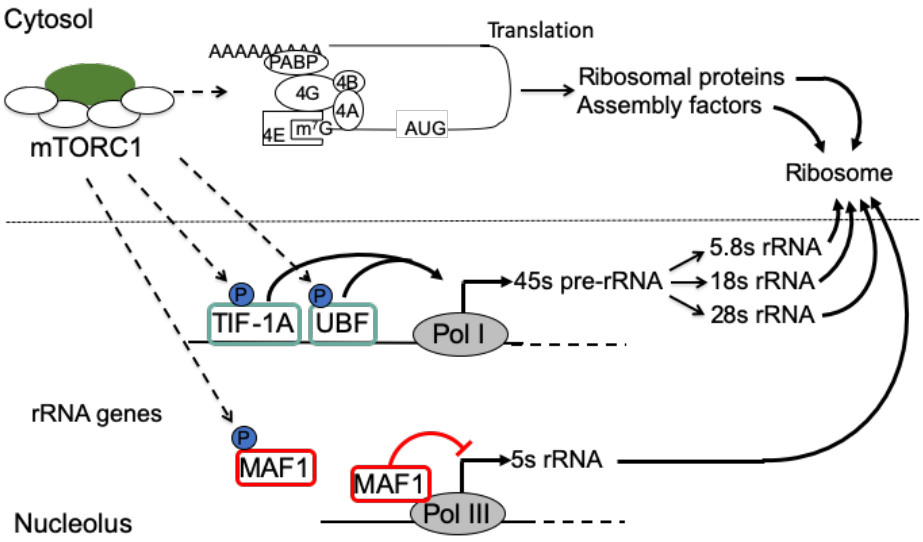

Figure 6- Effects of mTORC1 on ribosome biogenesis. Activation of mTORC1 in the cytosol promotes an increase in the translation of ribosomal proteins and ribosome assembly factors. mTORC1 induces the phosphorylation of the transcription factors TIF-1A and UBF in the nucleolus, which then activate RNA polymerase I (Pol I) to transcribe the precursor 45s ribosomal RNA (45s pre-rRNA), which is further processed into 5.8s, 18s and 28s rRNAs. mTORC1 also promotes the phosphorylation of the Pol III repressor MAF1, which leads to the activation of 5s rRNA transcription. These different effects of mTORC1 contribute together to an increase in ribosome biogenesis.

Ribosomes contain four rRNAs which are transcribed by two distinct RNA polymerases (Pol) I and III. RNA Pol I transcribes a precursor 45s rRNA that is further processed into 5.8s, 18s and 28s rRNAs (Mayer and Grummt, 2006). More specifically, the activation of S6K1 leads to the phosphorylation of the transcription intermediary factor 1(TIF-1A) and the carboxy terminal activation domain of the rDNA transcription upstream binding factor 1 (UBF), key regulators of rDNA transcription. The phosphorylated UBF-1 interacts with essential basal factor SL-1 and RNA Pol I in order to recruit them to rDNA promoter. Inhibition of mTORC1 by rapamycin results in a rapid dephosphorylation of UBF-1, leading to reduce its ability to promote rDNA

transcription (Panov et al., 2006). TIF-1A is essential for efficient transcription initiation by RNA Pol I, associated with the formation of the initiation-competent form of RNA Pol I (Mayer et al., 2004). TIF-1A plays a key role in muscle hypertrophy, mediating the upregulation of rRNA synthesis in response to extracellular stimulation such as physical activity (Fyfe et al., 2018). Interestingly, upon treatment with rapamycin, TIF-1A is not only phosphorylated at multiple site and inactivated but also translocated from the nucleolus to the cytoplasm and downregulates RNA Pol I transcription by sequestering various transcription factors (Mayer et al., 2004). Therefore, mTORC1 controls muscle growth through regulating TIF-IA in response to environmental stimuli or availability of nutrients and growth factors (Fyfe et al., 2018; Mayer and Grummt, 2006). In addition, mTORC1 increases the activity of RNA polymerase III which transcribes the 5s rRNA through the phosphorylation of MAF1, a key repressor of RNA polymerase III. Phosphorylation of MAF1 by mTOR promotes its dissociation from the Pol III complex and activation of 5s rRNA transcription (Michels et al., 2010).
It has been shown that Pol I-dependent rRNA synthesis in response to nutrient and growth factors is maintained even upon silencing of S6K1, however blocking mTORC1 with rapamycin prevents it (Mieulet et al., 2007; von Walden et al., 2016a). Therefore, phosphorylation S6K1 is not the only way that mTORC1 stimulates rRNA synthesis. In particular, mTOR is also localised in the nucleus and a helix-turn-helix motif has been found in mTOR, suggesting that it directly interacts with rDNA gene promoter in the nucleolus and regulate RNA pol I transcription of rDNA genes during myotube hypertrophy (Tsang et al., 2010; von Walden et al., 2016).

1.3.4 The mTORC1 activator RHEB

RHEB was originally identified as a gene whose expression is enriched in rat brain and upregulated in response to various stimuli to increase neuronal activity (Yamagata et al., 1994). RHEB is a small monomeric protein with a molecular weight of about 21KD (Mahoney et al., 2018), which is closely related to the small GTPases RAS, Rap, and Ral (Schöpel et al., 2017). RHEB is a highly conserved protein, from yeast to human, that consists of 184 amino acids. The N-terminal 169 amino acids encode the GTPase domain which contains 5 short stretches, the G1-G5 boxes that is followed by a short alpha helical linker known as the hypervariable region (Fig. 8). The G1 box is the binding site for guanine nucleotides. Binding of GDP or GTP leads to a

conformational change of the G2 box which is the effector region. The G3 box is the site for binding nucleotide-associated Mg^{2+} ion. The G4 box forms a hydrogen bond with the guanine ring, stabilizing the protein via an interaction with the G1 box. Finally, the G5 box residues form indirect links with the guanine nucleotide (Groenewoud M. 2013; Mizuki et al., 1996). The RHEB protein contains two switch regions (Switch I and Switch II) which are overlap with the G2 and G3 boxes, required for the recognition and interaction with GAPs and other effectors (Parmar and Tamanoi, 2010) (Fig.7). The switch I region is flexible and subjected to a conformational change when RHEB switches from the GTP to the GDP-bound form (Ma et al., 2008), while the switch II region keeps its configuration mainly unchanged (Long et al., 2007). Furthermore, RHEB switch I is essential to interact with FKBP38, the mTORC1 endogenous inhibitory protein, to sequester it and thereby to activate mTORC1 (Ma et al., 2008). The switch II region plays important role in GAP-stimulated GTP hydrolysis (Mazhab-Jafari et al., 2012). The last four C-terminal residues consist of a CAAX motif (in which "C" is cysteine, "A" is an aliphatic amino acid, and X is almost any amino acid), which is a signal for post-translational farnesylation (Parmar and Tamanoi, 2010). It has been reported that RHEB fanesylation plays an important role to promote the localisation of RHEB to membrane compartments such as the lysosome, Endoplasmic reticulum (ER) or Golgi (Buerger et al., 2006). However, a recent report showed that RHEB farnesylation is not necessary to activate mTORC1 (Ferguson and Angarola, 2020).

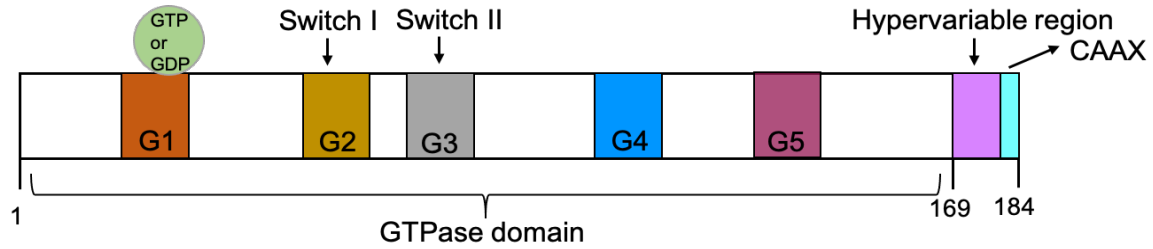

Figure 7- Schematic representation of RHEB structure. The N-terminal 169 amino acids constitute the GTPase domain and contains 5 short stretches, the G1-G5 boxes. G1 is essential for controlling the activaty of RHEB via binding GTP or GDP. Switch I and II regions are overlapping with G2 and G3 boxes. The last 15 amino acids are known as the hypervariable region. The last C-terminal residues are a CAAX motif for RHEB farnesylation. Modified from Groenewoud M. (2013).

To further characterize RHEB function, various mutants of RHEB have been created. For example, the switch II region has a highly conserved glutamine (Q64) which serves as a catalytic residue for GTP hydrolysis. Therefore, the RHEB Q64L mutant

(Fig. 8A) is constitutively bound to GTP and acts as a constitutively active mutant (Li et al., 2004; Long et al., 2005). The D60K mutation in the switch II region renders RHEB unable to bind either GTP or GDP (Fig. 8B). However, RHEB D60K binds strongly to FKBP38 on mTORC1 but does not displace it. Thereby, it competes with endogenous RHEB-GTP and inhibits mTORC1 activity, thus behaving as a dominant-negative mutant (Tabancay et al., 2003). Finally, the RHEB I39K mutant (Fig. 8C) harbours a mutation within the switch I region, which strongly reduces the ability of RHEB to interact with FKBP38 and to activate mTORC1(Ma et al., 2008).

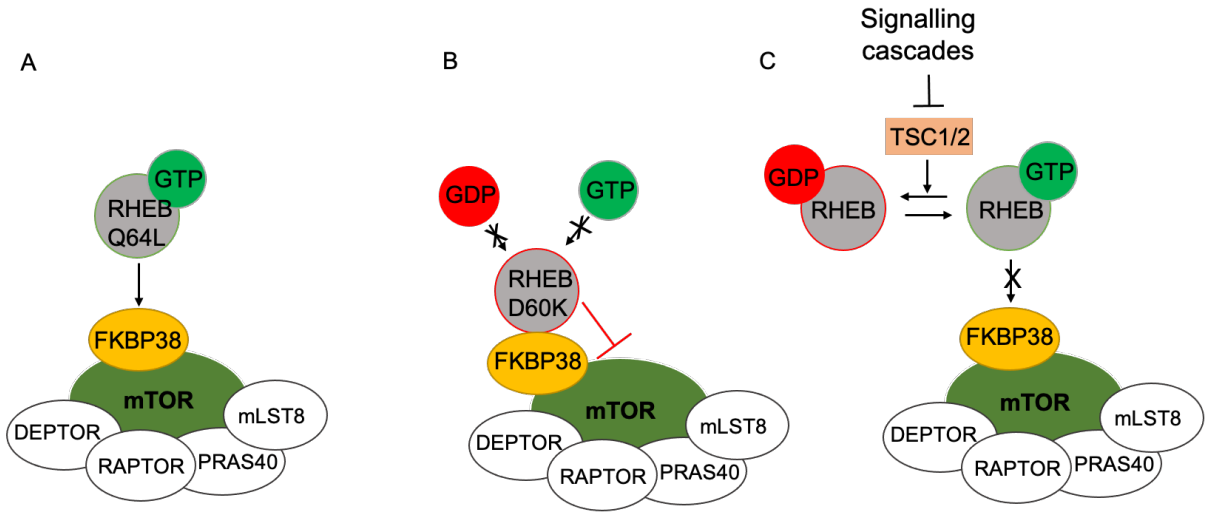

Figure 8- Schematic representation of RHEB mutants. **A)** RHEB-Q64L is constitutively bound to GTP, thus constantly activates mTORC1. **(B)** RHE- D60K is a dominant negative mutant which can bind neither GTP nor GDP, but still interacts with mTORC1 via FKBP38 and thus competes with endogenous RHEB-GTP. **(C)** RHEB I39K has a reduced ability to interact with FKBP38 and mTORC1.

While most studies focused on the lysosome as a most characterized site for RHEB to promote the canonical cytoplasmic activation of mTORC1, some evidence showed that RHEB can be detected also in the nucleus of several mammalian cell lines (Rosner and Hengstschläger, 2008). However, the functions of RHEB in the nucleus are unknown.

1.3.5 mTORC1-independent function of RHEB

Beside its effect on the mTORC1 pathway, RHEB has been shown to regulate other major signalling pathways, including the Notch (Karbowniczek et al., 2010) and the RAS-RAF-MEK signalling pathways (Karbowniczek et al., 2006). For example, it has been reported that in brown and beige adipose tissues, RHEB selectively activates Notch signalling. This activation promotes protein kinase A (PKA) signalling by repressing the binding of the regulatory subunit of PKA from its catalytic subunit. Thereby, RHEB selectively regulates thermogenic gene expression in an mTORC1-independent mechanism, thereby controls energy homeostasis (Meng et al., 2019). The other study using Drosophila sensory organ precursor (SOP) cell, a model of asymmetric cell division, suggests that RHEB regulates Notch signalling in an mTOR-independent manner to control SOP cell fate decision, which divides asymmetrically in a Notch-dependent manner. RHEB overexpression-mediated increase in the activity of Notch as well as asymmetric division in inhibited neither by rapamycin nor by downregulation of RAPTOR (Karbowniczek et al., 2010). In addition, overexpression of a farnesylation defective RHEB mutant induces elongation of axonal length via the phosphorylation of 4EBP even in presence of rapamycin. It indicated that nonfarnesylated RHEB can regulate axogenesis in an mTORC1-independent pathway (Choi et al., 2019). It has also shown that RHEB interferes with the MAPK pathway in an mTORC1-independent manner. RHEB interaction with B-Raf, which leads to the inhibition the heterodimerization of B-Raf and C-Raf, was insensitive to rapamycin. Therefore, RHEB suppresses the C-RAF kinase activity in a mTORC1-independent manner (Karbowniczek et al., 2006).

Thus, RHEB exerts several functions that are independent from its ability to activate mTORC1. However, whether RHEB in the nucleus can also exert mTORC1 independent functions has not been investigated.

1.3.6 Function of RHEB and mTORC1 in the control of muscle size

A direct link between mTORC1 interaction with RHEB and the regulation of protein synthesis and muscle mass has been reported (Baar and Esser, 1999; Marcotte et al., 2015; Song et al., 2017). The complex regulatory role of the mTORC1 pathway in

muscle fibre size has been intensively studied both *in vitro* and *in vivo* using different models. In these models, mTORC1 inhibitors such as rapamycin or various mutant of RHEB have been tested (Ogasawara et al., 2016). Collectively, all studies provide strong evidence that mTORC1 signalling is involved in muscle hypertrophy via modulating protein synthesis and ribosome biogenesis. More specifically, in addition to promoting an increase in the translation of multiple mRNAs in response to intra- and extracellular signals such as the availability of nutrients, growth factors or mechanical loading, mTORC1 promotes an increase in ribosome biogenesis which leads to an increase in the translation capacity of myofibres, consequently leading to an increase in protein synthesis and finally in myofibre size (Blaauw et al., 2017). As the direct activator of mTORC1, RHEB promotes muscle hypertrophy by increasing protein synthesis via an increase in both the translational efficiency (increased translation initiation) and translational capacity (increased ribosome biogenesis) (Long et al., 2005). Whether cytosolic or nuclear RHEB can induce muscle hypertrophy in an mTORC1-independent manner remains to be elucidated.

1.4 Hypotheses and aims

1.4.1 Muscle regeneration

The multistep process of muscle regeneration is tightly regulated by transcription factors which can exert different functions depending on the stage of adult myogenesis. Therefore, the temporal control of the activity of these transcription factors is critical to ensure the timely expression of their target genes (Bentzinger et al., 2012). The observation that nTRIP6 acts as a co-repressor for the transcription factor MEF2C in myoblast raised the hypothesis that nTRIP6 might have a role in the temporal control of myogenesis (Kemler et al., 2016). Therefore, the aim of the first part of my thesis was to investigate the possible role of nTRIP6 in regulating myogenesis *in vitro* and skeletal muscle regeneration *in vivo* in the mouse.

1.4.2 Muscle growth

The canonical mTORC1 pathway, which is activated in the cytosol by RHEB, is known to promote myofibre growth. However, RHEB is also present in the nucleus of various

cell types (Yadav et al., 2013). In the second part of my thesis, I investigated whether RHEB is present in the nucleus of myofibres, how it localises there as well as whether and how it regulates muscle growth, *in vivo* in Zebrafish embryos.

2. Materials and Methods

2.1 Materials

2.1.1 Consumables

All cell culture consumables, unless otherwise stated, were obtained from Greiner Bio-One, Frickenhausen, Germany.

2.1.2 Chemicals

Chemicals	**Company**
Collagen I (rat tail)	Corning
Collagenase	Sigma
Notexin	Latoxan
Lonafarnib	Sigma
Tamoxifen 99%	Sigma
Rapamycin	Sigma
PeqGOLD TriFast™	Peqlab Biotechnologie
Phenol red	Sigma
PTU (N-Phenylthioure)	Sigma
Tricaine (Ethyl 3-aminobenzoate methanesulfonate salt)	Sigma

All other chemicals if not stated otherwise were purchased from Carl Roth GmbH&Co, Karlsruhe, Germany; Gibco BRL, Eggenstein, Germany or Sigma, Deisenhofen, Germany.

2.1.3 Kits

Kits	Company
Amaxa Nucleofection V	Corning
Amersham ECL Prime	GE Healthcare
GeneJet Gel Extraction	Thermo Fischer
In-Fusion HD cloning Kit	Clonetech
Nano-Glo Luciferase Assay	Promega
Nuclear extract kit	Active Motif
PeqGold Xchange Plasmid Midi Kit	Promega
QUIAGEN Maxi Plasmid Kit	Quiagen
QuikChange Site-Directed Mutagenesis Kit	Stratagene
TransIT X2	Mirus

2.1.4 Hardware

Device	Company
Cell incubator	Hereus
Chemidoc X Touch Imaging System	Biorad
Femtojet	Eppendorf
LSM 800	Zeiss
Leica SP8 STED	Leica
Micropipet puller	Sutter Instruments
PeQstar PCR	VWR
Step one plus Real-time PCR system	Applied Biosystem
Trans blot turbo midi size	Biorad

2.1.5 Enzymes

All enzymes and their corresponding buffers, if not otherwise stated, were purchased from NEB or Promega.

2.1.6 Antibodies

2.1.6.1 Primary Antibodies

Name	Isotype	Dilution	Company (ordernumber)
α-mCherry	Rabbit	1:2000 (WB) 1:1000 (IF)	Abcam (167453)
glucocorticoid receptor (GR)	Rabbit	1:1000	Santa Cruz (sc1002)
α-HDAC II	Rabbit	1:1000	Santa Cruz (sc7899)
α-Laminin	Rat	1:5000	Abcam (ab11576)
α-MyoD	Rabbit	1:100	ThermoFischer (PA5-23078)
α-myHC (MYH3)	Mouse	1:100	DSHB (F1.652)
α-TRIP66/nTRIP6	Rabbit	1:100	Self made
Ki67	Rabbit	1:100	Cell signaling (12075)
RHEB	Rabbit	1:50	Abcam (ab25873)
mTOR	Rabbit	1:50	GeneTex (GTX124771)
α- Tubulin	Mouse	1:1000	Santa Cruz (sc8035)
Fibrillarin	Mouse	1:1000	Novus Biology (NB300-269)

2.1.6.2 Secondary Antibodies

Name	Isotype	Dilution	Company (ordernumber)
Alexa Fluor 488-conjugated anti-rabbit	Goat	1:1000	ThermoFischer (A-11059)
Alexa Fluor 546-conjugated anti-rat	Goat	1:1000	ThermoFischer (A-11081)
Alexa Fluor 546-conjugated anti-mouse	Goat	1:1000	ThermoFischer (A-11030)

Alexa Fluor 633-conjugated anti-mouse	Rabbit	1:1000	ThermoFischer (A-21063)
α-mouse- HRP	Goat	1:2000	DAKO (P0260)
α-rabbit-HRP	Goat	1:2000	DAKO P0448
α-rat-HRP	Goat	1:2000	DAKO P0450

2.1.7 Buffers

2.1.7.1 General buffers

RIPA	50mM Tris pH 7.5, 150mM NaCl, 1% NP-40; 0.5% NaDoc, 0.5% SDS
TAE	40 mM Tris acetate, 1mM EDTA (pH 8,2-8,4)

2.1.7.2 Protein measurement according to Lowry

Lowry I	20g/L Na_2CO_3, 4g/L NaOH in ddH_2O
Lowry II	1% $CuSO_4$
Lowry III	2% NaK Tartrat
Lowry IV (freshly mixed)	volume 100 Lowry I, volume 1 Lowry II, volume 1 Lowry III
1:1 Folin reagent (freshly mixed)	in ddH_2O

2.1.7.3 SDS- PAGE and Western Blot buffers

Separating gel	10% Acrylamid:Bisacrylamid, 375mM TrisHCL (pH 8.8), 0.1% SDS, 0.1% APS, 0.04% TEMED
Stacking gel	5 % Acrylamid:Bisacrylamid, 1 M Tris-HCL (pH 6.8), 10 % SDS, 10% APS, 0.1% TEMED

Electrophoresis buffer	25 mM Tris, 192mM Glycin, 0.1 % SDS
2x Sample buffer	125 mM tris-HCl (pH 6.8), 4 % SDS, 20 % glycerol, 0.01 % bromphenol blue, 2% 2-mercaptoethanol
TBST buffer	20 mM tris, 150 mM NaCl, pH 7.6; 0.05 % TWEEN 20
Transfer buffer	Trans-Blot Turbo 5x, 100% ethanol in ddH_20
Blocking buffer	5% skimmed milk powder in TBST 5% BSA in TBST

2.1.7.4 Luciferase Buffers

Buffer	**Content**
GlyGly buffer	25 mM Glycylglycine, 15 mM $MgSO_4$, 4 mM EGTA, pH 7.8
Reaction buffer	2 mM ATP, 1 mM DTT in GlyGly buffer
Substrate	0.2 mM FireFly substrate in GlyGly buffer

2.1.7.5 Immunofluorescence staining

Fixation Buffer	2% Parafomaldehyde in PBS -/- pH 7.2
Permeabilization buffer	0.5% Triton X-100 in PBS -/-
Blocking buffer	5% BSA in PBS -/- pH 7.2

2.1.8 Cell lines and cell culture medium

2.1.8.1 Cell lines

C2C12	Mus musculus muscle myoblast cells (ECACC No.: 91031101)
PAC2	Zebrafish embryonic fibroblast cell line

2.1.8.2 Cell culture medium

C2C12	Growth medium: Dulbecco's Modified Eagle Medium (DMEM) + 10% Fetal calf serum Differentiation medium: Dulbecco's Modified Eagle Medium (DMEM) + 2% Horse serum
PAC2	L-15 (Leibovitz-15) medium + 20% Fetal calf serum + 100 units/ml penicillin, 100 µg/ml streptomycin and 50µg/ml gentamicin
Starvation medium	Dulbecco's Modified Eagle Medium (DMEM) + 0,1% Fetal calf serum

2.1.9 Zebrafish strains and fish medium

2.1.9.1 Zebrafish strain

The wild-type zebrafish strain AB-B-KA were obtained from the KIT fish facility.

2.1.9.2 Fish medium

E3 medium (60x)	17.2 g NaCl, 0.76 g KCL, 2.6 g $CaCl_2.2H_2O$, 4.9 g $MgSo_4.7H_2O$ in dd H_2O
PTU (100x)	0.3% dissolved in dd H_2O
Anaesthetizing buffer	400 mg Tricaine, 2.1 ml 1M Tris pH 9 in ddH_2O. (final pH 7)

2.1.10 Bacterial strains and growth media

2.1.10.1 Bacterial strains

DH5α chemically competent *E.coli* cells

2.1.10.2 Growth media

Luria Both (LB):

Yeast extract	10 g/l
NaCl	5 g/l
Tryptone	5 g/l

pH 7.5

2.1.11 Plasmids

pminitol2	Empty vector contains Tol2 transposon with mini ITRs
tol2pUnc45MCSpA	a multiple cloning site (MCS) as well as a poly-adenylation signal of SV40, under a muscle specific promoter (pUnc45) was synthesised as a DNA string (GeneArt Strings DNA Fragments, ThermoFisher) and cloned to plasmid pminiTol2 (infusion cloning, see 2.2.7.10, using string DNA).
tol2pUnc45MCSLinker- mCherrypA	a flexible linker (3xGGS) as well as a cherry-red fluorescent protein (mCherry) was cloned in the MCS of the above described vector, under the control of a muscle specific promoter (pUnc45).
tol2pUnc45-hRHEBD60k- mCherry	A dominant negative RHEB mutant, RHEBD60K, was synthesised as a DNA string (GeneArt Strings DNA Fragments, ThermoFisher) and cloned C-terminally to the mCherry under the control of a muscle specific promoter (pUnc45).

tol2pUnc45-hRHEBQ64L- mCherry	A constitutively active RHEB mutant, RHEBQ64L, was synthesised as a DNA string (GeneArt Strings DNA Fragments, ThermoFisher) and cloned C-terminally to the mCherry under the control of a muscle specific promoter (pUnc45).
tol2pUnc45- mCherry- NLS	a functional Nuclear Localisation Signal (NLS) sequence was introduced N-terminally to the mCherry under the control of a muscle specific promoter (pUnc45)
tol2pUnc45-hRHEBQ64L- mCherry-NLS	a functional Nuclear Localisation Signal (NLS) sequence was introduced N-terminally to the mCherry tagged RHEB mutant Q64L under the control of a muscle specific promoter (pUnc45)
tol2pUnc45-hRHEBD60K- mCherry-NLS	a functional Nuclear Localisation Signal (NLS) sequence was introduced N-terminally to the mCherry tagged RHEB mutant D60K under the control of a muscle specific promoter (pUnc45)
tol2pUnc45-mCherry-NLS-T2A-eGFP	An eGFP fluorescent protein was introduced N-terminally to a nuclear targeted mCherry protein with a self-cleaving peptide (T2A) under the control of a muscle specific promoter (pUnc45) (PCR cloning see 2.2.7.6)
tol2pUnc45-hRHEBD60K-mCherry-NLS-T2A-eGFP	An eGFP fluorescent protein was introduced N-terminally to the mCherry tagged nuclear targeted RHEB mutant D60K with a self-cleaving peptide (T2A) under the control of a muscle specific promoter (pUnc45) (PCR cloning see 2.2.7.6)

tol2pUnc45-hRHEBQ64L-mCherry-NLS-T2A-eGFP	An eGFP fluorescent protein was introduced N-terminally to the mCherry tagged nuclear targeted RHEB mutant Q64L with a self-cleaving peptide (T2A) under the control of a muscle specific promoter (pUnc45) (PCR cloning, see 2.2.7.6)
tol2pUnc45- mCherry-NES	a functional Nuclear Export Signal (NES) sequence was introduced N-terminally to mCherry under the control of a muscle specific promoter (pUnc45) (PCR cloning, see 2.2.7.6)
tol2pUnc45-hRHEBD60K-mCherry-NES	a functional Nuclear Export Signal (NES) sequence was fused N-terminally to the mCherry tagged RHEB mutant D60K under the control of a muscle specific promoter (pUnc45) (infusion cloning, see 2.2.7.10, using oligos)
tol2pUnc45- hRHEBQ64L-mCherry-NES	a functional Nuclear Export Signal (NES) sequence was fused N-terminally to the mCherry tagged RHEB mutant D60K under the control of a muscle specific promoter (pUnc45) (infusion cloning, see 2.2.7.10, using oligos)
tol2pUnc45- mCherry-NES-T2A-eGFP	An eGFP fluorescent protein was introduced N-terminally to the mCherry with a self-cleaving peptide (T2A) under the control of a muscle specific promoter (pUnc45)

tol2pUnc45-hRHEBD60K-mCherry-NES-T2A-eGFP	An eGFP fluorescent protein was introduced N-terminally to the the mCherry tagged cytoplasmic RHEB mutant D60K with a self-cleaving peptide (T2A) under the control of a muscle specific promoter (pUnc45) (PCR cloning, see 2.2.7.6)
tol2pUnc45-hRHEBQ64L-mCherry-NES-T2A-eGFP	An eGFP fluorescent protein was introduced N-terminally to the mCherry tagged cytoplasmic RHEBD60K mutant with a self-cleaving peptide (T2A) under the control of a muscle specific promoter (pUnc45) (PCR cloning, see 2.2.7.6)
tol2pUnc45-hRHEBI39KQ64L-mCherry	A point mutation was conducted in the RHEB to mutate Isoleucine to Lysine using side directed mutagenesis (see 2.2.7.11)
tol2Unc45b-hRHEBI39Q64L-mCherry-NLS-T2A-eGFP	
tol2pUnc45-hRHEBI39KQ64L-mCherry- NES- T2A- eGFP	
tol2pUnc45-hRHEBI39KD60K-mCherry	
tol2Unc45b-hRHEBI39Q64L-mCherry-NLS-T2A-eGFP	
tol2pUnc45-hRHEBI39KD60K-mCherry- NES- T2A- eGFP	
pcDNA3.1(+)	Empty vector, basic mammalian expression cloning vector
pcDNA3.1(+)-hRHEBQ64L- mCherry	RHEB mutant Q64L was fused c-terminally to cherry-red fluorescent protein, under the control of a CMV promoter.
pcDNA3.1(+)-hRHEBD60K-mCherry	RHEB mutant D60K was fused c-terminally to cherry-red fluorescent protein, under the control of a CMV promoter.

pcDNA3.1(+) - mCherry- NES	The cDNA of a functional Nuclear Export Signal (NES) sequence was fused to the mcherry, under the control of a CMV promoter (provided by Markus Diefenbacher, ITG, KIT).
pcDNA3.1(+)-hRHEBD60K-mCherry-NES	a functional Nuclear Export Signal (NES) sequence was cloned N-terminally to the mCherry tagged RHEB mutant D60K under the control of a CMV promoter.
pcDNA3.1(+) - HA- mCherry- NLS	The cDNA of a functional Nuclear Localisation Signal (NLS) sequence was fused to the mCherry under the control of a CMV promoter (provided by Margarethe Litfin, IBCS, BIP, KIT).
pcDNA3.1(+) - hRHEBD60K- mCherry-NLS	a functional Nuclear Localisation Signal (NLS) sequence was introduced N-terminally to the mCherry tagged RHEB mutant D60K under the control of a CMV promoter.
pcDNA3.1 (+)- hRHEBQ64L- mCherry-NLS	a functional Nuclear Localisation Signal (NLS) sequence was introduced N-terminally to the mCherry tagged RHEB mutant Q64L under the control of a CMV promoter.
pcDNA3.1(+)- hRHEBI39KD60K-mCherry- NLS-T2A-eGFP **pcDNA3.1(+)- hRHEBI39KD60K-mCherry** **pcDNA3.1(+)- hRHEBI39KD60K-mCherry- NES- T2A- eGFP** **pcDNA3.1(+) - hRHEBI39KQ64L-mCherry- NLS-T2A-eGFP**	A point mutation was conducted in the RHEB to mutate Isoleucine to Lysine using side directed mutagenesis (see 2.2.7.11)

pcDNA3.1 (+) -hRHEBI39KQ64L-mCherry **pcDNA3.1 (+) -hRHEBI39KQ64L-mCherry- NES- T2A- eGFP**	A point mutation was conducted in the RHEB to mutate Isoleucine to Lysine using side directed mutagenesis (see 2.2.7.11)
pcDNA3.1 (+)- mCherryNLS- BP	Corresponds to the interaction domain 1 (ID1) of nTRIP6 (Diefenbacher et al., 2014; Kemler et al., 2016).
pcDNA3.1 (+)- mCherryNLS- cBP	Corresponds to the scrambled interaction domain 1 (ID1) of nTRIP6 (Diefenbacher et al., 2014; Kemler et al., 2016).
pcDNA3.1 (+)- YPET-IRES-Firefly	A Hoxa9b IRES sequence introduced to FireFly luciferase reporter under the control of CMV promopter.
PNL-1-1-ZFrRNA-Nluc (Nanoluc Zebrafish ribosomal RNA (pol1) reporter)	This construct was originally designed for measurements in vivo in zebrafish. It thus consists of a zebrafish rDNA promoter and terminator, which is transcribed by RNA pol1. However, in order to quantitate the transcription, the luciferase reporter gene (NanoLuc) coding sequence was introduced an Internal Ribosome Entry Site (IRES) before the NanoLuc coding sequence and a polyadenylation signal after.In a multi-step PCR cloning (see 2.2.7.6), the zebrafish rDNA terminator and promoter was fused to PNL1.1-NanoLuc vector, then an EMCV IRES sequence as well as a poly-adenylation signal of SV40 was C-terminally and N-terminally, respectively, introduced to NanoLuc coding sequence.

2.1.12 Primers

2.1.12.1 Genotyping

	Sequences 5’ to 3’
Trip6 $^{flox/flox}$	
mTrip6-28 For	TCACCTTTTCTCCCTTGCCTGCCTG
mTrip6-29 Rev	GGTACCCCCGGAGGCTGATAACAG
Pax7 $^{CRE\ ERT2}$	
gtPax7CreERT2 for	GCTGCTGTTGATTACCTGCC
gtPax7CreERT2m Rev	CTGCACTGAGACAGGACCG
gtPax7CreERT2wt Rev	CAAAAGACGGCAATATGGTG

2.1.12.2 Real-time PCR

Gene name	Forward primer (5’ to 3’)	Reverse primer (5’ to 3’)
Myog	GAGACATCCCCCTATTTCTACCA	GCTCAGTCCGCTCATAGCC
Rplp0	GGACCCGAGAAGACCTCCTT	GCACATCACTCAGAATTTCAATGG
Tnni2	CATGGAGGTGAAGGTGCAGA	CTCTTGAACTTGCCCCTCAGG

2.2 Methods

2.2.1 Animals and animal handling

2.2.1.1 Mouse methods

Experiments were performed on C57/BL6 mice. Use and care of the animals was approved by German authorities (Tierschutzkommission of the Regierungspräsidium Karlsruhe, licenses G-232/11 and G261/15) according to national law (TierSchG §7).

2.2.1.1.2 *Trip6* conditional knockout mouse (Cre/LoxP System)

To knock out *Trip6* conditionally in satellite cells, *TRIP6* floxed line mice, *Trip6*$^{fl/fl}$ (Shukla et al., 2019), were crossed with C57BL/6J-*Pax7*$^{tm1(Cre-ERT2)Gaka}$ mice, *Pax7*$^{Cre-ERT2}$ (Murphy et al., 2011). In *Trip6*$^{fl/fl}$ mice, *Trip6* is conditionally targeted by flanking exons 2 to 9 by loxP sites. In *Pax7*$^{Cre-ERT2}$ the tamoxifen-inducible version of Cre-recombinase (Cre-ERT2) is expressed only in satellite cells. In this version of Cre-Recombinase the T2 mutation in the ligand binding domain of the Estrogen Receptor (ER) renders the receptor unable to bind endogenous Estrogen but still to Tamoxifen which acts as an agonist. After treatment of *Trip6*$^{fl/fl}$; *Pax7*$^{Cre-ERT2/wt}$ offspring with Tamoxifen, the fusion protein shuttles to the nucleus, recognizes loxP sites and finally deletes the *Trip6* gene in satellite cells.

2.2.1.1.2.3 Genotyping

Trip6$^{fl/fl}$; *Pax7*$^{Cre-ERT2/wt}$ offspring were identified by PCR genotyping on tail DNA. Mice tails were digested in 200µl NID-buffer + 2µl (10mg/ml) Proteinase K at 55°C for overnight. Next day Proteinase K reaction was heat inactivated at 95°C for 30 min. Digested tails were then centrifuged at 13000rpm at 4°C for 15min. Genotyping was performed via PCR using the primers which are described in 2.1.12.1.

	Trip6 $^{flox/flox}$	**Pax7-Cre-ERT2**	**PCR program**	
5x Buffer	10µl	10µl	95°C	5 min
10mM dNTP	1µl	1µl	95°C	1 min
10µM Primer	2µl	2µl	71°C	1 min
Taq Polymerase	0.25µl	0.25µl	72°C	1 min
DNA	4µl	4µl	35-40 cycles	
Total volume	50µl	50µl	72°C	10 min

2.2.1.1.4 Treatment with Tamoxifen

To selectively knock out *Trip6* in satellite cells, Mice were injected intraperitoneally on 5 consecutive days with Tamoxifen (10mg/ml stock) diluted in peanut oil at a concentration of 5µl/g body weight.

2.2.1.1.5 Degeneration of Mice *M soleus*

Three days after the last injection, soleus muscle degeneration was induced by Notexin injection as described (Danieli-Betto et al., 2010). Briefly, animals were anesthetized by an intraperitoneal injection of Ketamin (100 mg/kg body weight) and Xylasin (16 mg/kg body weight). Notexin (10 µl of a 5 ng/µl solution in PBS-/-) was injected unilaterally in the soleus muscle exposed through a small cutaneous incision. Animals were sacrificed by cervical dislocation 7, 14, 28 and 45 days post- injury (dpi) and both the regenerating and contralateral soleus muscles were dissected.

2.2.2.2 Fish methods

2.2.2.2.1 Ethics statement

Zebrafish (Danio rerio) husbandry work was performed in accordance with the German Animal Welfare Act and was approved by the Regierungspräsidium Karlsruhe, Germany. A permit for experimental procedures or euthanasia was not required since no such procedures were carried out later than 5 days post fertilization (dpf).

2.2.2.2.2 Fish husbandry

Adult zebrafish were kept in tanks (50 fish per tank) with a water recirculation system at 28.5°C on a 14 hr/10 hr light-dark cycle. Adults were fed twice daily with commercial dry food and in-house hatched brine shrimp (live food).

2.2.2.2.3 Breeding

For pairwise breeding, small cages with divider were assembled in the late afternoon after the second feeding time. One male (slender and darker) and one female (with

bigger underbelly) were transferred to the opposite sites of a breeding cage. In the following morning, shortly after beginning the light cycle, divider was removed, and fish started mating. Eggs were collected every 20 minutes (mating time) using a strainer. Eggs were kept in a petri dish filled with egg water. (E3 medium + 2ml/l of 0.1% methylene blue).

2.2.2.2.4 Microinjection

For injection, purified plasmid DNA was diluted in distilled H_2O supplemented with 0.1% phenol red at a concentration of 35-40 ng/µl. Fertilized eggs were collected in the middle of a petri dish with a minimum amount of egg water. One- or two-cell stage embryos were injected (femtoJet, Eppendorf) through the chorion, directly into the yolk, with a drop of approximately 10% of the yolk volume, using injection needles. The injection needles were pulled from borosilicate glass capillary tubes with filament (0.58 mm diameter, Warner Instruments, Hamden, CT) using a micropipette puller (Sutter Instruments, Novato, CA). Injected embryos were raised in egg water at 28,5°C for further experiments.

2.2.2.2.5 Embryo treatment with rapamycin

For rapamycin treatment, embryos were co-injected with rapamycin (2.7nM of a 10mM stock solution in DMSO) together with the plasmid DNA (see above).

2.2.2 Immunofluorescence, microscopy and image analysis

2.2.2.1 preparing and sectioning

2.2.2.1.1 Mouse *M soleus* muscle

Mice were sacrificed by cervical dislocation 7, 14, 28 and 45 dpi. M. soleus was dissected by cutting the tendons, then immobilzed in a stretched position and frozen in liquid nitrogen. The muscle was cut in two halves with a scalpel. Half of the muscle was then fixed onto a sample holder using O.C.T. compound (Tissue-Tek) and 25µm thick transverse sections were cut using the cryostat. Sections were placed on glass slides, air-dried and kept in -80°C till use.

2.2.2.1.2 Zebrafish Embryo

2 dpf embryos were sacrificed using anesthetizing buffer and fixed in fixation buffer for 1h at RT. After several washes with PBS, fixed embryos were incubated in 30% sucrose in PBS at 4°C until embryos sanked to the bottom of the tube (12-24 h). Thereafter, embryos were transferred to a plastic mould that was filled with O.C.T. compound (Tissue-Tek) in the desired orientation and frozen gently in liquid nitrogen. To attach the frozen block to the sample holder, O.C.T. compound (Tissue-Tek) was dropped in the centre of sample holder and incubated in the main cryostat chamber at -20°C for 5 min. Embedded embryos were cut in 20µm tick longitudinal sections using the cryostat. Sections were placed on glass slides, air-dried and kept in -80°C till use.

2.2.2.1.3 Adult zebrafish trunk muscle

Adult zebrafish were anesthetized and euthanized using the rapid cooling method. The head, tail and fins were removed using a scalpel and the skin was removed with forceps. Fish muscles were removed longitudinally along one side of the fish, parallel to the backbone using a scalpel, transferred to the fixation buffer and incubated for 1h at RT. After several washes with PBS, fixed muscles were placed in 15% sucrose in PBS until they sank and then placed in 30% sucrose in PBS for overnight at +4°C. Afterward, each tissue was transferred to a plastic mould that was filled with O.C.T. compound (Tissue-Tek) and oriented in the longitudinal direction, and frozen gently in liquid nitrogen. Embedded tissues were cut in 25µm thick longitudinal sections using the cryostat. Sections were placed on glass slides, air-dried and kept in -80°C till use.

2.2.2.2 Immunofluorescence staining

After fixation in 4% PFA in PBS-/-, sections were washed 3 times for 5 min at RT in PBS -/-. Then, they were permeabilized in permeabilization buffer for 10 min at RT. After washing again with PBS -/-, sections were blocked in blocking solution for 1 h, at RT. The first antibody was diluted at an appropriate concentration in blocking solution and incubated on the section overnight at 4°C. On the next day, sections were washed with PBS -/- and proper secondary antibody was applied for 1h at RT in the dark and

sections were washed again with PBS-/-. In order to counterstain nuclei, diluted DAPI in blocking buffer (1:1000) was added on the sections and incubated for 10 min at RT in the dark. After washing with PBS-/-, sections were mounted with Mowiol 4-88 and a glass coverslip. The slides were maintained in the dark until imaging was performed. The same procedure was used for mouse *M soleus* muscle, adult zebrafish trunk muscle and embryos.

2.2.2.3 Confocal microscopy and image analysis

2.2.2.3.1 Regenerating Mouse *M soleus* muscle

Muscle sections were stained according to 2.2.2.2 and images were acquired in tiling mode to image the entire section using a 20x/0.8 Plan-Apochromat objective on a Zeiss LSM 800. Images were analysed using the Fiji software (Schindelin et al., 2012). The regenerated myofibres (central nuclei) were segmented using the Laminin staining in order to determine their number and minimum Feret's diameter as a measure of muscle fibre cross- sectional size (Schindelin et al., 2012). The number of Ki67 positive nuclei and the total number of nuclei were determined by automated segmentation whereas the number of nuclei within myofibres was determined by manual counting, in order to calculate the percentage of non-myofibre nuclei expressing Ki67. The number of MYOD positive cells normalized to the number of myofibres was determined by manually counting the MYOD positive nuclei, excluding those within myofibres. Linear brightness and contrast adjustments were made for illustration purposes, but only after the analysis had been made.

2.2.2.3.2 Cross sectioned Zebrafish myofibre imaging

Embryo and adult zebrafish muscle sections were stained according to 2.2.2.2 and imaged by confocal microscopy on a Zeiss LSM 800. Z- stack images were acquired using a 63x Plan- Apochromat oil immersion objective. Images were analysed using the Fiji software.

2.2.2.3.2 *In vivo* imaging of Zebrafish embryos and quantification of myofibre size

Zebrafish embryos were dechorionated by sharp forceps and anesthetized using anesthetizing buffer. Afterward, embryos were transferred to 35mm confocal dish and mounted in low melt agarose (preheated at 42°C). Once agarose was fully gelled, E3 medium containing tricaine was added to prevent drying out of agarose and embryos. Embryos were imaged by confocal microscopy on a Zeiss LSM 800. Images were acquired using a 20X/0.8 Plan- Apochromat objective. 3D reconstructed images were created from 70 stacks images using the Imaris software. On each image, single myofibre was segmented and the myofibre volume and mCherry intensity was measured using the Imaris software. The number of nuclear targeted RHEB constitutive active mutant (RHEB-Q64L) positive nuclei within myofibres were determined by manual counting.

2.2.2 Cell cultures methods

2.2.2.1 Cell culture conditions

C2C12 myoblast cells were cultured at 6 % CO2 and 95 % humidity at 37 °C. The zebrafish PAC2 fibroblast cell line was cultured under atmospheric CO2, in a non-humidified incubator at 26.5°C. The manipulation of cells was performed under a sterile hood. Media, buffers and glassware were sterilized before work (120 °C, 1.4 bar, 20 min).

2.2.2.2 Passaging and seeding of cells

First, the medium was removed, and cells were washed two times with PBS -/-. Thereafter cells were treated with trypsin solution and incubated for 3 min in the incubator. After detachment of the cells, the trypsin reaction was stopped by resuspending the cells with culture medium. Then cells were centrifuged, resuspended in culture medium, counted in a Neubauer chamber and cultured as follows:

Format	Cell number (PAC2 cells)	Format	Cell number (C2C12 cells)
T75 flask	1x 10^7	15 cm dish	2.5x 10^5
6 well plate	5x 10^5	6 well plate	5x 10^4
24 well plate	1x10^5	24 well plate	1x10^4

2.2.2.3 Differentiation of C2C12 myoblasts

A standardized protocol was used for the differentiation of C2C12 myoblasts. Cells were seeded at a density of 5.10^3 cells / cm^2 in growth medium (GM, 10% FCS-containing DMEM) at day -3, relative to the induction of differentiation at day 0. When cells reached confluence at day 0, differentiation was induced by changing the medium to differentiation medium (DM, 2% horse serum-containing DMEM), which was then replaced every day.

2.2.2.4 Collagen coating of coverslips

Glass coverslips were placed in a 24 well plate after sterilization by 70% ethanol and flaming. 500 µl of a sterile filtered 0.01 % collagen and 0.2 % acetic acid mixture was added on each coverslip and incubated for 1 h at RT. The mixture was removed, and the coverslips were dried overnight.

2.2.3 Transfection methods

2.2.3.1 Transfection of C2C12 cells with TransIT-X2

Cells were seeded either on collagen coated cover slips for imaging or in well plates according to 2.2.2.2 and incubated overnight. Proper amounts of DNA were diluted in serum-free medium. Then, TransiT-X2 (2.5 µl per 1 µg of DNA) was added and the mixture was incubated for 30 min at RT. During this time the growth medium on the cells was changed. Subsequently, the transfection mixture was added to the cells dropwise. The medium was changes after 6 h incubation.

siRNAs were also transfected at a concentration of 20 mM into C2C12 cells using this method.

2.2.3.2 Transfection of PAC2cells with FuGENE HD

Cells were seeded according to 2.2.2.2 and incubated overnight. Proper amounts of DNA were diluted in the serum-free medium. Then, FuGene HD (4 µl per 1 µg of DNA) was added and the mixture was incubated for 30 min at RT. During this time the growth medium on the cells was changed. Subsequently, the transfection mixture was added to the cells dropwise. The cells were incubated for 48h, however medium was changed after 24h.

2.2.3.3 Transfection C2C12 cells with Amaxa

$1x10^6$ cells were transfected by nucleofection using the Nucleofector® Kit V with 5µg of plasmid DNA according to manufacturer's protocol. Before reseeding, cells were stained with trypan blue and counted to estimate the number of viable cells.

2.2.4 Cells treatment with farnesyl transferase inhibitor (FTI)

$3x10^5$ C2C12 myoblast cells were seeded in 10 cm dish. The day after seeding, 4µM FTI (Lonafarnib) dissolved in DMSO was added to the cell culture medium. Treated cells were harvested after 24h incubation.

2.2.5 Edu staining

C2C12 myoblasts transfected with either the nTRIP6 blocking peptide (BP) or the control peptide (cBP) and grown on coverslips were pulsed for 1 h with 10 µM EdU and then fixed for 15 min with 2% paraformaldehyde, permeabilized for 20 min with 0.5% Triton X-100 in PBS and blocked for 1h in 5% BSA in PBS-/-. Incorporated EdU was reacted with 6-FAM-Azide as recommended by the manufacturer. Cells were then stained with a rabbit anti-mCherry primary antibody and an Alexa Fluor 546-conjugated anti-rabbit secondary antibody. Nuclei were counterstained with DAPI and analysed by confocal microscopy on a Zeiss LSM 800 (see 2.2.7).

2.2.6 Adhesion assay

For adhesion assays, plasmid or siRNA transfected C2C12 cells were re-seeded 48h post-transfection onto collagen-coated glass coverslips at a density of $2.5x10^4$ cells/cm2 and allowed to adhere for 1h. Non-adhered cells were washed away and adhered cells were fixed for 10 min fixation buffer. Nuclei were stained with DRAQ7, imaged and counted (see 2.2.7).

2.2.7 Immunofluorescence, microscopy and image analysis of cells

Immunofluorescence analysis was performed on C2C12 cells grown and differentiated on glass coverslips coated with collagen Type I, fixed for 10 min in fixation buffer, permeabilized for 10 min in 0.5% Triton X- 100 in PBS-/-and blocked for 1h in 5% BSA in PBS-/-. The primary antibodies were diluted at an appropriate concentration in blocking solution and incubated on the fixed cells overnight at 4°C. On the next day cells were washed three times with PBS-/- and the appropriate secondary antibody was applied for 1h at room temperature in the dark. After washing three times with PBS -/-, nuclei were counterstained with DAPI or DRAQ7 for 10 min in the dark. The coverslips were then mounted with Mowiol 4-88 and subjected to analysis.

For investigating nTRIP6 function to regulate the dynamics of myoblast differentiation *in vitro*, C2C12 myoblasts were transfected with either the nTRIP6 blocking peptide (BP) or the control peptide (cBP), grown and differentiated on coverslips and prepared for image analysis as described above. Imaging was performed using confocal microscopy on a Zeiss LSM 800.Cells images were acquired in tiling mode using a 10x/0.3 Plan- Neofluar objective resulting in 3 X 2 mm^2 images. The number of transfected cell nuclei (mCherry positive) and the number of MYH3 or of EdU positive cells (see 2.2.5) were determined by a combination of automated segmentation and manual counting in order to calculate the number of positive cells among transfected cells. The fusion index was calculated as the percentage of mCherry positive nuclei within fused myotubes.

To study the subcellular localisation of RHEB and mTOR, C2C12 cells were grown on glass coverslips coated with collagen Type I and prepared for image analysis as described above. Z- stack images were acquired using either a 63x Plan- Apochromat

oil immersion objective on a Zeiss LSM 800 or a 93x Plan- Apochromat glycerol immersion objective on a Leica 800. Images were analysed using the Fiji software.

2.2.6 Protein methods

2.2.6. Whole cell protein isolation (in RIPA Buffer)

Cells were washed twice with ice cold PBS -/-, lysed with appropriate amounts of RIPA (supplemented with the cocktail of protease/phosphatase inhibitors (PIC, PhIC and PMSF), scraped and transferred to the clean 1.5 ml tubes. Subsequently, cells were sonicated for 5 min with 20s pulse / 20s pause at the low intensity. To denature the proteins, the mixture was boiled at 94°C for 5 min, and 2x Laemmli buffer was used as a loading buffer.

2.2.6.2 Cytoplasmic, nuclear and nucleolar fractionation

Cytoplasm and nuclei from either untreated or C2C12 cells treated with FTI (see 2.2.4) were prepared using the Nuclear Extract Kit (Active Motif), according to manufacturer's protocol. Nucleoli were extracted from the nuclear. Briefly, Cells were washed with ice-cold PBS-/- supplemented with phosphatase inhibitor and collected as pellets. A hypotonic buffer was used to lyse the cells and extract the cytoplasm. After centrifuging and washing with the detergent-containing buffer, the nuclear pellet was collected. Pellets were resuspended in Buffer S2 (350mM Sucrose, 0.5mM $MgCl_2$, supplemented with phosphatase inhibitor (PhIC), sonicated, layered over Buffer S3 (880mM Sucrose, 0.5mM $MgCl_2$, supplemented with PhIC) and spun at 2800 xg for 5 min at 4 C. Supernatant was retained as the enriched nucleoplasmic fraction. The nucleolar pellet was resuspended in Buffer S2 and spun at 2800 xg for 5min at 4 C. The cleaned nucleolar pellet was resuspended in 1x RIPA (supplemented with PIC, PhIC, PMSF), briefly sonicated and centrifuged at 18000 xg for 10min at 4 C, and enriched lysates were collected.

2.2.6.3 Measurement of total protein concentration according to Lowry

The Lowry protein assay was used to measure total protein concentration in lysates. First, 250µl Lowry I -Buffer, then 500µl Lowry IV-buffer solution were added to 4µl of sonicated lysate. The mixture was incubated for 5 min at RT. Subsequently, 50µl Folin (1:1 in water) was added to the mixture and incubated for 30 min at RT in the dark. Two sets of BSA standards were mixed containing known amounts of protein. The protein concentration was evaluated by spectrometry at 595nm and the absorbance was measured and compared to a standard curve.

2.2.6.4 Separation of proteins via SDS-PAGE

Proteins were separated according to their size using an electrical field (Laemmli, 1970). The polyacrylamide gels were cast according to Sambrook (Sambrook, J., 2001). The gels were run in a Mini-PROTEAN Tetra Vertical Electrophoresis Cell (BioRad) at 100 V for 1 h.

2.2.6.5 Western bloting

After separation on the gel, the proteins were transferred to a Polyvinylidene fluoride (PVDF) membrane which was soaked and activated in Ethanol. For the transfer a trans-blot turbo (BioRad) at 1.3 mA/cm2 for 7 minutes was used with western blot buffer. Following this the membrane was incubated for 1 h at RT in blocking buffer. After blocking, the primary antibody (diluted in blocking buffer) was incubated on the membrane over night at 4°C under constant shaking. The next day the membrane were washed three times with TBST for 5 min at RT, then the secondary antibody (conjugated with HRP), again diluted in blocking buffer, was incubated on the membrane for 1 h at RT. The membrane was then washed three times in TBST. The specific signal of HRP was detected by enhanced chemoluminescence using the ChemiDoc Touch Imaging System (BioRad).

2.2.6.6 Luciferase assay

2.2.6.6.1 FireFly- Luciferase assay

After two washes with ice cold PBS-/-, cells were lysed with the Promega passive lysis buffer (5x lysis buffer diluted to 1x with ddH_2O). 10 µl of cell lysates were then transferred into a white 96 well plate and subjected to luciferase measurement. The luminometer automatically injected 70 µl of the reaction buffer together with 20 µl of the substrate buffer in each well. The luminescence was measured for 2 seconds.

2.2.6.6.2 Nanoluc- Luciferase assay

As with the FireFly-Luciferase Assay the cells were lysed with the Promega passive lyse buffer. 5 µl of the cell lysates were transferred into a white 96 well plate and 45 µl of Promega passive lyse buffer were added to the lysate. The Nano-Glo Luciferase Substrate was diluted 1:200 in Nano-Glo Luciferase Buffer (Promega). 50 µl of this substrate buffer mixture was added to each well and the luciferase activity was measured for 2 seconds.

2.2.7 DNA methods

2.2.7.1 DNA digestion

In order to double digest plasmid DNA, 2µg plasmid DNA was digested using 2 units of each corresponding restriction endonucleases in 10 times concentrated buffer. After 1 h incubation at 37°C, the separate digested plasmid DNA were mixed to complete digestion followed by 1 h incubation at 37°C.

2.2.7.2 Electrophoresis

Agarose gel electrophoresis was used to separate DNA fragments according to their size. To cast the gel, 1% agarose powder was dissolved in 1x TAE buffer under heating and ethidium bromide was added to it after cooling down. After loading DNA into the wells on the gel, an electric current with voltage of 100V was applied. The separation of DNA fragments lasted approximately 1 h and was visualized by UV- light.

2.2.7.3 Extraction of DNA fragment out of agarose gel

DNA fragments with the size of interest were cut out of the gel on a UV- light table using scalpel and purified from the piece of gel using GeneJet Gel Extraction Kit according to its protocol. The concentration of purified DNA was measured from its absorbance (A^{260}) using NanoDrop spectrophotometer.

2.2.7.4 Dephosphorylation of 5´end of DNA

In order to prevent self-ligation of plasmid DNA, 1 unit of rSAP was added to 1 pmol of DNA ends in 10 times concentrated buffer. After 30 min incubation at 37°C, the reaction was stopped by 5 min heat-inactivation at 65°C.

2.2.7.5 Ligation

According to manufacturer's instruction (NEB), 2µl of T4 DNA ligase was added to a combination of a vector and an insert in 10 times concentrated buffer (the molar ratio of vector to insert was calculated using NEB calculator). The reaction mix was incubated at 16°C overnight in a PCR cycler. The reaction was inactivated by 10 min heating at 65°C the next day.

2.2.7.6 PCR

To amplify the DNA of interest, a sequence specific primer pair was combined with DNA fragment in a PCR reaction mix which was involved, 10% DMSO, 0.2mM dNTPs, 1U Pfu-DNA-Polymerase in 5 times concentrated PCR buffer. The volume of DNA fragment and primers were different per reaction depending on the DNA construct and primers size. The PCR reaction was implemented in the PeQstar PCR device in a 30 cycles of denaturation (95°C, 1min), annealing (the temperature and duration was depended on melting point of each primer) and elongation (72°C, the duration was depended on the size of DNA fragment (2min/kb)) after 5 min primary denaturation (95°C). The PCR reaction was completed after another 10 min elongation and cooled down to 8°C.

2.2.7.7 Transformation of E. coli (DH5α)

0.1 µg of plasmid DNA was added to 100 µl of of chemically competent E. coli (DH5α), which were thawed on ice. After 30 min incubation of mix on ice, bacteria were heat shocked by 45 s heating at 42°C using a heating block subsequently placed on ice for 2 min. Afterwards, the mix was added to 900µl SOC medium in a sterile polypropylene tube and incubated at 37°C for 1 h under constant shaking. Thereafter, the transformed bacteria were transferred into a 1.5 ml reaction tube and centrifuged for 1 min at 13000 rpm. After removing the supernatant, the pellet was resuspended in 100 µl of remaining medium and transferred to preheated LB agar plate containing the antibiotic which was necessary to select the plasmid of interest. The transformed bacteria were incubated at 37°C to grow overnight.

2.2.7.8 Annealing of oligos

Equimolar concentration of each oligos in a total volume of 100µl were annealed at 95°C for 5 min and then slowly cooled to room temperature. Annealed oligos was kept in -20°C till use.

2.2.7.9 Phosphorylation of oligos

300 pmol of annealed oligos was phosphorylated using T4 PolynucleotideKinase (PNK) in 10 times concentrated Ligase buffer. The reaction mix was incubated at 37°C for 30 minutes and then heat inactivated at 65°C for 20 minutes.

2.2.7.10 Infusion Cloning

The infusion cloning was performed using the In-Fusion HD Cloning Kit of Clontech according to its protocol.

2.2.7.11 Site directed mutagenesis

Site directed mutation was conducted using QuikChange Site-Directed Mutagenesis Kit from Agilent according to its protocol.

2.2.7.12 Cloning

The cloning was accomplished in multiple steps. It was started with creating a desired expression vector and insert. The plasmids which were digested with the appropriate restriction enzymes, were used as the vector. The insert was either created by digestion, PCR, annealed oligos or by using pre-ordered string DNA. The vector and insert were then either ligated or fused and chemically transformed to the proper competent cell. The transformed construct was purified using peqGOLD Xchange Plasmid Midi Kit. The concentration of the purified DNA was determined from its absorbance (A^{260}) using the NanoDrop spectrophotometer and diluted to a concentration of 1 µg/µl and stored at -20°C until use. The plasmids that were cloned were sequence verified and are described in 2.1.11.

2.2.9. RNA isolation and quantitative real-time PCR

Total RNA was extracted using PeqGOLD TriFast^{TM}. Cells were collected in PeqGOLD TriFast^{TM}, mixed with Chlorofom and vortexed for one minute. Centrifugation was performed with 12000xg for 10 minutes. The RNA containing aqueous phase was transferred into a fresh reaction tube and was mixed with isopropanol for precipitation. After that, centrifugation was performed at 12000 xg for 10 minutes and the RNA pellet was washed with 75% EtOH, and, after drying resuspended in 20-50µl ddH_2O. RNA was then reverse-transcribed into cDNA. RNA samples were treated with DNase I and incubated for 30 minutes at 37 C. DNase I was then heat inactivated by adding EDTA and incubating for 10 min at 65 C. Thereafter, first strand was synthesized by incubating for min at 70 C in random primer and mixed with following reagents:

5x MLRVT Buffer	4 µl
dNTP (10mM)	2 µl
MLRVT	1 µl
H_2O	3 µl

and incubated for:

10 min	25°C
60 min	42°C
10 min	70°C
Store in	4°C

Synthesized cDNA was diluted in 50-100 µl RNase free water.

Myog (myogenin) and *Tnni2* mRNAs, as well as the transcript of the large ribosomal subunit P0 gene (*Rplp0*) used for normalization, were quantified by real-time PCR using the ABI Prism Sequence Detection System 7000 (Applied Biosystems, Foster City, CA) using SYBR green.

2x SYBR green	10 µl
Primer (10 pmol/µl)	2 µl
cDNA	4 µl
H_2O	4 µl

Program	
95°C	5 min
95°C	30 sec
60°C	30 sec
72°C	30 sec
35 cycles	
72°C	5 min
8°C	store

2.2.10 Statistical analysis

Statistical analyses were performed using R. Where indicated, significant differences were assessed by two-sided t-test analysis, with values of $P < 0.05$ sufficient to reject the null hypothesis. A Bonferroni correction was applied when multiple comparisons were performed. The normal distribution of myofibre size in zebrafish embryo was assessed by the Shapiro Wilk normality test (P=0.009).

3. Results

3.1 Function of nTRIP6 in myogenesis and skeletal muscle regeneration

3.1.1 nTRIP6 regulates the dynamics of myoblast differentiation *in vitro*

Our group has reported that nTRIP6 acts as a transcriptional co-repressor for MEF2C in myoblasts (Kemler et al., 2016), suggesting a role for nTRIP6 in the regulation of myogenesis. I first investigated this question in the C2C12 mouse myoblast cell line. In order to investigate the involvement of nTRIP6 in their differentiation, I used a genetically-encoded, nuclear targeted blocking peptide (BP) which was developed by our group. The peptide is fused to a nuclear localization sequence (NLS), to target it to the nucleus, and tagged with mCherry for visualization purposes. This blocking peptide competes with nTRIP6 to interact with MEF2C and selectively inhibits the function of nTRIP6 in the nucleus without interfering with TRIP6 in the cytosol (Diefenbacher et al., 2014; Kemler, 2017). As a control, I used a scrambled version of blocking peptide (cBP).

Upon transfection in C2C12 cells, both the blocking peptide and control peptide were exclusively located in the nucleus, as assessed by the mCherry florescence signal (Fig. 9A). Thereafter, I examined whether the blocking peptide affect the cytosolic function of TRIP6, i.e. cell adhesion (Gur'ianova et al., 2005; Yi et al., 2002). C2C12 cells were transfected with either the blocking peptide (BP), the control peptide or mCherry fused to an NLS as an additional negative control. As a positive control, an siRNA targeting *TRIP6* mRNA, which knocks down both the nuclear and cytosolic TRIP6 isoforms (Diefenbacher et al., 2008) was used. A nonspecific siRNA was used as a control. The adhesion assay results show that the blocking peptide did not have any effect on cell adhesion (Fig. 9B), whereas the siRNA significantly decreased it (Fig. 9C). Taken together, these results confirm the selectivity of the blocking peptide to block nTRIP6 function. I therefore used it to assess the function of nTRIP6 in myogenesis.

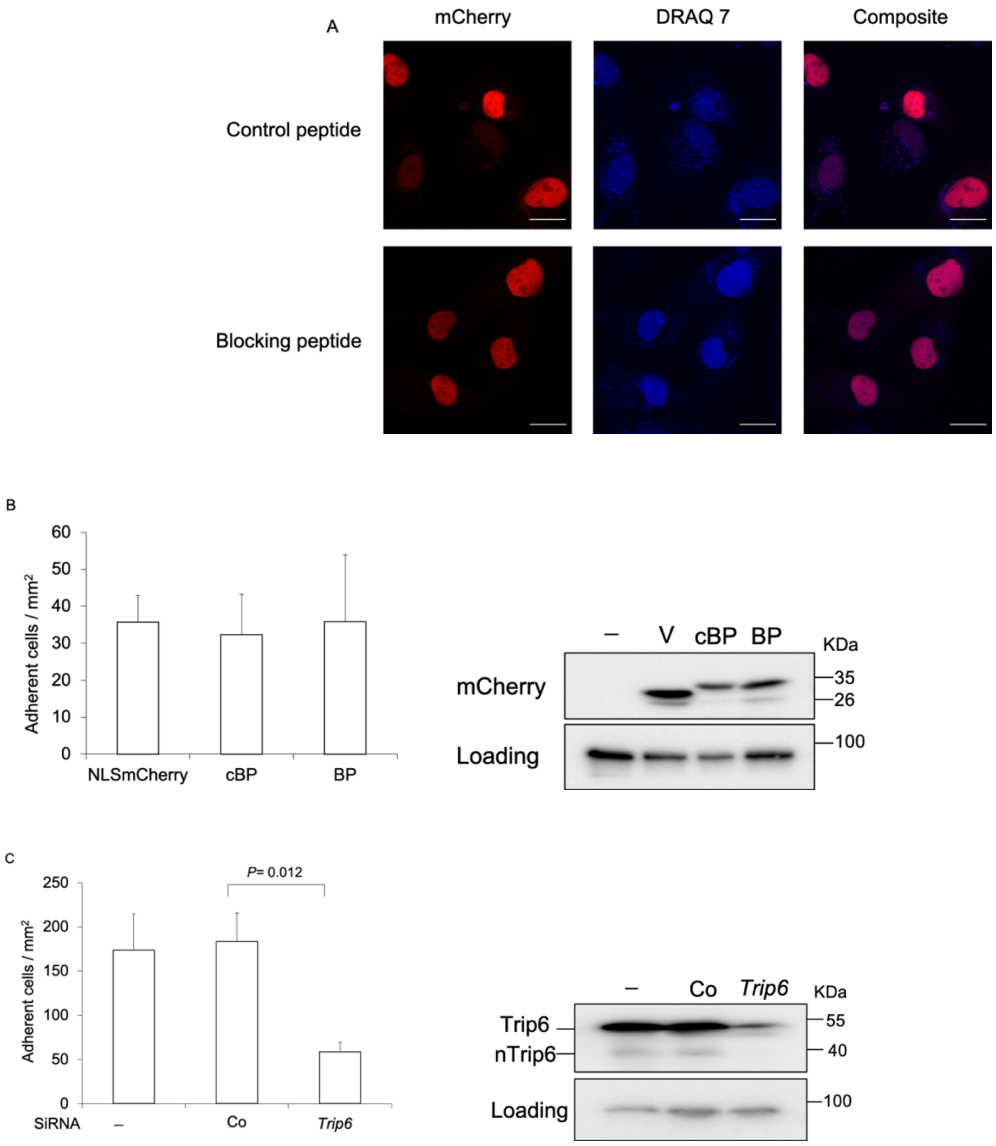

Figure 9- The blocking peptide does not interfere with the cytosolic functions of TRIP6. A) C2C12 myoblasts were transfected with the nuclear-targeted mCherry-tagged nTRIP6 blocking peptide or the control scrambled version of the peptide. Cell nuclei were counter stained with DRAQ7 and imaged by confocal microscopy (Scale bar: 20 µm). **(B)** C2C12 myoblasts were transfected with either nuclear-targeted mCherry as a vector control (V), the control peptide (cBP) or the blocking peptide (BP) and an adhesion assay was performed 48h later. The number of adhered transfected cells (mCherry positive) is presented as mean ± SD of 3 independent experiments. A representative Western Blot of the cell lysates probed with an anti-mCherry antibody and an anti-GR antibody as a loading control is presented. **(C)** C2C12 myoblasts were either untransfected (-) or transfected with a control siRNA (Co) or an siRNA targeting *Trip6* mRNA. An adhesion assay was performed 48h later and nuclei were stained with DRAQ7. The number of adhered cells is presented as mean ± SD of 3 independent experiments. A representative Western Blot of the cell lysates probed with an anti-TRIP6/nTRIP6 antibody and an anti-GR antibody as a loading control is presented.

I used a standardized protocol for the differentiation of C2C12 myoblasts. Cells were seeded at a low density in growth medium (GM) at day -3, relative to the induction of differentiation at day 0. When cells reached confluence at day 0, medium was switched to differentiation medium (DM), to induce the differentiation. To study the putative role of nTRIP6 in myoblast differentiation, we used *MyoG* (myogenin) mRNA as an indicator of early myocytic differentiation (Edmondson and Olson, 1990) and *Tnni2* a marker of late differentiation (Lin et al., 1994). In C2C12 cells expressing the blocking peptide, *MyoG* was expressed earlier in the proliferation phase and remained more elevated during the differentiation phase than in cells expressing the control peptide (Fig. 10A). In contrast, the expression of *Tnni2* was delayed in C2C12 cells expressing the blocking peptide compare to the control (Fig. 10B). These results suggest that blocking nTRIP6 function accelerates early differentiation and delays late differentiation.

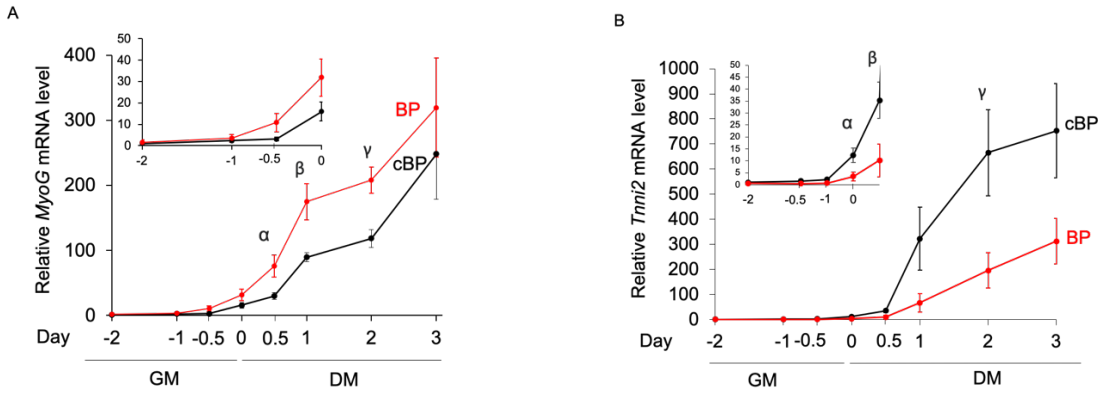

Figure 10- Blocking nTRIP6 function accelerates early differentiation and delays late differentiation. C2C12 cells were transfected with either the mCherry-tagged, nuclear-targeted nTRIP6 blocking peptide (BP) or the control, scrambled version of the peptide (cBP). After transfection, the cells were kept in growth medium (GM, 10% FCS-containing DMEM) for two days (day -2 till 0), then switched to the differentiation medium at day 0 (DM, 2% horse serum-containing DMEM). Cells were harvested at the indicated day and the relative levels of the *Myog* **(A)** and *Tnni2* **(B)** mRNAs were determined by real-time PCR. Results are plotted relative to the expression of the *RPLP0* gene (mean ± SD of three independent experiments). Bonferroni corrected *P* values are for A) α= 0.044, β= 0.027 and γ=0.012 and for B) α =0.050, β =0.053 and γ=0.047.

Myoblast exit from the cell cycle and entry into the differentiation phase are coordinated process (Ruijtenberg and van den Heuvel, 2016). Thus, the accelerated early differentiation in cells expressing the blocking peptide could be due to an accelerated cell cycle exit.

Therefore, I tested whether blocking nTRIP6 function affects myoblast proliferation and cell cycle exit, using again the blocking peptide. There was no difference between the number of C2C12 cells transfected with the blocking peptide and those expressing the control peptide during the proliferation and early differentiation phases (Fig. 11A). Furthermore, there was no difference in the kinetics of cell cycle exit, as assessed by Edu pulsed labelling, between cells expressing the blocking peptide and cells expressing the control peptide (Fig. 11B). Thus, blocking nTRIP6 function in myoblasts has no effect on cell proliferation or on the kinetics of cell cycle exit, although it accelerated early differentiation.

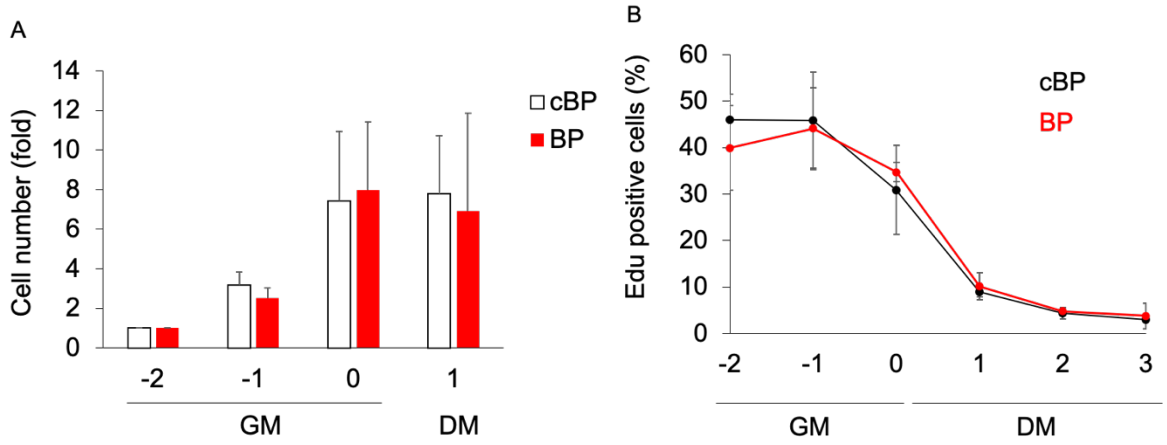

Figure 11 - Blocking nTRIP6 function does not affect myoblast proliferation and cell cycle exit. C2C12 cells were transfected with either the mCherry-tagged, nuclear-targeted nTRIP6 blocking peptide (BP) or the control, scrambled version of the peptide (cBP). After transfection, the cells were kept in growth medium (GM) for two days, then switched to the differentiation medium (DM) at day 0. **(A)** Cells were counted at the indicated day and results are shown relative to the cBP-transfected cells at day -2 and are mean ± SD of three independent experiments. **(B)** Cells were pulsed with EdU for 1 h at the indicated time point, fixed, stained for EdU incorporation and peptide expression (mCherry) and analysed by confocal microscopy. The percentage of EdU-positive nuclei among transfected cells (mCherry positive) is presented as mean ± SD of three independent experiments.

To confirm the effect of blocking nTRIP6 function on late differentiation, in collaboration with Denise Kemler, the number of C2C12 cells expressing MYH3 (embryonic skeletal myosin heavy chain 3) was quantified upon transfection with the nTRIP6 blocking peptide or the control peptide. MYH3 is a contractile protein which is expressed during myogenic differentiation and provides a specific marker of the late differentiation phase (Schiaffino et al., 2015). At day 0, one day before the induction of differentiation, very few cells expressed MYH3, as expected. At day 1, about 10%

of the cells transfected with the control peptide expressed MYH3, whereas this number was significantly decreased in the cells transfected with the nTRIP6 blocking peptide (Fig. 12). Therefore, blocking nTRIP6 function delays late differentiation.

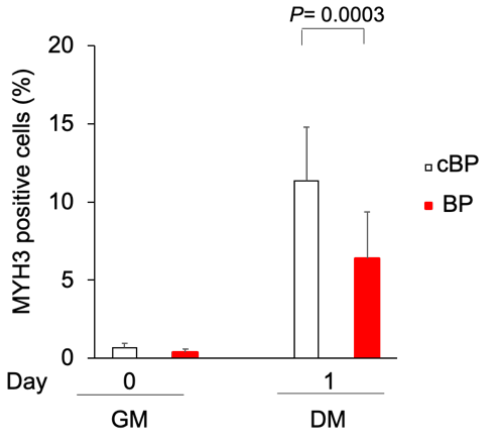

Figure 12- Blocking nTRIP6 function delays late differentiation. C2C12 cells were transfected with either the mCherry-tagged, nuclear-targeted nTRIP6 blocking peptide (BP) or the control, scrambled version of the peptide (cBP). After transfection, the cells were kept in growth medium (GM, 10% FCS-containing DMEM) for two days, then switched to the differentiation medium at day 0 (DM). Cells were fixed at the indicated day and subjected to immunofluorescence analysis using antibodies against MYH3 and mCherry. Nuclei were counterstained using DAPI. The percentage of MYH3 expressing cells among transfected cells (mCherry positive) is presented as mean ± SD of three independent experiments.

I then tested whether blocking nTRIP6 function has also an effect on myocyte fusion. In cells transfected with the control peptide, cell fusion started at day 2 of differentiation and strongly increased at day 3 to reach of fusion index of about 40%. However, in cells transfected with the blocking peptide, cell fusion was significantly inhibited at both day 2 and day 3. (Fig. 13). Thus, blocking nTRIP6 function leads to impaired myocyte fusion.

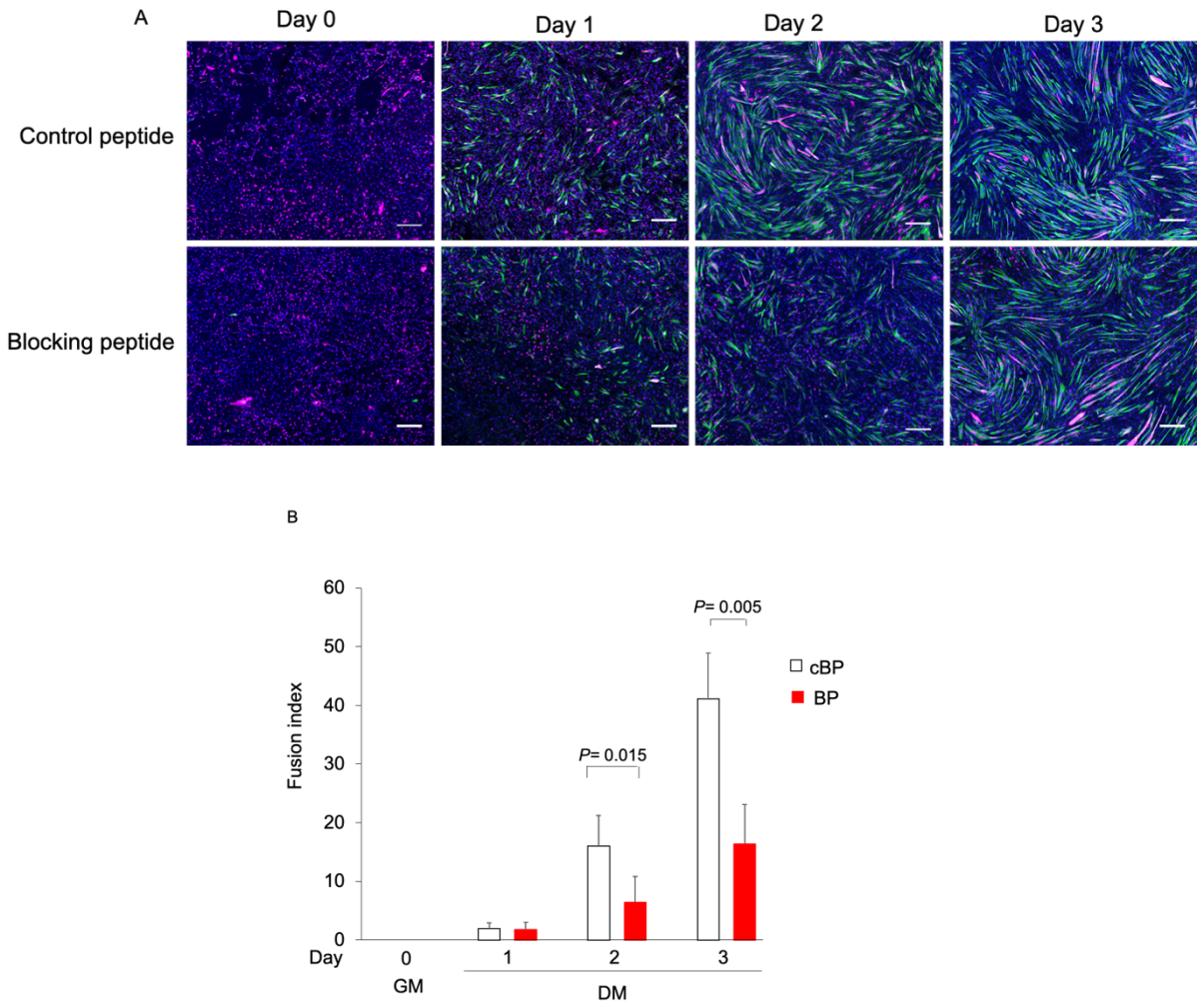

Figure 13 - Blocking nTRIP6 function leads to impaired myocyte fusion. C2C12 cells were transfected with either the mCherry-tagged, nuclear-targeted nTRIP6 blocking peptide (BP) or the control, scrambled version of the peptide (cBP). After transfection, the cells were kept in growth medium (GM) for two days (day -2 till 0), then switched to the differentiation medium at day 0 (DM). Cells were fixed at the indicated day and subjected to immunofluorescence analysis using antibodies against MYH3 and mCherry. Nuclei were counterstained using DAPI. **(A)** Representative images are shown (Scale bar: 200 µm). **(B)** The fusion index (percentage of mCherry positive nuclei within fused myotubes) is presented as mean ± SD of three independent experiments.

3.1.2 Skeletal muscle regeneration in *Trip6* knockout mouse

In order to investigate the *in vivo* relevance of the results showing the regulatory role of nTRIP6 in myoblast differentiation *in vitro,* I studied skeletal muscle regeneration in a mouse model in which the *Trip6* gene is knocked out in satellite cells. To this end, I used the C57BL/6J-*Trip6*$^{Tm(loxP)}$ line, hereafter termed *Trip6*$^{fl/fl}$, in which *Trip6* is conditionally targeted by flanking exons 2 to 9 by loxP sites (Shukla et al., 2019).

Trip6$^{fl/fl}$ mice were crossed with C57BL/6J-*Pax7*$^{tm1(Cre-ERT2)Gaka}$ (short name *Pax7*$^{Cre-ERT2}$) mice, in which the tamoxifen-inducible version of Cre-recombinase (Cre-ERT2) is expressed only in satellite cells (Murphy et al., 2011). The *Trip6*$^{fl/fl}$; *Pax7*$^{Cre-ERT2/wt}$ offspring were treated with Tamoxifen for 5 consecutive days to delete *Trip6* only in satellite cells. I then tested the muscle repair capacity of these *Trip6* knockout mice, hereafter termed *Trip6*^{scko}. The wild type *Trip6*$^{fl/fl}$ mice were used as a control. To this end, in collaboration with Denise Kemler, the animals were subjected to a muscle injury by injection of Notexin directly into the soleus muscle. Notexin promotes a complete degeneration of the muscle, followed by a complete regeneration (Danieli-Betto et al., 2010). Then muscle regeneration was followed at time 7, 14, 28 and 45 days post injury (dpi) (Fig. 14A). As an index of myogenic differentiation during regeneration, I counted the number of mononuclear cells expressing MYOD, which includes both proliferating myoblasts and differentiated myocytes (Füchtbauer and Westphal, 1992; Yablonka-Reuveni and Rivera, 1994) (Fig. 14B). Seven, 14 and 28 dpi, the number of MYOD-positive cells was significantly higher in the regenerating soleus muscle of *Trip6*^{scko} animals than in the soleus muscle of the *Trip6*$^{fl/fl}$ control mice. At 45 dpi, the number of MYOD-positive cells had strongly decreased and no difference between the knockout and control group was observed at this day (Fig14. C). This increase in the number of MYOD-positive cells might due to an increased myoblast proliferation. To address this hypothesis, the number of cells expressing the Ki67 proliferation marker was quantified (Fig. 14B). At 7 dpi, the number of cells expressing Ki67 was not different between the *Trip6*^{scko} and *Trip6*$^{fl/fl}$ regenerating muscles. However, at 14 dpi, this number had increased more in the *Trip6*$^{fl/fl}$ than in the *Trip6*^{scko} regenerating muscles. At 28 and 45 dpi, it had strongly decreased in muscles from both genotypes compared to 14 dpi (Fig. 14D). These results showed that the higher number of MYOD-expressing cells in the *Trip6*^{scko} muscle is not caused by an increased myoblast proliferation. An alternative hypothesis would be a decreased myocyte fusion.

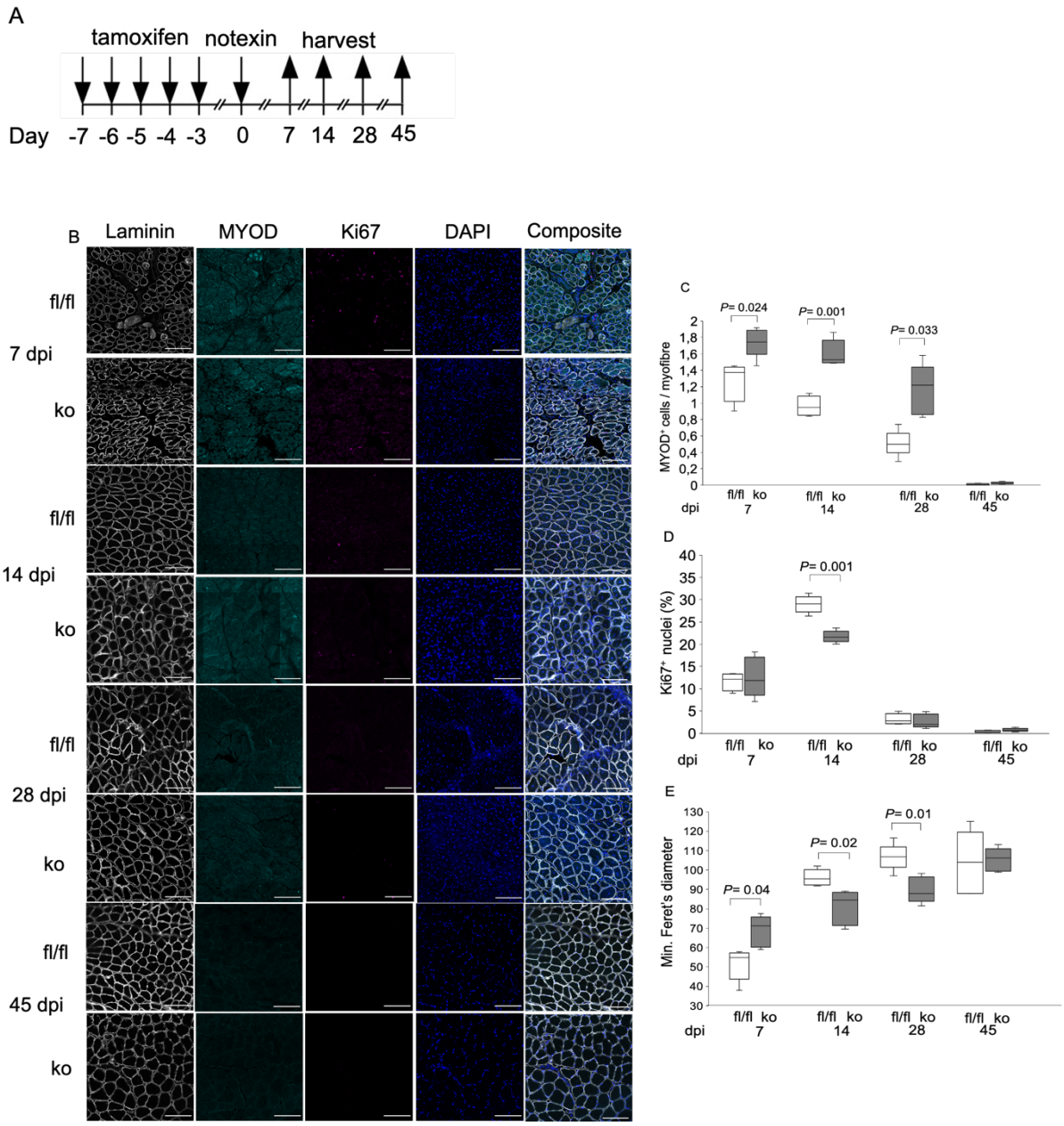

Figure 14 - Skeletal muscle regeneration in *Trip6* knockout mice. A) Schematic representation of the protocol. The *Trip6* gene was knocked out in satellite cells by intraperitoneal injection of tamoxifen in *Trip6*$^{fl/fl}$; *Pax7*$^{Cre\text{-}ERT2/wt}$ mice and muscle degeneration was induced by injection of notexin in the M. soleus. **(B-D)** The regenerating and uninjured contralateral muscles of *Trip6*^{scko} (ko) and *Trip6*$^{fl/fl}$ control animals (fl/fl) were harvested at the indicated day post-injury (dpi). Transverse cross sections of M. soleus muscles were immunostained with antibodies against Laminin (gray) to delineate the myofibres, MYOD (green) to visualize myoblasts and myocytes, Ki67 (red) to visualize proliferating cells. Nuclei were counterstained with DAPI (blue). Section were imaged by confocal microscopy. **(B)** Representative images are shown (Scale bar: 100 µm). **(C)** Number of MYOD-positive mononuclear cells normalized to the number of myofibres; **(D)** Percentage of non-myofibres nuclei expressing Ki67; **(E)** Minimum Feret's diameter of the regenerating myofibres expressed as percent of the contralateral uninjured muscle. Bonferroni corrected *P* values are presented (5 animals per group).

To investigate this hypothesis, I measured the size of regenerating myofibres (the minimum Feret's diameter), as an index of fusion during regeneration. At 7 dpi, the size of the myofibres was larger in *Trip6*^{scko} than in *Trip6*$^{fl/fl}$ muscles. On the contrary, at 14 and 28 dpi, the size of myofibres was larger in *Trip6*$^{fl/fl}$ muscles. Finally, at 45 dpi, there was no more observable difference in the size of the regenerated myofibres in both genotypes (Fig. 14E). Therefore, the delay in the increase in myofibre size despite the higher number of MYOD expressing cells in the *Trip6*^{scko} muscle is very similar to our *in vitro* observations that blocking nTRIP6 functions delays myocyte fusion.

Taken together, these results show that the loss of nTRIP6 expression in satellite cells delays muscle regeneration.

3.2 Nuclear function of RHEB in muscle growth in the zebrafish embryo

3.2.1 Subcellular localisation of mTOR and RHEB *in vitro* in C2C12 myoblast cells and *in vivo* in Zebrafish myofibres

It has been reported that mTOR and RHEB are localised in the cytoplasm and nucleus in many cell lines. In addition, a study in murine myoblasts revealed that mTOR is mainly nuclear during myogenic differentiation (Zhang et al., 2002). Whether RHEB is also localised in the nucleus in these cells is unknown. Therefore, I first studied the subcellular localisation of mTOR and RHEB in C2C12 myoblasts. In proliferating myoblasts (day-2 and -1), mTOR and RHEB immunoreactivity was detected mainly in the nucleus. By day 4 of differentiation, mTOR and RHEB were observed more in the nucleus with detectable level in the cytoplasm of fused myotubes (Fig. 15). These results indicate that RHEB and mTOR are localised mainly in the nucleus in C2C12 myoblast cells during proliferation and differentiation, with an increase in cytoplasmic localization towards the late differentiation phase.

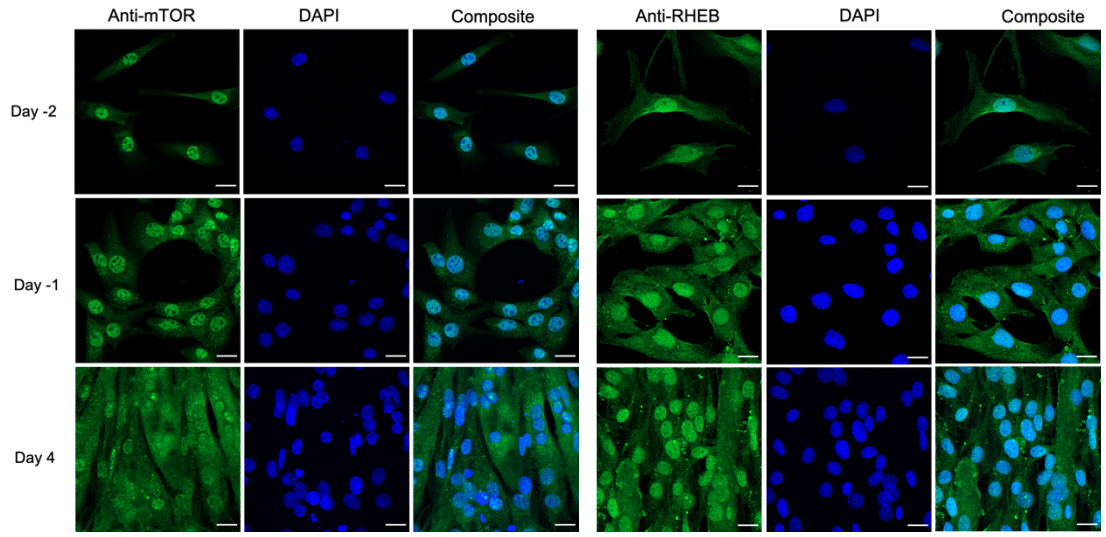

Figure 15 - Subcellular localisation of mTOR and RHEB in C2C12 myoblasts. C2C12 cells were seeded at low density and kept in proliferation medium for 2 days (day -2 till 0). At day 0 the medium was switched to low serum containing differentiation medium and kept for 4 days (day +4). Cells were fixed at the indicated day and subjected to immunofluorescence analysis using antibodies against mTOR and RHEB (green). Nuclei were counterstained using DAPI (blue) and imaged by confocal microscopy. Images representative of three experiments are shown (Scale bar: 20μm).

What could be the determinant of the nuclear localisation of RHEB? Farnesylation of the C-terminal CAAX motif of RHEB by the cytoplasmic farnesyl transferase supports its subcellular localisation to membrane comportments like the lysosome, Golgi or Endoplasmic reticulum (ER) (Buerger et al., 2006). Farnesyl transferase inhibitors prevent this step of RHEB post-translational modification, leading to the scattering of RHEB in the cytosol (Ferguson and Angarola, 2020). To investigate whether farnesylation plays a role in the nuclear localization of RHEB, I used a farnesyl transferase inhibitor (Lonafarnib) (Basso et al., 2005) in proliferating C2C12 myoblasts. Western blot analysis of subcellular fractions showed an increase in the nuclear localisation of RHEB upon treatment with Lonafarnib, while its cytoplasmic localisation was reduced (Fig. 16). This preliminary result suggests that the lack of farnesylation is a major determinant of RHEB nuclear accumulation.

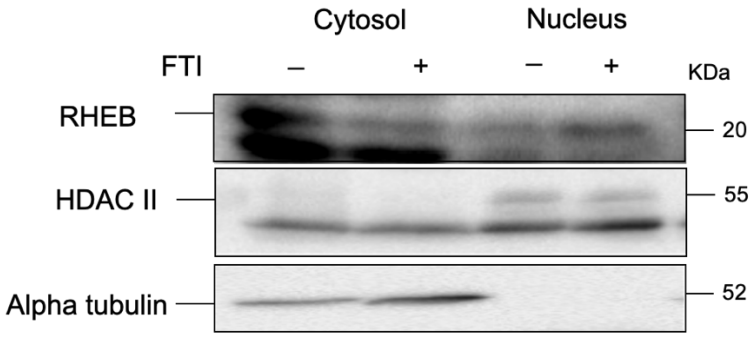

Figure 16 - Nonfarnesylated RHEB accumulates in the nuclei of C2C12 myoblast cells. C2C12 cells were seeded at low density and were kept in proliferation medium for one day in the presence or absence of a farnesyl transferase inhibitor (FTI). Cytosolic and nuclear fractions were subjected to western blot analysis using an anti-RHEB antibody, an anti-HDAC II antibody as a nuclear marker and an anti-alpha tubulin antibody as a cytosolic marker. The presented western blot is representative of three independent experiments.

mTORC1 regulates cell growth rather than cell proliferation (Khor et al. 2019) and the over-expression of RHEB induces skeletal muscle hypertrophy (Emerman et al., 2010). If RHEB is also expressed in the nucleus of growing muscle, its effect on muscle growth might not be only due to its canonical function in the cytosol, but also to a nuclear function. Therefore, I assessed the subcellular localisation of mTOR and RHEB *in vivo*, in the myofibres of fast-growing 2 days post fertilization zebrafish embryo, as well as in adult zebrafish in which muscles grow at a much slower rate (Keenan and Currie, 2019; Rowlerson et al., 1995). In longitudinal cross section, immunostaining revealed a predominantly nuclear localisation of mTOR and RHEB in

the embryonic myofibres (Fig. 17A), whereas they were nearly exclusively cytosolic in the adult (Fig. 17B). Thus, the mostly nuclear localisation of RHEB of embryonic myofibres might be a feature of fast-growing muscles during embryonic development. This prompted us to study the effect of RHEB on muscle growth in the developing embryo.

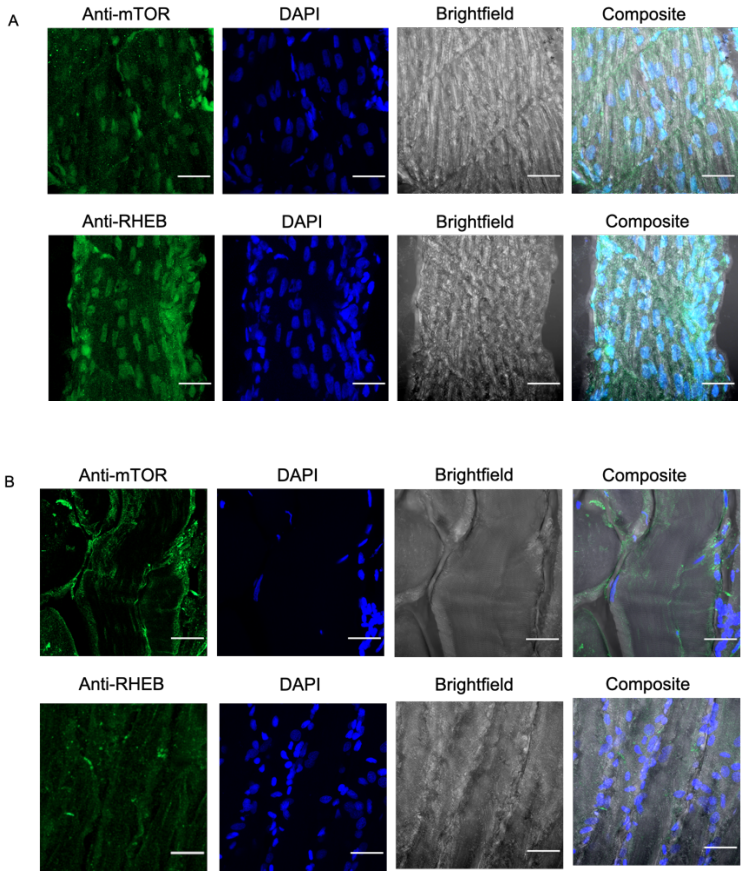

Figure 17 - Localization of mTOR and RHEB in Zebrafish myofibres. Longitudinal cross sections through the trunk region of zebrafish embryos at 2 dpf **(A)** and adult zebrafish **(B)** were subjected to immunofluorescence analysis using antibodies against mTOR and RHEB (green). Nuclei were counterstained with DAPI (blue). Representative images (n=3) are shown. (Scale bar: 20 µm).

3.2.2 The effect of RHEB mutants on myofibre size

To this end, I quantified the volume of myofibres expressing mCherry-tagged versions of constitutively active (Q64L) and dominant negative (D60K) mutants of RHEB in the

developing zebrafish embryo. The expression of the constructs from the injected plasmids was driven by a promoter fragment of the muscle-specific myosin chaperone, Unc45b, which directs gene expression exclusively in zebrafish skeletal muscle (Rudeck et al., 2016). Single cell stage embryos were injected with RHEB-Q64L, RHEB-D60K and mCherry plasmids (Fig. 18A) and raised for two days. The expression of the RHEB constructs was clearly visible in both the cytoplasm and nucleus of myofibres two days post-fertilization (2dpf) (Fig. 18B). Quantifying the volume of the myofibres expressing the RHEB-Q64L mutant showed a significant increase in size compared to the mCherry expressing myofibres. Conversely, in the myofibres expressing RHEB-D60K, I observed a strongly decrease in size, or they were even not detectable anymore (Fig. 18C). Together, these results validate the effect of RHEB mutants *in vivo* on zebrafish myofibre size. Given that the mutants are localised both in the cytoplasm and in the nucleus, these effects could be due to the function of cytosolic RHEB in the activation of the canonical mTORC1 pathway in the cytosol, or to a nuclear function of RHEB.

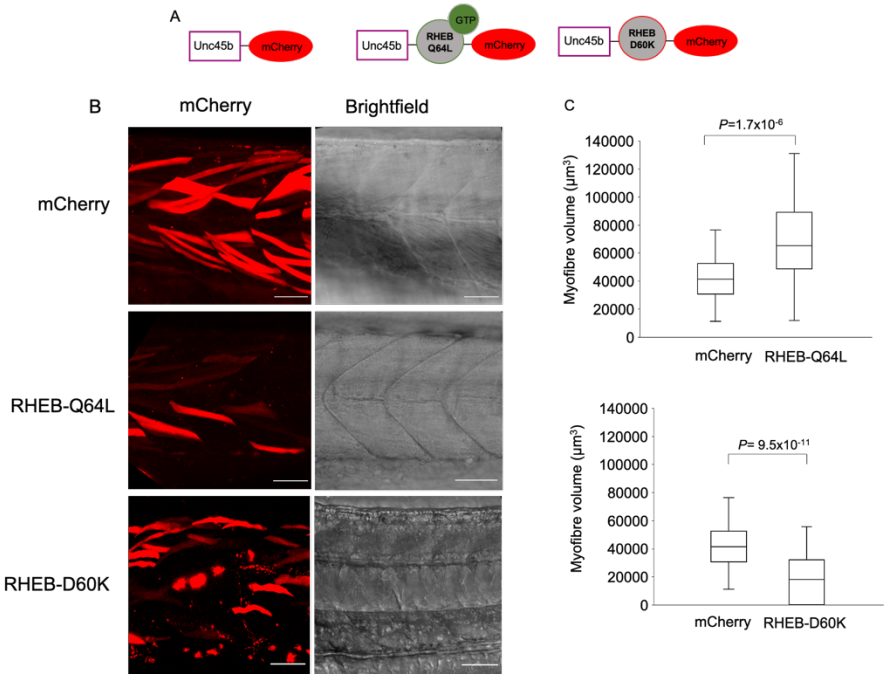

Figure 18 - Effect of RHEB mutants on myofibre size. A) Schematic representation of the constructs used. **B, C)** Zebrafish embryos at the first cell stage were injected with plasmids in which the unc45b promoter drives the expression of either mCherry, RHEB- Q64L or RHEB-D60K fused to mCherry. **(B)** The trunk region of the 2dpf embryos were imaged by confocal microscopy. The images of the mCherry and bright field channels represent a restricted expression in the myofibres (Scale bar: 50 µm). **(C)** Embryos were imaged by confocal microscopy to generate Z-stacks covering the entire depth of the embryo trunk region. The mCherry-positive myofibres were segmented in 3D using Imaris to determine their volume. Five animals with 20 myofibres per animal were analyzed per group.

To address this question, the RHEB mutants were first targeted to the cytosol by fusing them to the strong nuclear export signal (NES) of the mitogen-activated protein kinase kinase (MEK) (Adachi et al. 2000). I then tested the effect of these cytosolic RHEB mutants on zebrafish myofibre size. RHEB-Q64L-NES, RHEB-D60K-NES and mCherry-NES were injected in the single cell stage embryos (Fig. 19A) and raised for two days. Confocal imaging confirmed that RHEB constructs were localised only in the cytoplasm of myofibres at 2dpf (Fig. 19B). In order to quantify the volume of the whole myofibre, a green fluorescent protein (eGFP) was introduced to the constructs using the self-cleaving peptide T2A. I observed a significant increase in the volume of myofibres which expressed RHEB-Q64L-NES at 2dpf compared to the mCherry control. Conversely, the volume of myofibres expressing RHEB-D60K-NES was significantly reduced (Fig. 19C). These results are compatible with the known function of RHEB in the activation of the canonical mTORC1 pathway in the cytosol.

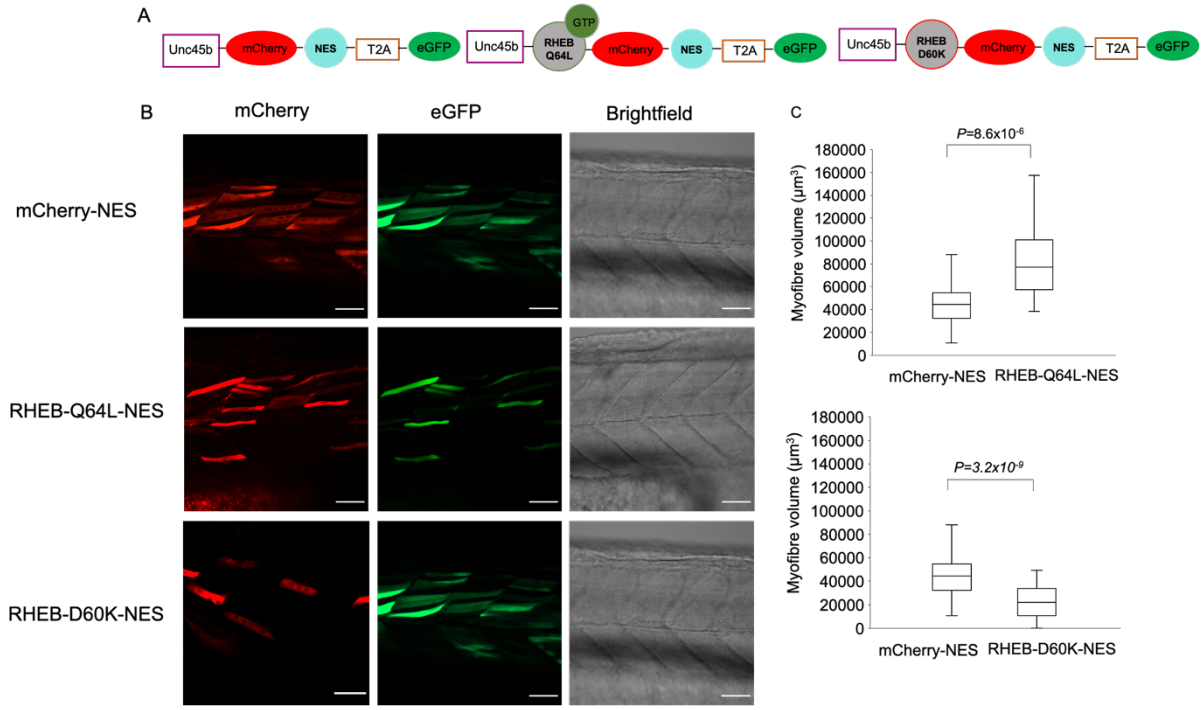

Figure 19 - Effect of cytosolic RHEB mutants on myofibre size. A) Schematic representation of the constructs used. **(B, C)** Zebrafish embryos at the first cell stage were injected with plasmids in which the unc45b promoter drives the expression of either mCherry-NES, RHEB- Q64L-NES or RHEB-D60K-NES fused to mCherry. In order to visualise the whole fibres for quantifying the volume, the constructs also include T2A-eGFP. **(B)** The trunk region of the 2dpf embryos were imaged by confocal microscopy. The images of the mCherry, eGFP and bright field channels represent a restricted expression of the RHEB mutants in the myofibres cytosol (red) (scale bar: 50 µm). **(C)** Embryos were imaged by confocal microscopy to generate Z-stacks covering the entire depth of the embryo trunk region. The mCherry-positive myofibres were segmented in 3D using Imaris to determine their volume. Five animals with 20 myofibres per animal were analyzed per group.

In order to investigate the nuclear effect of RHEB on muscle growth, the strong nuclear localisation sequence (NLS) from Simian virus 40 (SV40) T antigen (Collas and Aleström, 1996), was introduced to the RHEB mutants (Fig. 20A).

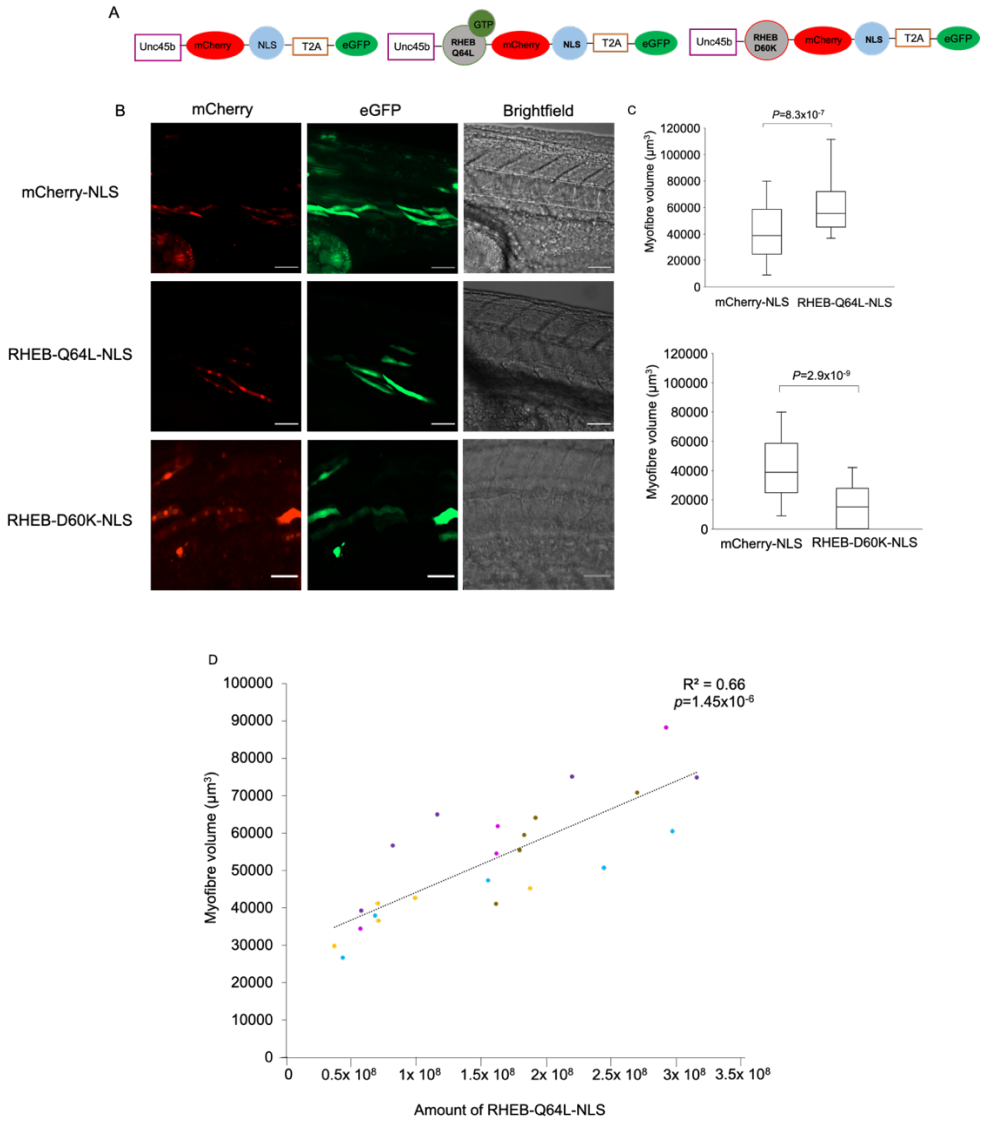

Figure 20 - Effect of nuclear RHEB mutants on myofibre size. Zebrafish embryos at the first cell stage were injected with plasmids in which the unc45b promoter drives the expression of either mCherry-NLS, RHEB-Q64L-NLS or RHEB-D60K-NLS fused to mCherry. In order to visualise the whole fibres for quantifying the volume, the constructs also include T2A-eGFP. **(A)** Schematic representation of the constructs used. **(B)** The trunk region of the 2dpf embryos were imaged by confocal microscopy. Representative images of the mCherry, eGFP and bright field channels are presented (scale bar: 50 µm). **(C)** Embryos were imaged by confocal microscopy to generate Z-stacks covering the entire depth of the embryo trunk region. The mCherry-positive myofibres were segmented in 3D using Imaris to determine their volume. Five animals with 20 myofibres per animal were analyzed per group. **(D)** The correlation between the volume of the myofibres expressing RHEB-Q64L-NLS and the expression level of the construct, assessed by the intensity of the mCherry signal was performed by linear regression analysis. The correlation coefficient (R^2) and the *P* value of the linear regression t-test are presented.

The expression of the RHEB constructs was clearly visible in the myofibres nuclei (Fig. 20B). The volume of the myofibres expressing the RHEB-Q64L-NLS mutant was significantly increased at 2 dpf compared to the mCherry control (Fig. 20C). This effect was dose-dependent, as the myofibre volume was linearly correlated to the amount of expressed RHEB-Q64L-NLS (Fig. 20D). Conversely, the volume of the myofibres expressing the RHEB-D60K-NLS mutant was significant decreased. Furthermore, I observed a lot of collapsed myofibres among RHEB-D60K-NLS expressed cells (Fig. 20C). These results show that nuclear RHEB promotes myofibre growth.

3.2.3 Mechanism of the effect of nuclear RHEB

3.2.3.1 Nuclear effect of RHEB on myofibre size: Myofibre hypertrophy or myocyte fusion?

The increase in myofibre size occurs by either the incorporation of more nuclei by the fusion of myocytes or by hypertrophy of the myofibres (Wagner, 1996). In mammals, muscle growth via an increase in the number of myonuclei through myocyte fusion mostly stops after birth, and therefore in adults the increase in muscle mass is mostly related to myofibre hypertrophy. In contrast, in teleost fish, reaching the ultimate body size is the results of a combination between myofibre hypertrophy and myocytes fusion as a result of multiple waves of myogenesis during adult life (Rossi and Messina, 2014; Vo et al., 2016). To investigate whether the effect of the nuclear-targeted RHEB-Q64L mutant on myofibre size in zebrafish embryos is related to hypertrophy or myocyte fusion, I counted the number of myonuclei per myofibre expressing RHEB- Q64L in the nucleus. There was no significant difference in the number of myonuclei between myofibres expressing RHEB-Q64L-NLS and those expressing the mCherry-NLS control (Fig. 21). Thus, the nuclear effect of RHEB on myofibre size is not related to myocyte fusion but to myofibre hypertrophy.

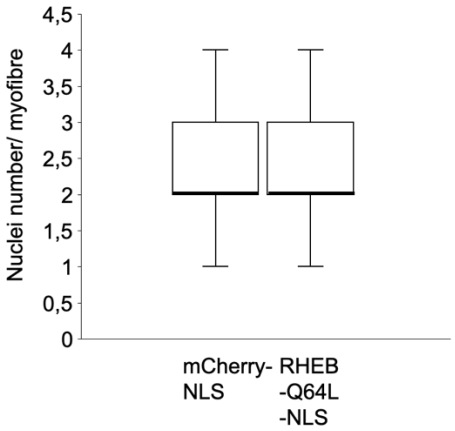

Figure 21 –Effect of nuclear RHEB on myocyte fusion. The trunk region of the 2dpf embryos injected with RHEB-Q64L-NLS or mCherry-NLS was imaged by confocal microscopy. The mCherry-positive myofibres were segmented in 3D using Imaris to count their myonuclei as an index of myocyte fusion. Five animals with 20 myofibres per animal were analyzed per group.

3.2.3.2 Dependence on mTORC1 of the effect of RHEB on myofibre size

Given that mTORC1 is the main driver of myofibre hypertrophy, I investigated whether the effect of nuclear RHEB is mTORC1-dependent. Two approaches were used to address this question, I introduced another mutation in the constitutive active RHEB-Q64L mutant, I39K, to reduce its interaction with mTORC1 (Ma et al., 2008), and treated the RHEB-Q64L injected embryos with rapamycin, a potent chemical inhibitor of mTORC1 (Reijnders et al., 2017).

I first examined the effect of the cytosolic RHEB-I39K-Q64L on muscle growth *in vivo* in the zebrafish (Fig. 22A-B). mCherry-NES and RHEB-Q64L-NES injected embryos were used as controls. While the embryos injected with RHEB-Q64L-NES showed a significant increase in myofibre size, as compared to mCherry-NES, the embryos injected with RHEB-I39K-Q64L-NES did not (Fig. 22C). Thus, reducing the interaction between the mTORC1 and RHEB via the I39K mutation, abolishes the ability of the cytosolic constitutively active RHEB mutant to increase muscle fibre size. This result confirms that cytosolic RHEB regulate muscle growth via the activation of the canonical mTORC1 pathway. Furthermore, this result validates the use of the I39K mutation to investigate the mTOR dependency of the nuclear function of RHEB.

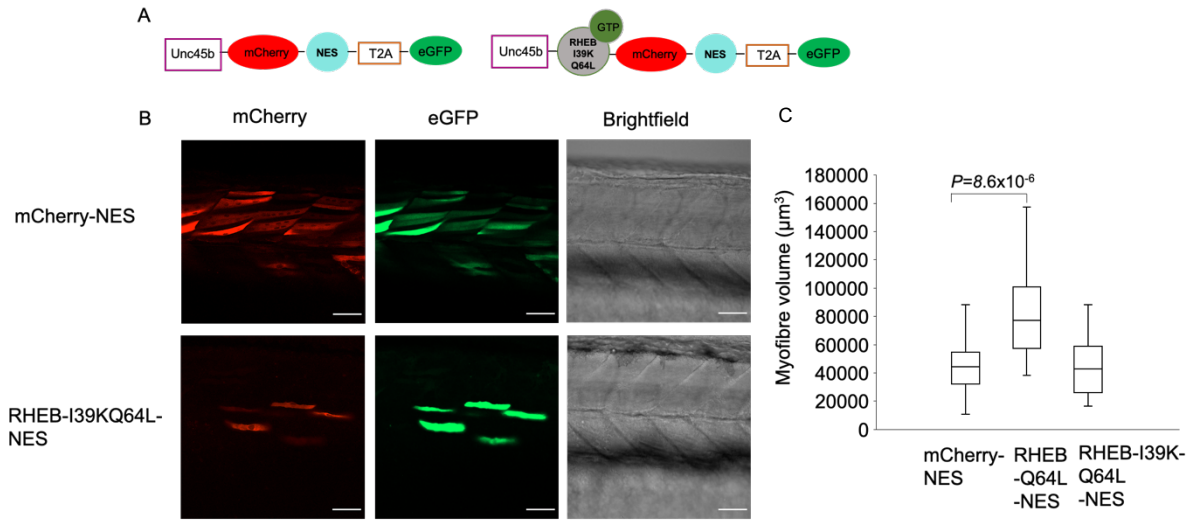

Figure 22 - Effect of cytosolic constitutive active RHEB-I39K mutant on myofibre size. Zebrafish embryos at the first cell stage were injected with plasmids in which the unc45b promoter drives the expression of either mCherry-NES, RHEB-Q64L-NES or RHEB-I39K-Q64L-NES fused to mCherry. In order to visualise the whole fibres for quantifying the volume, the constructs also include T2A-eGFP. **(A)** Schematic representation of the constructs used. **(B)** The trunk region of the 2dpf embryos was imaged by confocal microscopy. Representative images of the mCherry, eGFP and bright field channels are shown (scale bar: 50 µm). **(C)** Embryos were imaged by confocal microscopy to generate Z-stacks covering the entire depth of the embryo trunk region. The mCherry-positive myofibres were segmented in 3D using Imaris to determine their volume. Five animals with 20 myofibres per animal were analyzed per group.

I thus tested the effect of the nuclear-targeted RHEB-I39K-Q64L on muscle growth in the zebrafish embryo (Fig. 23A-B). A significant increase in the size of myofibres which expressed RHEB-I39K- Q64L in the nucleus was observed compare to the mCherry-NLS control at 2dpf (Fig. 23C). The size of the myofibres expressing RHEB-I39K-Q64L-NLS was even significantly larger than those expressing RHEB-Q64L-NLS. This result suggests that nuclear RHEB regulates muscle growth in an mTORC1 independent manner.

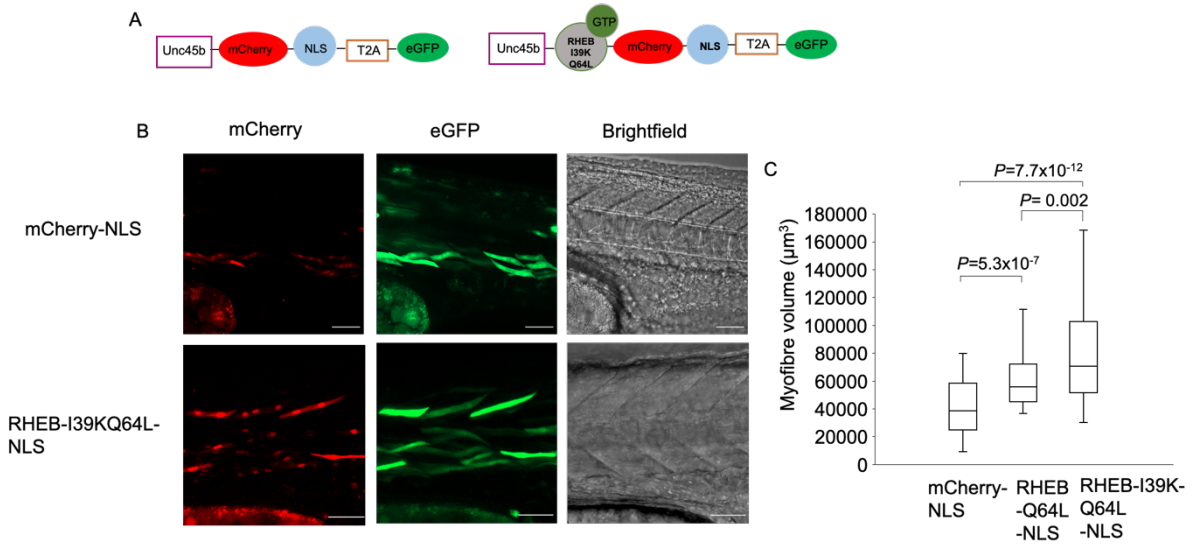

Figure 23 - Effect of nuclear constitutive active RHEB-I39K mutant on myofibre size. Zebrafish embryos at the first cell stage were injected with plasmids in which the unc45b promoter drives the expression of either mCherry-NLS, RHEB-Q64L-NLS or RHEB-I39K-Q64L-NLS fused to mCherry. In order to visualise the whole fibres for quantifying the volume, the constructs also include T2A-eGFP. **(A)** Schematic representation of the constructs used. **(B)** The trunk region of the 2dpf embryos was imaged by confocal microscopy. Representative images of the mCherry, eGFP and bright field channels are shown (scale bar: 50 µm). **(C)** Embryos were imaged by confocal microscopy to generate Z-stacks covering the entire depth of the embryo trunk region. The mCherry-positive myofibres were segmented in 3D using Imaris to determine their volume. Five animals with 20 myofibres per animal were analyzed per group.

To confirm this result, I used rapamycin to inhibit mTORC1. To do so, rapamycin was co-injected together with either RHEB-Q64L-NES or RHEB-Q64L-NLS, or their respective control constructs mCherry-NES and mCherry-NLS (Fig. 24 A). Although the increase in myofibre size elicited by RHEB-Q64L-NES was totally abolished by the rapamycin treatment. (Fig. 24 B), that elicited by RHEB-Q64L-NLS was not affected by rapamycin (Fig. 24 C).

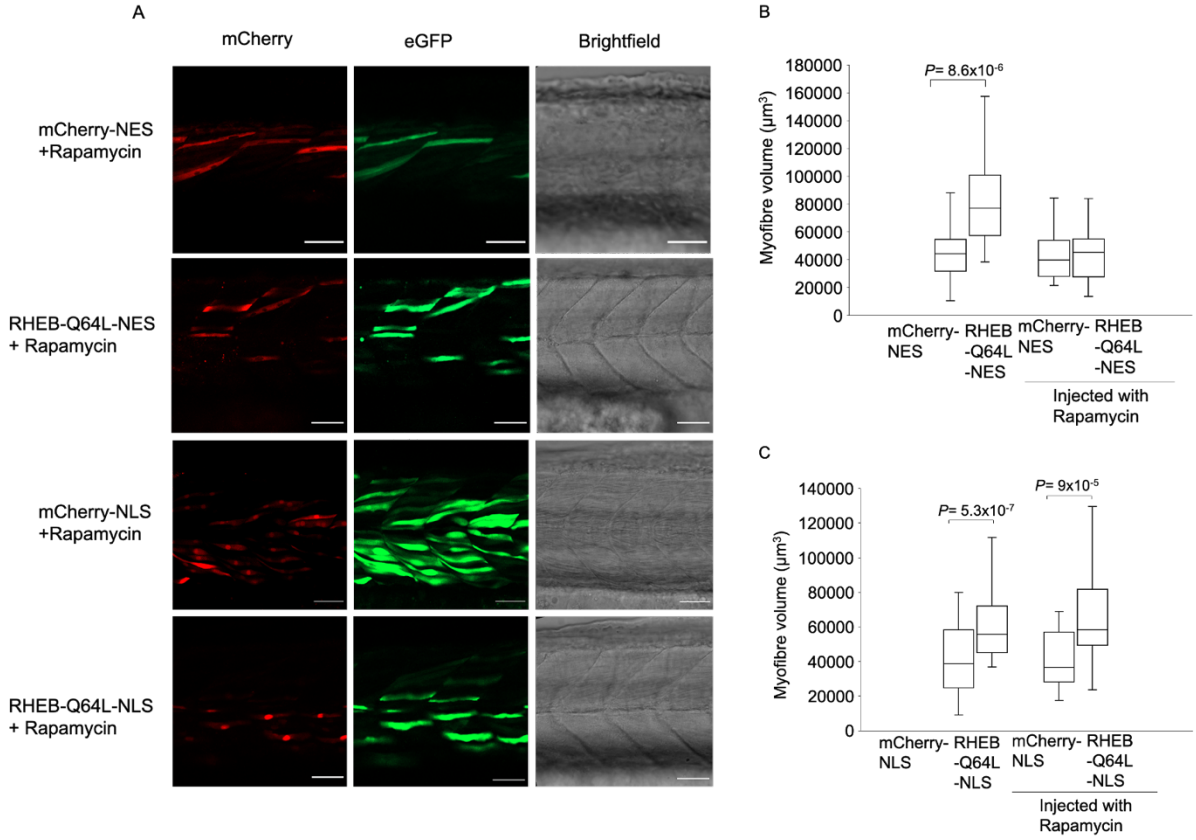

Figure 24 - Effect of Rapamycin on RHEB-mediated increase in myofibre size. Zebrafish embryos at the first cell stage were co-injected with rapamycin together with plasmids in which the unc45b promoter drives the expression of either mCherry-NLS, RHEB-Q64L-NLS fused to mCherry, mCherry-NES or RHEB-Q64L-NES fused to mCherry. In order to visualise the whole fibres for quantifying the volume, the constructs also include T2A-eGFP. **(A)** The trunk region of the 2dpf embryos was imaged by confocal microscopy. Representative images of the mCherry, eGFP and bright field channels are shown (scale bar: 50 µm). **(B)** Embryos were imaged by confocal microscopy to generate Z-stacks covering the entire depth of the embryo trunk region. The mCherry-positive myofibres were segmented in 3D using Imaris to determine their volume. Five animals with 20 myofibres per animal were analyzed per group.

Taken together these results show that the nuclear effect of RHEB on myofibre growth is independent of mTORC1.

3.2.3.3 Effect of nuclear RHEB on rRNA transcription

The increase in protein synthesis capacity is essential for myofibre hypertrophy and is associated with the increase in ribosomal DNA (rDNA) transcription by RNA polymerase I (Pol I), leading to ribosomal RNA (rRNA) accumulation, and to an increase in ribosome content (von Walden et al., 2012). Cytosolic RHEB-mTORC1

and nuclear mTOR are involved in this process (Ghosh et al., 2014; Mayer et al., 2004; von Walden et al., 2016). However, the role of nuclear RHEB in stimulating rRNA transcription is unknown.

Ribosome biogenesis occurs in the nucleolus (Abraham et al., 2020; Chen and Huang, 2001). Therefore, I first studied whether RHEB is localised in the nucleolus. Immunofluorescence staining showed no RHEB immunoreactivity in nucleoli, which were visualized by an anti-fibrillarin antibody (Fig. 25A). To confirm this result, I also performed subcellular fractionations. RHEB was not detected in the nucleolus as shown by western blot analysis (Fig. 25B).

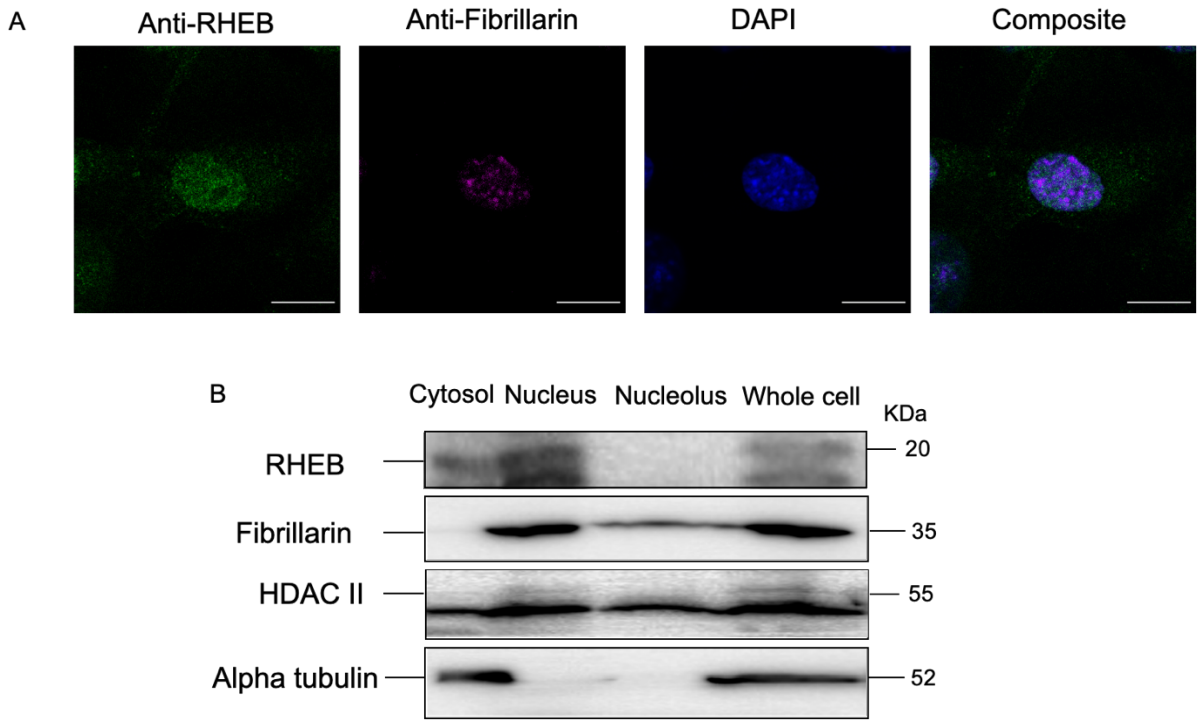

Figure 25 - RHEB is not localised in the nucleolus. C2C12 cells were seeded at low density and kept in proliferation medium for one day. **(A)** Cells were fixed and subjected to immunofluorescence analysis using antibodies against RHEB (green) and Fibrillarin (nucleolar marker, red). Nuclei were counterstained using DAPI (blue) and imaged by confocal microscopy. Representative images are shown (Scale bar: 10µm). **(B)** Representative Western Blot of cytosolic, nuclear, nucleolar fractions and whole cell lysates of C2C12 cells probed with an anti-RHEB antibody, an anti-Fibrillarin antibody as a marker of nucleolus, anti-HDAC II antibody as nuclear marker and anti-alpha tubulin antibody as a cytosolic marker. The presented western blot is representative of three independent experiments.

Yet, nuclear RHEB could regulate rRNA transcription in an indirect manner. To address this question, we used a luciferase reporter gene to measure the transcription of the 45s pre-rRNA. This construct consists of a zebrafish rDNA promoter and terminator so that it is transcribed by RNA Pol I. However, in order to quantitate the transcription, the luciferase reporter gene (NanoLuc) coding sequence should be translated. For this reason, we flanked the NanoLuc coding sequence by a 5' Internal Ribosome Entry Site (IRES) and a 3' polyadenylation signal (Fig. 26A). This reporter was transfected in Zebrafish PAC2 fibroblasts together with either RHEB-Q64L-NLS or mCherry-NLS as a negative control. As a positive control, RHEB-Q64L-NES, which is expected to increase 45s rRNA transcription via the canonical mTORC1 pathway, as well as mCherry-NES as a negative were used. In order to normalize for possible differences in transfection efficiency, PAC2 cells were also co-transfected with an expression vector for Firefly luciferase which is translated from the same IRES (Fig. 26A). As expected, RHEB-Q64L-NES, as compared to mCherry-NES, significantly increased 45s rRNA transcription. Similarly, cells which expressed RHEB-Q64L-NLS showed a significant increase in rRNA transcription (Fig. 26B). These results indicate that nuclear RHEB stimulates rRNA transcription, most likely in an indirect manner given that RHEB is not present in the nucleolus.

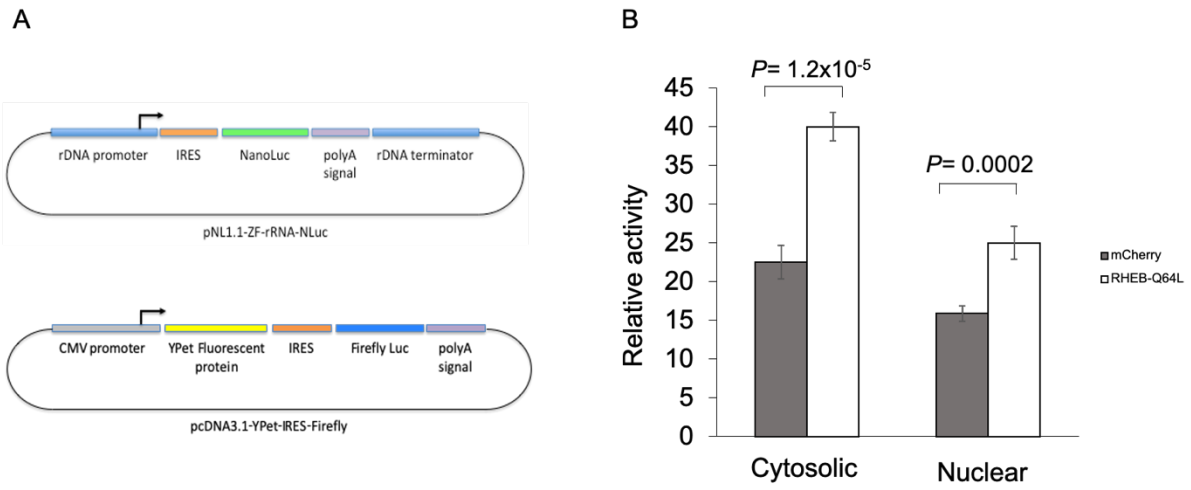

Figure 26 – Effect of RHEB on rRNA transcription. A) Schematic representation of the reporters used. **(B)** PAC2 cells were transfected with the NanoLuc rRNA reporter together with an expression vector for Firefly luciferase for normalization, and either expression vector for nuclear targeted RHEB-Q64L, nuclear targeted mCherry as control vector, or cytoplasmic RHEB-Q64L and cytoplasmic mCherry as a control. Cells were serum starved for 24 h after serum, lysed, and NanoLuc and Firefly luciferase activities were determined. The relative Luciferase activity, i.e. NanoLuc activity normalized against Firefly activity, is presented as mean ± SD of three independent experiments.

4. Discussion

In this work, I have investigated two aspects of skeletal muscle plasticity, muscle regeneration and the regulation of myofibre size.

In the first part, I have unravelled the role of nTRIP6 in the temporal control of myogenesis. At early stages, nTRIP6 temporarily represses myoblast differentiation, allowing proper myocyte differentiation and fusion at later stages. In the second part, I have uncovered that in the zebrafish embryo nuclear RHEB regulates myofibre growth via an mTORC1-independent mechanism.

4.1 Skeletal muscle regeneration

Our first finding is that nTRIP6 prevents premature differentiation. Indeed, blocking nTRIP6 function using a nuclear-targeted peptide (Diefenbacher et al., 2014; Kemler et al., 2016) accelerated early differentiation. Given the coordination between cell cycle exit and entry into differentiation (Singh and Dilworth, 2013), the accelerated expression of early differentiation markers upon blocking nTRIP6 function could have been due to an accelerated cell cycle exit. However, the blocking peptide had no effect on myoblast proliferation and cell cycle exit. Thus, nTRIP6 appears to mainly repress early differentiation. What could be the mechanism of such an effect of nTRIP6? Our group has shown that this transcriptional co-regulator exerts a co-repressor function for the transcription factor MEF2C in myoblasts (Kemler et al., 2016). Although involved in late differentiation and fusion (Hinits and Hughes, 2007; Potthoff et al., 2007), MEF2C is already expressed during the myoblast proliferation phase (Liu et al., 2014; Mokalled et al., 2012) and its activity must be repressed to prevent premature differentiation. Therefore, I propose that nTRIP6 prevents premature differentiation at least in part by repressing MEF2C activity during the late myoblast proliferation phase.

We also observed that blocking nTRIP6 function inhibits late differentiation and fusion. The lack of nTRIP6 activity delayed the expression of the late differentiation genes Tnni2 and MYH3. The expression of both these genes is directly (Tnni2) or indirectly

(MYH3) driven by MEF2C (Nakayama et al., 1996). Thus, one would have expected an increase in their expression upon blocking the co-repressor function of nTRIP6 for MEF2C. An explanation for this apparently contradictory result is given by the dynamics of nTRIP6 expression during myogenesis. Indeed, previous results of our group have shown that nTRIP6 expression is very low at the beginning of myoblast proliferation. It is then transiently up-regulated at the transition between myoblast proliferation and differentiation to reach a maximum towards the late proliferation phase, then it progressively decreases along with late differentiation and fusion (Kemler, 2017). Thus, nTRIP6 expression is maximal at the transition between proliferation and differentiation, when MEF2C activity has to be repressed, but back to very low levels for late differentiation and fusion, when MEF2C activity is required. Therefore, the inhibitory effect of blocking nTRIP6 function on late differentiation and fusion seems to be an indirect consequence of the loss of nTRIP6 function at earlier time points. The resulting premature activation of MEF2C and the subsequent premature expression of proteins of the contractile apparatus could be the cause of the impaired fusion observed upon blocking nTRIP6 function. Taken together, nTRIP6 prevents premature myoblast differentiation to allow proper myocyte differentiation and fusion at later stages.

The *in vivo* relevance of these findings is confirmed by our results on muscle regeneration in mice in which *Trip6* is knocked out in satellite cells. I observed an increase in the number of MYOD-expressing cells in *Trip6*^{scko} regenerating muscle. Given that both myoblasts and myocytes express MYOD (Füchtbauer and Westphal, 1992; Yablonka-Reuveni and Rivera, 1994), this increase could be due to either an increased myoblast proliferation or a decreased myocyte fusion. I did not observe an increased number of proliferating cells (myoblasts) in the *Trip6*^{scko} regenerating muscle but rather a decrease at 14 dpi. Thus, the increased number of MYOD-positive cells corresponds to an increased number of myocytes, which matches the accelerated early differentiation that was observed upon blocking nTRIP6 function *in vitro*. Furthermore, the delay in the increase in myofibre size in the *Trip6*^{scko} regenerating muscle despite the increased number of myocytes is clearly indicative of a delay in myocyte fusion. This observation is very similar to the inhibitory effect the blocking peptide on myocyte fusion *in vitro*. Therefore, the deregulated dynamics of muscle

regeneration in the *Trip6*^{scko} animal is very reminiscent of the deregulated dynamics of *in vitro* myogenesis that we observed upon blocking nTRIP6 function.

Finally, in the *Trip6*^{scko} knock out animals the expression of both the long cytosolic isoforms (TRIP6) and short nuclear isoform (nTRIP6) is lost. Thus, the observed regeneration phenotype could be due to the loss of either nTRIP6 in the nucleus or TRIP6 in the cytosol or both. The main function of the cytosolic isoform TRIP6, like that the other members of the ZYXIN family of focal adhesion LIM domain proteins (Smith et al., 2014), is to regulate adhesion (Lin and Lin, 2011; Willier et al., 2011). However, no general phenotype was observed upon the total deletion of the *Trip6* gene in the mouse, as could have been expected from the loss of such an important function (Shukla et al., 2019). This observation, together with the absence of obvious phenotypes in the *Zyxin* (Hoffman et al., 2003), *Lpp* (Vervenne et al., 2009) , *Ajuba* (Pratt et al., 2005), *Limd*1 (Feng et al., 2007) and *Migfilin* (Moik et al., 2011) knockout mice, strongly suggests that TRIP6 and the other ZYXIN family members are redundant for their cytosolic function. It is therefore unlikely that the muscle regeneration phenotype that we observed in *Trip6*^{scko} animals is due to the loss of the cytosolic function of TRIP6. Furthermore, the similarities between the phenotype of the *Trip6*^{scko} knockout mouse and the *in vitro* effects of the nTRIP6 blocking peptide, which is targeted to the nucleus and can therefore only block the function of nTRIP6, very strongly suggests that the delayed muscle regeneration in the knockout is a consequence of a loss of nTRIP6.

4.2 Muscle growth

In the second part of this thesis, I report that nuclear RHEB promotes myofibre growth in an mTORC1-independent manner. My first observation is that while RHEB is mostly cytosolic in adult zebrafish myofibres, it is nearly exclusively nuclear in embryonic myofibres. Although RHEB is reported to be associated with the lysosomal membrane and other membrane compartment (Buerger et al., 2006; Takahashi et al., 2005), a nuclear localisation has already been described (Yadav et al., 2013). However, my results represent the first report of a nearly exclusive nuclear localisation. RHEB is

targeted to lysosomal and other membranes via the farnesylation of its C-terminal CAAX motif (Buerger et al., 2006; Clark et al., 1997; Moores et al., 1991). In this regard, RHEB differs from the other members of the RAS superfamily, which contain additional membrane-targeting motifs. For example, in addition to the farnesylated CAAX motif, H-RAS and K-RAS-4B also harbour palmitoylated cysteines and polybasic domains in their hypervariable regions, which together contribute to their enrichment at the plasma membrane (Takahashi et al., 2005). The hypervariable region of RHEB does not harbour any of these additional membrane-targeting signal and RHEB is therefore not specifically targeted to the plasma membrane. RHEB CAAX motif is necessary and sufficient for transient farnesylation-dependent membrane interactions. Thus, RHEB has a weak interaction with the lysosome via farnesylation, which is sufficient to activate mTORC1 (Angarola and Ferguson, 2019). However, it has been recently shown that RHEB localisation is not restricted to the surface of lysosome but that it can also scatter in the cytosol (Ferguson and Angarola, 2020). However, whether this “free” cytosolic form of RHEB as well as RHEB in the nucleus are also farnesylated is not known. My results *in vitro*, in cells where RHEB is both cytosolic and nuclear, showed that a farnesyl transferase inhibitor increased the nuclear localisation of RHEB, suggesting that nonfarnesylated RHEB passively diffuses to the nucleus where it can accumulate. Thus, two pools of RHEB might coexist in the cell, one farnesylated and retained at membranes, and the other nonfarnesylated and freely diffusing to and accumulating in the nucleus. However, such a nuclear accumulation implies that RHEB is somehow retained within this compartment, presumably via an interaction with resident proteins. Whether a lack of farnesylation is the cause of the nearly exclusive nuclear localisation of RHEB in embryonic myofibres remains to be investigated. The striking difference in the subcellular localisation of RHEB between embryonic and adult myofibres strongly suggests a major difference in the control of myofibre growth. In adult zebrafish, farnesylated RHEB associated to lysosomal membranes is most likely involved in the activation of the canonical mTORC1 pathway, which is required for muscle growth in response to various hypertrophic stimuli (Khor et al., 2019). In the embryo, the nuclear localisation of RHEB strongly suggests that muscle growth is not driven primarily by the canonical mTORC1 pathway. Thus, nuclear RHEB appears to be a feature of fast-growing muscles.

The second prominent finding of this work is that nuclear RHEB promotes embryonic myofibre growth. In the embryo, over-expression of the nuclear-targeted, constitutively active mutant RHEB-Q64L (Scheffzek, 1997) increased myofibre size, while the nuclear-targeted dominant negative mutant RHEB-D60K decreased myofibre size. Given that the nuclear localisation of the RHEB mutants was achieved through fusion to an NLS, which promotes cytosol to nucleus shuttling, one might argue that during its residence time in the cytosol, RHEB-Q64L-NLS might have activated mTORC1 and thereby increased myofibre size. However, while rapamycin inhibited the growth promoting effect of the mutant when targeted to the cytosol, it did not inhibit the effect of the nuclear-targeted mutant. Similarly, the I39K mutation in RHEB switch one region which reduces mTORC1-RHEB interaction (Ma et al., 2008) abolished the growth promoting effect of RHEB-Q64L when targeted to the cytosol, but not when targeted to the nucleus. Therefore, the increase in myofibre growth is indeed a direct consequence of RHEB- Q64L presence in the nucleus. Furthermore, these results clearly show that nuclear RHEB regulates myofibre growth via an mTORC1-independent mechanism.

What could be the mechanism of nuclear RHEB mediated myofibre growth? The two main mechanisms that can drive an increase in myofibre volume are either increased myocyte fusion or increased protein synthesis (Mommsen, 2001). Given that myogenic differentiation and fusion is negatively regulated by RHEB (Ge et al., 2011), the growth promoting effect of nuclear RHEB is unlikely to be due to an effect on myocytes fusion. This putative mechanism is further excluded by my results showing that nuclear targeted RHEB-Q64L does not increase the number of myonuclei per myofibre. Thus, the myofibre growth promoted by nuclear RHEB most likely relies on increased protein synthesis. One mechanism could be through ribosomal biogenesis (Liu et al., 2014b). Indeed, ribosomal protein synthesis and ribosomal DNA (rDNA) transcription by RNA Pol I are initial events that are required to increase the protein synthesis capacity during muscle hypertrophy (von Walden et al., 2016). My results showed that nuclear targeted RHEB-Q64L promotes an increase in rRNA transcription, suggesting that this might be one of the mechanisms of nuclear RHEB-mediated myofibre growth. However, RHEB was not localised to the nucleolus, where rRNA transcription takes place. rRNA synthesis by RNA Pol I requires the cooperative interaction of the transcription initiation factors TIF-IA, B and the upstream binding

factor UBF-1. Given that TIF-IA plays an essential role in the regulation of rRNA synthesis in growing myofibres and that its activity is regulated by diverse extracellular signals like resistance training and growth factors (Fyfe et al., 2018; Ghosh et al., 2014), it is tempting to speculate that nuclear RHEB may indirectly stimulate rRNA transcription in part via TIF-IA.

Another possible mechanism of mTORC1-independent effect of nuclear RHEB on myofibre size could be through Notch signaling which plays a key role in skeletal muscle maintenance and growth (Al Jaam et al., 2016). Indeed, RHEB was shown to stimulate Notch signaling in a mTORC1-independent manner: the activated form of Notch, NotchR intracellular domain (NICD), interacts with RHEB in the cytoplasm of brown adipocytes (Meng et al., 2019). However, NICD due to its nuclear localisation domain localised mainly in the nucleus of myofibres (Bröhl et al., 2012). A possibility is therefore that nuclear RHEB promotes the interaction of NICD with the primary transcriptional mediator of Notch signaling, Rbpj, and with mastermind-like (Maml), to initiate the expression of direct Notch target genes such as HeyL which is required for muscle hypertrophy (Fukuda et al., 2019; Jarriault et al., 1995). Therefore, RHEB might regulate myofibre size in a mTORC1-independent manner via the Notch signaling pathway.

Furthermore, in brown adipocytes, RHEB promotes a Notch-dependent activation of the PKA signaling pathway, which in turn activates the cyclic AMP (cAMP) response element binding protein (CREB) transcription factor (Meng et al., 2019). Interestingly, CREB stimulates the expression of genes that are involved in the regulation of skeletal muscle mass (Rahnert et al., 2016). For example, the Nr4a family nuclear hormone receptors and the transcription factor JunB, which are both direct CREB target genes, are involved in myofibre hypertrophy (Kawasaki et al., 2011; Raffaello et al., 2010). Thus, it is tempting to speculate that nuclear RHEB promotes myofibre growth in a mTORC1-independent mechanism at least in part through the Notch signaling pathway, although additional experiments have to be performed to dissect these possibilities.

4.3 Conclusion

In this thesis work, I have investigated two essential aspects of skeletal muscle plasticity, muscle regeneration and muscle growth.

The first part revealed a novel function for the transcriptional co-regulator nTRIP6 in the regulation of regenerative myogenesis. I propose that during the late myoblast proliferation phase, nTRIP6, whose expression is transiently upregulated (Kemler, 2017), prevents premature differentiation. This early anti-differentiation function appears necessary to allow a timely myocyte differentiation and fusion at later stages. Thus, nTRIP6 modulates the dynamics of myogenesis *in vitro* and of skeletal muscle regeneration *in vivo* by preventing premature differentiation.

The second part of this work uncovered an unconventional function of the mTORC1 activator RHEB. In zebrafish embryo myofibres, RHEB, which is nearly exclusively localised in the nucleus promotes the growth of myofibres in an mTORC1-independent manner. Although some reports have described mTORC-1 independent functions of RHEB as well as its nuclear localisation, to my knowledge, this work represents the first description of an mTORC1 independent function of RHEB in the nucleus. This nuclear function appears essential to regulate the growth of myofibres in the embryo.

Together, this work illustrates the diversity and complexity of the molecular mechanisms involved in the regulation of skeletal muscle plasticity.

5. References

Abraham, K.J., Khosraviani, N., Chan, J.N.Y., Gorthi, A., Samman, A., Zhao, D.Y., Wang, M., Bokros, M., Vidya, E., Ostrowski, L.A., et al. (2020). Nucleolar RNA polymerase II drives ribosome biogenesis. Nature *585*, 298–302.

Adachi, M., Fukuda, M., and Nishida, E. (2000). Nuclear export of MAP kinase (ERK) involves a MAP kinase kinase (MEK)-dependent active transport mechanism. J. Cell Biol. *148*, 849–856.

Angarola, B., and Ferguson, S.M. (2019). Weak membrane interactions allow Rheb to activate mTORC1 signaling without major lysosome enrichment. Mol. Biol. Cell *30*, 2750–2760.

Aoyagi, S., and Archer, T.K. (2008). Dynamics of coactivator recruitment and chromatin modifications during nuclear receptor mediated transcription. Mol. Cell. Endocrinol. *280*, 1–5.

Baar, K., and Esser, K. (1999). Phosphorylation of p70(S6k) correlates with increased skeletal muscle mass following resistance exercise. Am. J. Physiol. - Cell Physiol. *276*, 120–127.

Basso, A.D., Mirza, A., Liu, G., Long, B.J., Bishop, W.R., and Kirschmeier, P. (2005). The farnesyl transferase inhibitor (FTI) SCH66336 (lonafarnib) inhibits Rheb farnesylation and mTOR signaling: Role in FTI enhancement of taxane and tamoxifen anti-tumor activity. J. Biol. Chem. *280*, 31101–31108.

Bentzinger, C.F., Wang, Y.X., and Rudnicki, M.A. (2012). Building Muscle: Molecular Regulation of Myogenesis. Cold Spring Harb. Perspect. Biol. *4*, a008342–a008342.

Blaauw, B., Mccarthy, J.J., and Yoon, M.-S. (2017). mTOR as a Key Regulator in Maintaining Skeletal Muscle Mass. Front. Physiol. Front. Physiol *8*, 88.

Bonaldo, P., and Sandri, M. (2013). Cellular and molecular mechanisms of muscle atrophy. DMM Dis. Model. Mech. *6*, 25–39.

Bröhl, D., Vasyutina, E., Czajkowski, M.T., Griger, J., Rassek, C., Rahn, H.P., Purfürst, B., Wende, H., and Birchmeier, C. (2012). Colonization of the Satellite Cell Niche by Skeletal Muscle Progenitor Cells Depends on Notch Signals. Dev. Cell *23*, 469–481.

Buerger, C., DeVries, B., and Stambolic, V. (2006). Localization of Rheb to the

endomembrane is critical for its signaling function. Biochem. Biophys. Res. Commun. *344*, 869–880.

Cadot, B., Gache, V., and Gomes, E.R. (2015). Moving and positioning the nucleus in skeletal muscle-one step at a time. Nucleus *6*, 373–381.

Carosio, S., Berardinelli, M.G., Aucello, M., and Musarò, A. (2011). Impact of ageing on muscle cell regeneration. Ageing Res. Rev. *10*, 35–42.

Chal, J., and Pourquié, O. (2017). Making muscle: skeletal myogenesis *in vivo* and *in vitro*. Development *144*, 2104–2122.

Chen, D., and Huang, S. (2001). Nucleolar components involved in ribosome biogenesis cycle between the nucleolus and nucleoplasm in interphase cells. J. Cell Biol. *153*, 169–176.

Chen, S.L., Loffler, K.A., Chen, D., Stallcup, M.R., and Muscat, G.E.O. (2002). The coactivator-associated arginine methyltransferase is necessary for muscle differentiation: CARM1 coactivates myocyte enhancer factor-2. J. Biol. Chem. *277*, 4324–4333.

Chen, Y., Gucek, M., Puertollano, R., and Martina, J. a. (2012). MTORC1 functions as a transcriptional regulator of autophagy by preventing nuclear transport of TFEB. Autophagy *8*, 877–876.

Choi, S., Sadra, A., Kang, J., Ryu, J.R., Kim, J.H., Sun, W., and Huh, S.O. (2019). Farnesylation-defective rheb increases axonal length independently of mTORC1 activity in embryonic primary neurons. Exp. Neurobiol. *28*, 172–182.

Chromiak, J.A., and Antonio, J. (2008). Skeletal Muscle Plasticity. In Essentials of Sports Nutrition Study Guide, J. Antonio, D. Kalman, J.R. Stout, M. Greenwood, D.S. Willoughby, and G.G. Haff, eds. (Totowa, NJ: Humana Press), pp. 16–36.

Ciciliot, S., and Schiaffino, S. (2010). Regeneration of Mammalian Skeletal Muscle: Basic Mechanisms and Clinical Implications. Curr. Pharm. Des. *16*, 906–914.

Clark, G.J., Kinch, M.S., Rogers-Graham, K., Sebti, S.M., Hamilton, A.D., and Der, C.J. (1997). The Ras-related Protein Rheb Is Farnesylated and Antagonizes Ras Signaling and Transformation. J. Biol. Chem. *272*, 10608–10615.

Collas, P., and Aleström, P. (1996). Nuclear localization signal of SV40 T antigen directs import of plasmid DNA into sea urchin male pronuclei in vitro. Mol. Reprod.

Dev. *45*, 431–438.

Cornelison, D.D.W., and Wold, B.J. (1997). Single-cell analysis of regulatory gene expression in quiescent and activated mouse skeletal muscle satellite cells. Dev. Biol. *191*, 270–283.

Danieli-Betto, D., Peron, S., Germinario, E., Zanin, M., Sorci, G., Franzoso, S., Sandonà, D., and Betto, R. (2010). Sphingosine 1-phosphate signaling is involved in skeletal muscle regeneration. Am. J. Physiol. - Cell Physiol. *298*, 550–558.

Dawid, I.B., Breen, J.J., and Toyama, R. (1998). LIM domains: Multiple roles as adapters and functional modifiers in protein interactions. Trends Genet. *14*, 156–162.

Diefenbacher, M., Sekula, S., Heilbock, C., Maier, J. V., Litfin, M., van Dam, H., Castellazzi, M., Herrlich, P., and Kassel, O. (2008). Restriction to Fos Family Members of Trip6-Dependent Coactivation and Glucocorticoid Receptor-Dependent Trans-Repression of Activator Protein-1. Mol. Endocrinol. *22*, 1767–1780.

Diefenbacher, M.E., Litfin, M., Herrlich, P., and Kassel, O. (2010). The nuclear isoform of the LIM domain protein Trip6 integrates activating and repressing signals at the promoter-bound glucocorticoid receptor. Mol. Cell. Endocrinol. *320*, 58–66.

Diefenbacher, M.E., Reich, D., Dahley, O., Kemler, D., Litfin, M., Herrlich, P., and Kassel, O. (2014). The LIM Domain Protein nTRIP6 Recruits the Mediator Complex to AP-1-Regulated Promoters. PLoS One *9*, e97549.

Dorrello, N.V., Peschiaroli, A., Guardavaccaro, D., Colburn, N.H., Sherman, N.E., and Pagano, M. (2006). S6K1- and TRCP-Mediated Degradation of PDCD4 Promotes Protein Translation and Cell Growth. Science. *314*, 467–471.

Edmondson, D.G., and Olson, E.N. (1990). Erratum: A gene with homology to the myc similarity region of MyoD1 is expressed during myogenesis and is sufficient to activate the muscle differentiation program. Genes Dev. *4*, 1450.

Emerman, A.B., Zhang, Z.-R., Chakrabarti, O., and Hegde, R.S. (2010). A Phosphatidylinositol 3-Kinase/Protein Kinase B-independent Activation of Mammalian Target of Rapamycin Signaling Is Sufficient to Induce Skeletal Muscle Hypertrophy. Mol. Biol. Cell *21*, 4325–4337.

Feng, Y., Zhao, H., Luderer, H.F., Epple, H., Faccio, R., Ross, F.P., Teitelbaum, S.L., and Longmore, G.D. (2007). The LIM Protein, LIMD1, Regulates AP-1 Activation

through an Interaction with TRAF6 to Influence Osteoclast Development. J. Biol. Chem. *282*, 39–48.

Ferguson, S.M., and Angarola, B. (2020). Coordination of Rheb lysosomal membrane interactions with mTORC1 activation. F1000Research *9*, 450.

Frias, M.A., Thoreen, C.C., Jaffe, J.D., Schroder, W., Sculley, T., Carr, S.A., and Sabatini, D.M. (2006). mSin1 Is Necessary for Akt/PKB Phosphorylation, and Its Isoforms Define Three Distinct mTORC2s. Curr. Biol. *16*, 1865–1870.

Frontera, W.R., and Ochala, J. (2015). Skeletal Muscle: A Brief Review of Structure and Function. Behav. Genet. *45*, 183–195.

Füchtbauer, E. -M, and Westphal, H. (1992). MyoD and myogenin are coexpressed in regenerating skeletal muscle of the mouse. Dev. Dyn. *193*, 34–39.

Fukuda, S., Kaneshige, A., Kaji, T., Noguchi, Y.T., Takemoto, Y., Zhang, L., Tsujikawa, K., Kokubo, H., Uezumi, A., Maehara, K., et al. (2019). Sustained expression of HeyL is critical for the proliferation of muscle stem cells in overloaded muscle. Elife *8*, 1–21.

Fyfe, J.J., Bishop, D.J., Bartlett, J.D., Hanson, E.D., Anderson, M.J., Garnham, A.P., and Stepto, N.K. (2018). Enhanced skeletal muscle ribosome biogenesis, yet attenuated mTORC1 and ribosome biogenesis-related signalling, following short-term concurrent versus single-mode resistance training. Sci. Rep. *8*, 1–21.

García-Martínez, J.M., and Alessi, D.R. (2008). mTOR complex 2 (mTORC2) controls hydrophobic motif phosphorylation and activation of serum- and glucocorticoid-induced protein kinase 1 (SGK1). Biochem. J. *416*, 375–385.

Ge, Y., Yoon, M.S., and Chen, J. (2011). Raptor and rheb negatively regulate skeletal myogenesis through suppression of insulin receptor substrate 1 (IRS1). J. Biol. Chem. *286*, 35675–35682.

Ghosh, A., Rideout, E.J., and Grewal, S.S. (2014). TIF-IA-Dependent Regulation of Ribosome Synthesis in Drosophila Muscle Is Required to Maintain Systemic Insulin Signaling and Larval Growth. PLoS Genet. *10*, e1004750.

Gingras, A.C., Gygi, S.P., Raught, B., Polakiewicz, R.D., Abraham, R.T., Hoekstra, M.F., Aebersold, R., and Sonenberg, N. (1999). Regulation of 4E-BP1 phosphorylation: A novel two step mechanism. Genes Dev. *13*, 1422–1437.

Glass, D.J. (2003). Molecular mechanisms modulating muscle mass. Trends Mol. Med. *9*, 344–350.

Goldberg, L. (1969). Protein turnover in skeletal muscle. J. Biol. Chem. *244*, 3217–3222.

Goodman, C.A., Frey, J.W., Mabrey, D.M., Jacobs, B.L., Lincoln, H.C., You, J.S., and Hornberger, T.A. (2011). The role of skeletal muscle mTOR in the regulation of mechanical load-induced growth. J. Physiol. *589*, 5485–5501.

Groenewoud, M. (2013). Rheb in mTORC1 signalling and metabolism (Utrecht).

Guertin, D.A., Stevens, D.M., Thoreen, C.C., Burds, A.A., Kalaany, N.Y., Moffat, J., Brown, M., Fitzgerald, K.J., and Sabatini, D.M. (2006). Ablation in Mice of the mTORC Components raptor, rictor, or mLST8 Reveals that mTORC2 Is Required for Signaling to Akt-FOXO and PKCα, but Not S6K1. Dev. Cell *11*, 859–871.

Gur'ianova, O.A., Sablina, A.A., Chumakov, P.M., and Frolova, E.I. (2005). Down-regulation of TRIP6 expression induces actin cytoskeleton rearrangements in human carcinoma cell lines. Mol. Biol. (Mosk). *39*, 905–909.

Hara, K., Yonezawa, K., Weng, Q.P., Kozlowski, M.T., Belham, C., and Avruch, J. (1998). Amino acid sufficiency and mTOR regulate p70 S6 kinase and eIF- 4E BP1 through a common effector mechanism. J. Biol. Chem. *273*, 22160.

Harris, T.E., Chi, A., Shabanowitz, J., Hunt, D.F., Rhoads, R.E., and Lawrence, J.C. (2006). mTOR-dependent stimulation of the association of eIF4G and eIF3 by insulin. EMBO J. *25*, 1659–1668.

Hernández-Hernández, J.M., García-González, E.G., Brun, C.E., and Rudnicki, M.A. (2017). The myogenic regulatory factors, determinants of muscle development, cell identity and regeneration. Semin. Cell Dev. Biol. *72*, 10–18.

Hervy, M., Hoffman, L., and Beckerle, M.C. (2006). From the membrane to the nucleus and back again: bifunctional focal adhesion proteins. Curr. Opin. Cell Biol. *18*, 524–532.

Hinits, Y., and Hughes, S.M. (2007). Mef2s are required for thick filament formation in nascent muscle fibres. Development *134*, 2511–2519.

Hoffman, L.M., Nix, D.A., Benson, B., Boot-Hanford, R., Gustafsson, E., Jamora, C., Menzies, A.S., Goh, K.L., Jensen, C.C., Gertler, F.B., et al. (2003). Targeted

Disruption of the Murine zyxin Gene. Mol. Cell. Biol. *23*, 70–79.

Hoppeler, H., Klossner, S., and Vogt, M. (2008). Training in hypoxia and its effects on skeletal muscle tissue. Scand. J. Med. Sci. Sports *18*, 38–49.

Inoki, K. (2003). Rheb GTPase is a direct target of TSC2 GAP activity and regulates mTOR signaling. Genes Dev. *17*, 1829–1834.

Ishibashi, J., Perry, R.L., Asakura, A., and Rudnicki, M.A. (2005). MyoD induces myogenic differentiation through cooperation of its NH 2- and COOH-terminal regions. J. Cell Biol. *171*, 471–482.

al Jaam, B., Heu, K., Pennarubia, F., Segelle, A., Magnol, L., Germot, A., Legardinier, S., Blanquet, V., and Maftah, A. (2016). Reduced Notch signalling leads to postnatal skeletal muscle hypertrophy in Pofut1cax/cax mice. Open Biol. *6*.160211

Jacinto, E., Loewith, R., Schmidt, A., Lin, S., Rüegg, M.A., Hall, A., and Hall, M.N. (2004). Mammalian TOR complex 2 controls the actin cytoskeleton and is rapamycin insensitive. Nat. Cell Biol. *6*, 1122–1128.

Jarriault, S., Brou, C., Logeat, F., Schroeter, E.H., Kopan, R., and Israel, A. (1995). Signalling downstream of activated mammalian Notch. Nature *377*, 355–358.

Jhanwar-Uniyal, M., Wainwright, J. V., Mohan, A.L., Tobias, M.E., Murali, R., Gandhi, C.D., and Schmidt, M.H. (2019). Diverse signaling mechanisms of mTOR complexes: mTORC1 and mTORC2 in forming a formidable relationship. Adv. Biol. Regul. *72*, 51–62.

Karagounis, L.G., and Hawley, J.A. (2010). Skeletal muscle: Increasing the size of the locomotor cell. Int. J. Biochem. Cell Biol. *42*, 1376–1379.

Karalaki, M., Fili, S., Philippou, A., and Koutsilieris, M. (2009). Muscle regeneration: cellular and molecular events. In Vivo *23*, 779–796.

Karbowniczek, M., Robertson, G.P., and Henske, E.P. (2006). Rheb inhibits C-Raf activity and B-Raf/C-Raf heterodimerization. J. Biol. Chem. *281*, 25447–25456.

Karbowniczek, M., Zitserman, D., Khabibullin, D., Hartman, T., Yu, J., Morrison, T., Nicolas, E., Squillace, R., Roegiers, F., and Henske, E.P. (2010). The evolutionarily conserved TSC/Rheb pathway activates Notch in tuberous sclerosis complex and Drosophila external sensory organ development. J. Clin. Invest. *120*, 93–102.

Karlsson, O., Thor, S., Norberg, T., Ohlsson, H., and Edlund, T. (1990). Insulin gene

enhancer binding protein Isl-1 is a member of a novel class of proteins containing both a homeo-and a Cys–His domain. Nature *344*, 879–882.

Kassel, O., Schneider, S., Heilbock, C., Litfin, M., Göttlicher, M., and Herrlich, P. (2004). A nuclear isoform of the focal adhesion LIM-domain protein Trip6 integrates activating and repressing signals at AP-1- and NF-κB-regulated promoters. Genes Dev. *18*, 2518–2528.

Kawasaki, E., Hokari, F., Sasaki, M., Sakai, A., Koshinaka, K., and Kawanaka, K. (2011). The effects of β-adrenergic stimulation and exercise on NR4A3 protein expression in rat skeletal muscle. J. Physiol. Sci. *61*, 1–11.

Keenan, S.R., and Currie, P.D. (2019). The developmental phases of zebrafish myogenesis. J. Dev. Biol. *7*.

Kemler, D. (2017). The Role of nTRIP6 in Adult Myogenesis (PhD Thesis). Karlsruhe; Karlsruhe Inst. Technol.

Kemler, D., Dahley, O., Roßwag, S., Litfin, M., Kassel, O., Potthoff, M.J., Olson, E.N., Bharathy, N., Ling, B.M.T., Taneja, R., et al. (2016). The LIM domain protein nTRIP6 acts as a co-repressor for the transcription factor MEF2C in myoblasts. Sci. Rep. *6*, 27746.

Khor, E.-S., Noor, S.M., and Wong, P.-F. (2019). Understanding the Role of ztor in Aging-related Diseases Using the Zebrafish Model. In Vivo (Brooklyn). *33*, 1713–1720.

Kim, D.-H., Sarbassov, D.D., Ali, S.M., King, J.E., Latek, R.R., Erdjument-Bromage, H., Tempst, P., and Sabatini, D.M. (2002). mTOR Interacts with Raptor to Form a Nutrient-Sensitive Complex that Signals to the Cell Growth Machinery. Cell *110*, 163–175.

Kim, D.-H., Sarbassov, D.D., Ali, S.M., Latek, R.R., Guntur, K.V.., Erdjument-Bromage, H., Tempst, P., and Sabatini, D.M. (2003). GβL, a Positive Regulator of the Rapamycin-Sensitive Pathway Required for the Nutrient-Sensitive Interaction between Raptor and mTOR. Mol. Cell *11*, 895–904.

Kobayashi, J., Uchida, H., Kofuji, A., Ito, J., Shimizu, M., Kim, H., Sekiguchi, Y., and Kushibe, S. (2019). Molecular regulation of skeletal muscle mass and the contribution of nitric oxide: A review. FASEB BioAdvances *1*, 364–374.

Kou, X., Chen, D., and Chen, N. (2019). Physical activity alleviates cognitive

dysfunction of alzheimer's disease through regulating the mtor signaling pathway. Int. J. Mol. Sci. *20*.

Laemmli, U.K. (1970). Cleavage of Structural Proteins during the Assembly of the Head of Bacteriophage T4. Nature *227*, 680–685.

Lee, S.J. (2004). Regulation of muscle mass by myostatin. Annu. Rev. Cell Dev. Biol. *20*, 61–86.

Li, Y., Inoki, K., and Guan, K.-L. (2004). Biochemical and Functional Characterizations of Small GTPase Rheb and TSC2 GAP Activity. Mol. Cell. Biol. *24*, 7965–7975.

Li Y, Corradetti MN, Inoki K, G.K. (2004). TSC2: filling the GAP in the mTOR signaling pathway. Trends Biochem. Sci. *29*, 32–38.

Lin, V.T.G., and Lin, F. (2011). TRIP6: An adaptor protein that regulates cell motility, antiapoptotic signaling and transcriptional activity. Cell. Signal. *23*, 1691–1697.

Lin, Z., Lu, M. -H, Schultheiss, T., Choi, J., Holtzer, S., Dilullo, C., Fischman, D.A., and Holtzer, H. (1994). Sequential appearance of muscle-specific proteins in myoblasts as a function of time after cell division: Evidence for a conserved myoblast differentiation program in skeletal muscle. Cell Motil. Cytoskeleton *29*, 1–19.

Liu, G.Y., and Sabatini, D.M. (2020). mTOR at the nexus of nutrition, growth, ageing and disease. Nat. Rev. Mol. Cell Biol. *21*.

Liu, N., Nelson, B.R., Bezprozvannaya, S., Shelton, J.M., Richardson, J.A., Bassel-Duby, R., and Olson, E.N. (2014). Requirement of MEF2A, C, and D for skeletal muscle regeneration. Proc. Natl. Acad. Sci. U. S. A. *111*, 4109–4114.

Liu, R., Iadevaia, V., Averous, J., Taylor, P.M., Zhang, Z., and Proud, C.G. (2014b). Impairing the production of ribosomal RNA activates mammalian target of rapamycin complex 1 signalling and downstream translation factors. Nucleic Acids Res. *42*, 5083–5096.

Long, X., Lin, Y., Ortiz-Vega, S., Yonezawa, K., and Avruch, J. (2005). Rheb Binds and Regulates the mTOR Kinase. Curr. Biol. *15*, 702–713.

Long, X., Lin, Y., Ortiz-Vega, S., Busch, S., and Avruch, J. (2007). The Rheb Switch 2 Segment Is Critical for Signaling to Target of Rapamycin Complex 1. J. Biol. Chem. *282*, 18542–18551.

Ma, D., Bai, X., Guo, S., and Jiang, Y. (2008). The switch I region of Rheb is critical

for its interaction with FKBP38. J. Biol. Chem. *283*, 25963–25970.

Mahoney, S.J., Narayan, S., Molz, L., Berstler, L.A., Kang, S.A., Vlasuk, G.P., and Saiah, E. (2018). A small molecule inhibitor of Rheb selectively targets mTORC1 signaling. Nat. Commun. *9*, 1–12.

Marcotte, G.R., West, D.W.D., and Baar, K. (2015). The Molecular Basis for Load-Induced Skeletal Muscle Hypertrophy. Behav. Genet. *45*, 196–210.

Mayer, C., and Grummt, I. (2006). Ribosome biogenesis and cell growth: mTOR coordinates transcription by all three classes of nuclear RNA polymerases. Oncogene *25*, 6384–6391.

Mayer, C., Zhao, J., Yuan, X., and Grummt, I. (2004). mTOR-dependent activation of the transcription factor TIF-IA links rRNA synthesis to nutrient availability. Genes Dev. *18*, 423–434.

Mazhab-Jafari, M.T., Marshall, C.B., Ishiyama, N., Ho, J., Di Palma, V., Stambolic, V., and Ikura, M. (2012). An autoinhibited noncanonical mechanism of GTP hydrolysis by Rheb maintains mTORC1 homeostasis. Structure *20*, 1528–1539.

Meng, W., Liang, X., Xiao, T., Wang, J., Wen, J., Luo, H., Teng, J., Fei, Y., Zhang, Q., Liu, B., et al. (2019). Rheb promotes brown fat thermogenesis by Notch-dependent activation of the PKA signaling pathway. J. Mol. Cell Biol. *11*, 781–790.

Michels, A.A., Robitaille, A.M., Buczynski-Ruchonnet, D., Hodroj, W., Reina, J.H., Hall, M.N., and Hernandez, N. (2010). mTORC1 Directly Phosphorylates and Regulates Human MAF1. Mol. Cell. Biol. *30*, 3749–3757.

Mieulet, V., Roceri, M., Espeillac, C., Sotiropoulos, A., Ohanna, M., Oorschot, V., Klumperman, J., Sandri, M., and Pende, M. (2007). S6 kinase inactivation impairs growth and translational target phosphorylation in muscle cells maintaining proper regulation of protein turnover. Am. J. Physiol. Physiol. *293*, C712–C722.

Mizuki, N., Kimura, M., Ohno, S., Miyata, S., Sato, M., Ando, H., Ishihara, M., Goto, K., Watanabe, S., Yamazaki, M., et al. (1996). Isolation of cDNA and Genomic Clones of a Human Ras-Related GTP-Binding Protein Gene and Its Chromosomal Localization to the Long Arm of Chromosome 7, 7q36. Genomics *34*, 114–118.

Moik, D. V., Janbandhu, V.C., and Fassler, R. (2011). Loss of migfilin expression has no overt consequences on murine development and homeostasis. J. Cell Sci. *124*,

414–421.

Mokalled, M.H., Johnson, A.N., Creemers, E.E., and Olson, E.N. (2012). MASTR directs MyoD-dependent satellite cell differentiation during skeletal muscle regeneration. Genes Dev. *26*, 190–202.

Mommsen, T.P. (2001). Paradigms of growth in fish. Comp. Biochem. Physiol. - B Biochem. Mol. Biol. *129*, 207–219.

Moores, S.L., Schaber, M.D., Mosser, S.D., Rands, E., O'Hara, M.B., Garsky, V.M., Marshall, M.S., Pompliano, D.L., and Gibbs, J.B. (1991). Sequence dependence of protein isoprenylation. J. Biol. Chem. *266*, 14603–14610.

Moretti, I., Ciciliot, S., Dyar, K.A., Abraham, R., Murgia, M., Agatea, L., Akimoto, T., Bicciato, S., Forcato, M., Pierre, P., et al. (2016). MRF4 negatively regulates adult skeletal muscle growth by repressing MEF2 activity. Nat. Commun. *7*.

Murphy, M.M., Lawson, J.A., Mathew, S.J., Hutcheson, D.A., and Kardon, G. (2011). Satellite cells, connective tissue fibroblasts and their interactions are crucial for muscle regeneration. Development *138*, 3625–3637.

Musarò, A. (2014). The Basis of Muscle Regeneration. Adv. Biol. *2014*, 1–16.

Nakayama, M., Stauffer, J., Cheng, J., Banerjee-Basu, S., Wawrousek, E., and Buonanno, A. (1996). Common core sequences are found in skeletal muscle slow- and fast-fiber-type-specific regulatory elements. Mol. Cell. Biol. *16*, 2408–2417.

Nojima, H., Tokunaga, C., Eguchi, S., Oshiro, N., Hidayat, S., Yoshino, K.I., Hara, K., Tanaka, N., Avruch, J., and Yonezawa, K. (2003). The mammalian target of rapamycin (mTOR) partner, raptor, binds the mTOR substrates p70 S6 kinase and 4E-BP1 through their TOR signaling (TOS) motif. J. Biol. Chem. *278*, 15461–15464.

Ogasawara, R., Fujita, S., Hornberger, T.A., Kitaoka, Y., Makanae, Y., Nakazato, K., and Naokata, I. (2016). The role of mTOR signalling in the regulation of skeletal muscle mass in a rodent model of resistance exercise. Sci. Rep. *6*, 31142.

Panov, K.I., Friedrich, J.K., Russell, J., and Zomerdijk, J.C.B.M. (2006). UBF activates RNA polymerase I transcription by stimulating promoter escape. EMBO J. *25*, 3310–3322.

Parmar, N., and Tamanoi, F. (2010). Rheb G-proteins and the activation of mTORC1. Enzymes *27*, 39–56.

Pavlath, G.K., Dominov, J.A., Kegley, K.M., and Millert, J.B. (2003). Regeneration of transgenic skeletal muscles with altered timing of expression of the basic helix-loop-helix muscle regulatory factor MRF4. Am. J. Pathol. *162*, 1685–1691.

Pende, M., Um, S.H., Mieulet, V., Sticker, M., Goss, V.L., Mestan, J., Mueller, M., Fumagalli, S., Kozma, S.C., and Thomas, G. (2004). S6K1−/−/S6K2−/− Mice Exhibit Perinatal Lethality and Rapamycin-Sensitive 5′-Terminal Oligopyrimidine mRNA Translation and Reveal a Mitogen-Activated Protein Kinase-Dependent S6 Kinase Pathway. Mol. Cell. Biol. *24*, 3112–3124.

Perl, A. (2015). MTOR activation is a biomarker and a central pathway to autoimmune disorders, cancer, obesity, and aging. Ann. N. Y. Acad. Sci. *1346*, 33–44.

Peterson, T.R., Laplante, M., Thoreen, C.C., Sancak, Y., Kang, S.A., Kuehl, W.M., Gray, N.S., and Sabatini, D.M. (2009). DEPTOR Is an mTOR Inhibitor Frequently Overexpressed in Multiple Myeloma Cells and Required for Their Survival. Cell *137*, 873–886.

Peterson, T.R., Sengupta, S.S., Harris, T.E., Carmack, A.E., Kang, S.A., Balderas, E., Guertin, D.A., Madden, K.L., Carpenter, A.E., Finck, B.N., et al. (2011). mTOR Complex 1 Regulates Lipin 1 Localization to Control the SREBP Pathway. Cell *146*, 408–420.

Potthoff, M.J., Arnold, M.A., McAnally, J., Richardson, J.A., Bassel-Duby, R., and Olson, E.N. (2007). Regulation of Skeletal Muscle Sarcomere Integrity and Postnatal Muscle Function by Mef2c. Mol. Cell. Biol. *27*, 8143–8151.

Pratt, S.J., Epple, H., Ward, M., Feng, Y., Braga, V.M., and Longmore, G.D. (2005). The LIM protein Ajuba influences p130Cas localization and Rac1 activity during cell migration. J. Cell Biol. *168*, 813–824.

Raffaello, A., Milan, G., Masiero, E., Carnio, S., Lee, D., Lanfranchi, G., Goldberg, A.L., and Sandri, M. (2010). JunB transcription factor maintains skeletal muscle mass and promotes hypertrophy. J. Cell Biol. *191*, 101–113.

Rahnert, J.A., Zheng, B., Hudson, M.B., Woodworth-Hobbs, M.E., and Price, S.R. (2016). Glucocorticoids Alter CRTC-CREB Signaling in Muscle Cells: Impact on PGC-1α Expression and Atrophy Markers. PLoS One *11*, e0159181.

Reijnders, M.R.F., Kousi, M., Van Woerden, G.M., Klein, M., Bralten, J., Mancini,

G.M.S., Van Essen, T., Proietti-Onori, M., Smeets, E.E.J., Van Gastel, M., et al. (2017). Variation in a range of mTOR-related genes associates with intracranial volume and intellectual disability. Nat. Commun. *8*, 1–11.

Rennie, M.J., Wackerhage, H., Spangenburg, E.E., and Booth, F.W. (2004). Control of the Size of the Human Muscle Mass. Annu. Rev. Physiol. *66*, 799–828.

Robitaille, A.M., Christen, S., Shimobayashi, M., Cornu, M., Fava, L.L., Moes, S., Prescianotto-Baschong, C., Sauer, U., Jenoe, P., and Hall, M.N. (2013). Quantitative phosphoproteomics reveal mTORC1 activates de novo pyrimidine synthesis. Science. *339*, 1320–1323.

Rommel, C., Bodine, S.C., Clarke, B.A., Rossman, R., Nunez, L., Stitt, T.N., Yancopoulos, G.D., and Glass, D.J. (2001). Mediation of IGF-1-induced skeletal myotube hypertrophy by PI(3)K/Alt/mTOR and PI(3)K/Akt/GSK3 pathways. Nat. Cell Biol. *3*, 1009–1013.

Rosner, M., and Hengstschläger, M. (2008). Cytoplasmic and nuclear distribution of the protein complexes mTORC1 and mTORC2: Rapamycin triggers dephosphorylation and delocalization of the mTORC2 components rictor and sin1. Hum. Mol. Genet. *17*, 2934–2948.

Rossi, G., and Messina, G. (2014). Comparative myogenesis in teleosts and mammals. Cell. Mol. Life Sci. *71*, 3081–3099.

Rowlerson, A., Mascarello, F., Radaelli, G., and Veggetti, A. (1995). Differentiation and growth of muscle in the fish Sparus aurata (L): II. Hyperplastic and hypertrophic growth of lateral muscle from hatching to adult. J. Muscle Res. Cell Motil. *16*, 223–236.

Rudeck, S., Etard, C., Khan, M.M., Rottbauer, W., Rudolf, R., Strähle, U., and Just, S. (2016). A compact unc45b-promoter drives muscle-specific expression in zebrafish and mouse. Genesis *54*, 431–438.

Ruijtenberg, S., and van den Heuvel, S. (2016). Coordinating cell proliferation and differentiation: Antagonism between cell cycle regulators and cell type-specific gene expression. Cell Cycle *15*, 196–212.

Sambrook, J., Fritsch, E. F. and Maniatis, T. (2001). Molecular cloning : a laboratory manual (Cold Spring Harbor Laboratory).

Sancak, Y., Peterson, T.R., Shaul, Y.D., Lindquist, R.A., Thoreen, C.C., Bar-Peled, L., and Sabatini, D.M. (2008). The Rag GTPases Bind Raptor and Mediate Amino Acid Signaling to mTORC1. Science. *320*, 1496–1501.

Sanders, S.S., De Simone, F.I., and Thomas, G.M. (2019). mTORC1 Signaling Is Palmitoylation-Dependent in Hippocampal Neurons and Non-neuronal Cells and Involves Dynamic Palmitoylation of LAMTOR1 and mTOR. Front. Cell. Neurosci. *13*.

Sandri, M. (2008). Signaling in muscle atrophy and hypertrophy. Physiology *23*, 160–170.

Sarbassov, D.D., Guertin, D.A., Ali, S.M., and Sabatini, D.M. (2005). Phosphorylation and regulation of Akt/PKB by the rictor-mTOR complex. Science. *307*, 1098–1101.

Sartore, S., Gorza, L., and Schiaffino, S. (1982). Fetal myosin heavy chains in regenerating muscle. Nature *298*, 294–296.

Scheffzek, K. (1997). The Ras-RasGAP Complex: Structural Basis for GTPase Activation and Its Loss in Oncogenic Ras Mutants. Science. *277*, 333–338.

Schiaffino, S., and Mammucari, C. (2011). Regulation of skeletal muscle growth by the IGF1-Akt/PKB pathway: Insights from genetic models. Skelet. Muscle *1*, 4.

Schiaffino, S., Dyar, K.A., Ciciliot, S., Blaauw, B., and Sandri, M. (2013). Mechanisms regulating skeletal muscle growth and atrophy. FEBS J. *280*, 4294–4314.

Schiaffino, S., Rossi, A.C., Smerdu, V., Leinwand, L.A., and Reggiani, C. (2015). Developmental myosins: Expression patterns and functional significance. Skelet. Muscle *5*, 1–14.

Schindelin, J., Arganda-Carreras, I., Frise, E., Kaynig, V., Longair, M., Pietzsch, T., Preibisch, S., Rueden, C., Saalfeld, S., Schmid, B., et al. (2012). Fiji: an open-source platform for biological-image analysis. Nat. Methods *9*, 676–682.

Schöpel, M., Potheraveedu, V.N., Al-Harthy, T., Abdel-Jalil, R., Heumann, R., and Stoll, R. (2017). The small GTPases Ras and Rheb studied by multidimensional NMR spectroscopy: Structure and function. Biol. Chem. *398*, 577–588.

Shi, X., and Garry, D.J. (2006). Muscle stem cells in development, regeneration, and disease. Genes Dev. *20*, 1692–1708.

Shukla, S., Urbanek, P., Frappart, L., Hänold, R., Nagel, S., Monajembashi, S., Grigaravicius, P., Min, W.K., Tapias, A., Kassel, O., et al. (2019). Novel function of

TRIP6, in brain ciliogenesis. BioRxiv 777052.

Singh, K., and Dilworth, F.J. (2013). Differential modulation of cell cycle progression distinguishes members of the myogenic regulatory factor family of transcription factors. FEBS J. *280*, 3991–4003.

Smith, M.A., Hoffman, L.M., and Beckerle, M.C. (2014). LIM proteins in actin cytoskeleton mechanoresponse. Trends Cell Biol. *24*, 575–583.

Song, Z., Moore, D.R., Hodson, N., Ward, C., Dent, J.R., O'Leary, M.F., Shaw, A.M., Hamilton, D.L., Sarkar, S., Gangloff, Y.G., et al. (2017). Resistance exercise initiates mechanistic target of rapamycin (mTOR) translocation and protein complex co-localisation in human skeletal muscle. Sci. Rep. *7*, 1–14.

Tabancay, A.P., Gau, C.L., Machado, I.M.P., Uhlmann, E.J., Gutmann, D.H., Guo, L., and Tamanoi, F. (2003). Identification of dominant negative mutants of Rheb GTPase and their use to implicate the involvement of human Rheb in the activation of p70S6K. J. Biol. Chem. *278*, 39921–39930.

Takahashi, K., Nakagawa, M., Young, S.G., and Yamanaka, S. (2005). Differential membrane localization of ERas and Rheb, two Ras-related proteins involved in the phosphatidylinositol 3-kinase/mTOR pathway. J. Biol. Chem. *280*, 32768–32774.

Taylor, M. V., and Hughes, S.M. (2017). Mef2 and the skeletal muscle differentiation program. Semin. Cell Dev. Biol. *72*, 33–44.

Thébault, S., Verdin, E., Lu, J., McKinsey, T.A., Zhang, C.L., and Olson, N.E. (2001). Regulation of skeletal myogenesis by association of the MEF2 transcription factor with class II histone deacetylases. Chemtracts *14*, 720–726.

Thoreen, C.C., Kang, S.A., Chang, J.W., Liu, Q., Zhang, J., Gao, Y., Reichling, L.J., Sim, T., Sabatini, D.M., and Gray, N.S. (2009). An ATP-competitive mammalian target of rapamycin inhibitor reveals rapamycin-resistant functions of mTORC1. J. Biol. Chem. *284*, 8023–8032.

Tidball, J.G., and Wehling-Henricks, M. (2007). Macrophages promote muscle membrane repair and muscle fibre growth and regeneration during modified muscle loading in mice in vivo. J. Physiol. *578*, 327–336.

Tsang, C.K., Liu, H., and Zheng, X.F.S. (2010). mTOR binds to the promoters of RNA polymerase I- and III-transcribed genes. Cell Cycle *9*, 953–957.

Vervenne, H.B.V.K., Crombez, K.R.M.O., Delvaux, E.L., Janssens, V., Van de Ven, W.J.M., and Petit, M.M.R. (2009). Targeted disruption of the mouse Lipoma Preferred Partner gene. Biochem. Biophys. Res. Commun. *379*, 368–373.

Vo, T.A., Galloway, T.F., Bardal, T., Halseth, C.K., Øie, G., and Kjørsvik, E. (2016). Skeletal muscle growth dynamics and the influence of first-feeding diet in Atlantic cod larvae (Gadus morhua L.). Biol. Open *5*, 1575–1584.

Wagner, D.R. (1996). Skeletal Muscle Growth: Hypertrophy and Hyperplasia. Strength Cond. J. *18*, 1524-1602.

von Maltzahn, J., Jonas, A., Parks, R.J., and Rudnicki, MA. (2013). PAX7 is critical for the normal function of satellite cells in adult skeletal muscle. PNAS.*110*, 16474-16479.

von Walden, F., Casagrande, V., Farrants, A.K.Ö., and Nader, G.A. (2012). Mechanical loading induces the expression of a Pol I regulon at the onset of skeletal muscle hypertrophy. Am. J. Physiol. - Cell Physiol. *302*, 1523–1530.

von Walden, F., Liu, C., Aurigemma, N., and Nader, G.A. (2016). mTOR signaling regulates myotube hypertrophy by modulating protein synthesis, rDNA transcription, and chromatin remodeling. Am. J. Physiol. - Cell Physiol. *311*, C663–C672.

Wang, Y., and Gilmore, T.D. (2003). Zyxin and paxillin proteins: Focal adhesion plaque LIM domain proteins go nuclear. Biochim. Biophys. Acta - Mol. Cell Res. *1593*, 115–120.

Wang, L., Harris, T.E., Roth, R.A., and Lawrence, J.C. (2007). PRAS40 regulates mTORC1 kinase activity by functioning as a direct inhibitor of substrate binding. J. Biol. Chem. *282*, 20036–20044.

Wang, Y., Dooher, J.E., Koedood Zhao, M., and Gilmore, T.D. (1999). Characterization of mouse Trip6: A putative intracellular signaling protein. Gene *234*, 403–409.

Willier, S., Butt, E., Richter, G.H.S., Burdach, S., and Grunewald, T.G.P. (2011). Defining the role of TRIP6 in cell physiology and cancer. Biol. Cell *103*, 573–591.

Wolfe, R.R. (2006). The underappreciated role of muscle in health and disease. Am. J. Clin. Nutr. *84*, 475–482.

Wyzykowski, J.C., Winata, T.I., Mitin, N., Taparowsky, E.J., and Konieczny, S.F. (2002). Identification of Novel MyoD Gene Targets in Proliferating Myogenic Stem

Cells. Mol. Cell. Biol. *22*, 6199–6208.

Yablonka-Reuveni, Z., and Rivera, A.J. (1994). Temporal expression of regulatory and structural muscle proteins during myogenesis of satellite cells on isolated adult rat fibers. Dev. Biol. *164*, 588–603.

Yadav, R.B., Burgos, P., Parker, A.W., Iadevaia, V., Proud, C.G., Allen, R.A., O'Connell, J.P., Jeshtadi, A., Stubbs, C.D., and Botchway, S.W. (2013). mTOR direct interactions with Rheb-GTPase and raptor: Sub-cellular localization using fluorescence lifetime imaging. BMC Cell Biol. *14*, 1.

Yamagata, K., Sanders, L.K., Kaufmann, W.E., Yee, W., Barnes, C.A., Nathans, D., and Worley, P.F. (1994). Rheb, a Growth Factor- and Synaptic Activity-Regulated Gene, Encodes a Novel Ras-Related Protein. J. Biol. Chem. *269*, 16333–16339.

Yamamoto, M., Legendre, N.P., Biswas, A.A., Lawton, A., Yamamoto, S., Tajbakhsh, S., Kardon, G., and Goldhamer, D.J. (2018). Loss of MyoD and Myf5 in Skeletal Muscle Stem Cells Results in Altered Myogenic Programming and Failed Regeneration. Stem Cell Reports *10*, 956–969.

Yi, J., Kloeker, S., Jensen, C.C., Bockholt, S., Honda, H., Hirai, H., and Beckerle, M.C. (2002). Members of the zyxin family of LIM proteins interact with members of the p130Cas family of signal transducers. J. Biol. Chem. *277*, 9580–9589.

Yin, H., Price, F., and Rudnicki, M.A. (2013). Satellite Cells and the Muscle Stem Cell Niche. Physiol. Rev. *93*, 23–67.

Yin Zheng, Y.J. (2018). mTOR Inhibitors at a Glance. Physiol. Behav. *176*, 139–148.

Yoshimoto, Y., Ikemoto-Uezumi, M., Hitachi, K., Fukada, S.I., and Uezumi, A. (2020). Methods for Accurate Assessment of Myofiber Maturity During Skeletal Muscle Regeneration. Front. Cell Dev. Biol. *8*, 1–12.

You, J.S., Anderson, G.B., Dooley, M.S., and Hornberger, T.A. (2015). The role of mTOR signaling in the regulation of protein synthesis and muscle mass during immobilization in mice. DMM Dis. Model. Mech. *8*, 1059–1069.

Zammit, P.S. (2017). Function of the myogenic regulatory factors Myf5, MyoD, Myogenin and MRF4 in skeletal muscle, satellite cells and regenerative myogenesis. Semin. Cell Dev. Biol. *72*, 19–32.

Zhang, X., Shu, L., Hosoi, H., Gopal Murti, K., and Houghton, P.J. (2002). Predominant

nuclear localization of mammalian target of rapamycin in normal and malignant cells in culture. J. Biol. Chem. *277*, 28127–28134.

Zheng, Q., and Zhao, Y. (2007). The diverse biofunctions of LIM domain proteins: determined by subcellular localization and protein-protein interaction. Biol. Cell *99*, 489–502.

Zhou, Z., and Bornemann, A. (2001). MRF4 protein expression in regenerating rat muscle. J. Muscle Res. Cell Motil. *22*, 311–316.

6. Acknowledgements

First and foremost, I would like to thank Dr. Olivier Kassel, who gave me the priceless opportunity to work in his group and for his supervision in which he went above and beyond with his support in all aspects of my work. I really appreciate the time that I spent working with Margarethe Litfin, from whom I learned alot on both the professional and personal level. Moreover, I am deeply thankful all the lab members, without them my PhD time would not have been so amazing, especially Zita Gonda for being always there as a colleague and friend, and of course Raphael Fettig for his great help. I am also truly thankful of Denise Kemler, who was a great supervisor and has always been there for me even after leaving the lab. Furthermore, I would like to acknowledge endless support from Dr. Sepand Rastegar, Dr. Christelle Etard, Dr. Volker Middel and Dr. Masanary Takamiya for allowing me to come to them with any questions regarding to work with Zebrafish. Lastly, I would like to give my special thanks to my wonderful parents and my dear aunt, Shiva, for their everlasting support and their encouragement for me to pursue my dreams.

Publications

Kemler, D.*, **Norizadeh Abbariki, T**.*, Urbanek, P., Litfin M., Wang, ZQ., Herrlich, P., Kassel O. (2020, under revision). The LIM domain protein nTRIP6 modulates the dynamic of myogenic differentiation. (* equal contribution)

Molle, E., Le, D., **Norizadeh Abbariki, T**., Akdemir, M., Takami, M., Miceli, E., Kassel, O., Delaittre G. (2019). Access to Photoreactive Core-Shell Nanomaterials by Photoinitiated Polymerization-Induced Self-Assembly. ChemPhotoChem. *3*, 1084-1089.

Saberi, M., Pu Q., Valasek, P., **Norizadeh Abbariki, T.**, Patel, K., Huang R. (2017). The hypaxial origin of the epaxially located rhomboid muscles. Annals of Anatomy. *214*, 15-20.

Moraveji, M., Haghighipour, N ., Keshvari, H., Shokrgozar, MA., **Nourizadeh Abbariki, T.**, Amanzadeh A. (2016). Effect of extremely low frequency electromagnetic field on Map2 and Nestin gene expression of hair follicle dermal papillae cells. Artificial Organs. *6*, 294-299.

Jazayeri, M., Shokrgozar, MA., Haghighipour, N., Mahdian, R., farrokhi, M., Bonakdar, Sh., Mirahmadi, F., **Norizadeh Abbariki, T.** (2015) Evaluation of mechanical and chemical stimulation on osteocalcin and Runx2 expression in mesenchymal stem cells. Molecular and Cellular Biomechanics (MCB). *3*, 197-213.

Norizadeh Abbariki, T., Mashinchian, O., Shokrgozar, MA., Haghighipour, N., Sen, T., Mahmoudi, M. (2014) Superparamagnetic nanoparticles direct differentiation of embryonic stem cells into skeletal muscle, Journal of Biomaterials and Tissue Engineering (JBT). *4*, 579-585.

Norizadeh Abbariki, T., Shokrgozar, MA., Haghighipour, N ., Aghdami, N., Mahdian R., Amanzadeh, A., Jazayeri, M. (2014) Comparing the effect of uniaxial cyclic mechanical stimulation and chemical factors on Myogenin and Myh2 expression in mouse embryonic and bone marrow derived mesenchymal stem cells, Molecular and

Cellular Biomechanics (MCB). *1*, 19-37.